Université catholique de Louvain

Faculté des Sciences Appliquées
Centre for systems engineering and applied mechanics

The role of gravity in dexterous manipulation: a driving force rather than a perturbation

Doctoral Dissertation presented by

Olivier White

in fulfillment of the requirements for the degree of
Doctor in Applied Sciences

Prof. Vincent Blondel (chair)	Université catholique de Louvain	Belgium
Prof. Philippe Lefèvre (supervisor)	Université catholique de Louvain	Belgium
Dr. Joseph McIntyre	Université Paris 5	France
Prof. Rodolphe Sepulchre	Université de Liège	Belgium
Prof. Allan Smith	Université de Montréal	Canada
Prof. Jean-Louis Thonnard (supervisor)	Université catholique de Louvain	Belgium
Prof. Alan Wing	University of Birmingham	UK

Louvain-la-Neuve June 2007

To my wonderful Héloïse, a gift from Heaven,

To her fabulous Mother, Evelyne,
a constant source of motivation and love in my life,

To her Grand-Mother, Dominique,
whose unswerving Faith in Life was an Inspiration,
whose Generosity is a bye-word;

This work is dedicated, as a mark of Love, Gratitude and Affection.

Acknowledgments

Nowadays, richness and potential in ideas often emerge from multicultural views. Over the last five years, I had the unique chance to benefit from expertises in the engineering and biomedical domains.

I am most grateful to Professors Jean-Louis Thonnard from the Rehabilitation and Physical Medicine Unit (READ) and to Philippe Lefèvre from the Centre for Systems Engineering and Applied Mechanics (CESAME), at the Université catholique de Louvain. The collaboration with Jean-Louis dates back to the time when I was working as a student to update programs of the first set-up. Over the years, I discovered his numerous qualities as a leader and advisor. In particular, his scientific rigor and perseverance have been of great value and proven extremely useful. Our common passion for cycling let us discover another side of working together. Hearty acknowledgments also go to Philippe. His expertise was extremely valuable to complete this work. His availability and humanity were ingredients for an excellent scientific supervision. During hard time, he knew how to motivate and encourage his researchers to reach their objectives.

I also wish to thank all members of my PhD jury for their comments and suggestions. In particular, I sincerely appreciated our meetings during the ESA topical teams with Alan, Allan and Joe as well as more focused exchanges in other contexts in Birmingham or in Liège.

My gratitude also goes to all my numerous colleagues and friends in READ and CESAME with whom I did not address only scientific issues but also memorable conferences and activities beyond office hours.

Finally, I deeply thank my whole family and particularly my parents and parents-in-law, for their active involvement and support during those years of work despite very hard ordeals. More than anyone else, I thank my wife and our little sunshine Héloïse for their unlimited love and their organization which was perfectly synchronized with the redaction of my manuscript, day and night.

This research was supported by grants from Prodex, OSTC (Belgian Federal Office for Scientific, Technical and Cultural affairs) and ESA, ESTEC Contract 14725/00/NL/JS to JLT.

Contents

1 Introduction **1**
- 1.1 Background . . . 1
- 1.2 Control theory . . . 3
  - 1.2.1 Feedback control . . . 4
  - 1.2.2 Feedforward control . . . 4
  - 1.2.3 Hybrid feedforward/feedback control . . . 6
  - 1.2.4 Motor planning . . . 8
- 1.3 Experimental evidence of internal models . . . 10
  - 1.3.1 Planning . . . 11
  - 1.3.2 Feedback control . . . 14
  - 1.3.3 Forward models . . . 16
    - 1.3.3.1 Arm dynamic models . . . 18
    - 1.3.3.2 Object dynamic models . . . 19
    - 1.3.3.3 Sensorimotor memory . . . 20
    - 1.3.3.4 Learning . . . 21
- 1.4 Role of gravity in motor control . . . 23
- 1.5 Parabolic flights manœuvres . . . 25
- 1.6 Content of the thesis . . . 27
- 1.7 List of publications . . . 30
  - 1.7.1 Journal articles . . . 30
  - 1.7.2 Journal articles submitted and in preparation . . . 30
  - 1.7.3 Conference abstracts . . . 30

2 Altered gravity highlights Central Pattern Generators mechanisms **33**
- 2.1 Abstract . . . 33
- 2.2 Introduction . . . 34
- 2.3 Methods . . . 35

2.3.1 Participants 35
2.3.2 Experimental procedure 35
2.3.3 Equipment 36
2.3.4 Manipulation of the gravitational context 36
2.3.5 Pendulum model 37
2.3.6 Data analysis 37
2.4 Results 39
2.5 Discussion 39

3 Do novel gravitational environments alter the grip force/load force coupling at the fingertips? 43
3.1 Abstract 43
3.2 Introduction 44
3.3 Methods 45
3.3.1 Subjects 45
3.3.2 Parabolic flights 46
3.3.3 Apparatus 46
3.3.4 Experimental procedure 47
3.3.5 Data processing 48
3.3.6 Inertial and gravitational components of the load 50
3.3.7 Statistical analysis 51
3.4 Results 51
3.4.1 Description of the task across gravitational fields 51
3.4.2 Cross Correlation analysis 53
3.4.3 Comparison between the levels of force 53
3.4.4 Adaptation to inertial and gravitational components of the load 56
3.4.5 Asymmetry in load and normal grip forces 56
3.5 Discussion 59
3.5.1 Arm and grip force controllers are decoupled 59
3.5.2 Interaction between gravity and inertia to predict GF . 61
3.5.3 Asymmetrical GF and LF are pre-programmed 62

4 The grip force controller differentiates the inertial and gravitational components of the load 65
4.1 Abstract 65
4.2 Introduction 66
4.3 Methods 68
4.3.1 Subjects 68

4.3.2 Equipment . . . 68
4.3.3 Experimental procedure . . . 69
4.3.4 Data analysis . . . 70
4.4 Results . . . 71
4.4.1 Typical trials . . . 71
4.4.2 Global effects of acceleration and mass . . . 71
4.4.3 Grip force control in a given range of load force . . . 72
4.4.4 Model prediction . . . 75
4.5 Discussion . . . 75
4.5.1 Global adjustments of the grip-load force coupling . . . 76
4.5.2 Inertial and gravitational forces are independent in the CNS . . . 77

5 Grip-load force coupling and gaze-hand coordination in high impact loads 79
5.1 Abstract . . . 79
5.2 Introduction . . . 80
5.3 Methods . . . 81
5.3.1 Equipment . . . 81
5.3.2 Experimental procedure . . . 82
5.3.3 Data processing . . . 84
5.3.4 Inertial and gravitational components of the load . . . 85
5.4 Results . . . 85
5.4.1 Transport and collision phases . . . 86
5.4.2 Grip force maximum is pre-programmed . . . 89
5.4.3 Gaze and hand coupling in the transport phase . . . 90
5.4.4 Target fixation strategy is direction-dependent . . . 92
5.5 Discussion . . . 93
5.5.1 Grip force/load force coupling in a collision task . . . 94
5.5.2 Gaze strategy in transport and collision phases . . . 95
5.6 Appendix . . . 97

6 Predictive grip for high impact loads in altered gravity 99
6.1 Abstract . . . 99
6.2 Introduction . . . 100
6.3 Methods . . . 101
6.3.1 Manipulation of gravitational context . . . 101
6.3.2 Experimental procedure and equipment . . . 102
6.3.3 Data processing . . . 103

6.3.4 Inertial and gravitational components of the load 104
6.4 Results 104
6.4.1 Grip force strategy in transport and collision phases . . 105
6.4.2 Microgravity dissociates transport and collision phases . 108
6.4.3 Pre-programming of grip force 109
6.4.4 Gaze saccades onsets are time-locked to peak hand acceleration 110
6.5 Discussion 112
6.5.1 Microgravity highlights a switch from transport to collision modes 113
6.5.2 A conceptual internal model of eye-hand coordination during a collision task 114

7 Conclusions and perspectives 117
7.1 Main findings 117
7.2 Future prospects 121
7.2.1 Rhythmic movements 121
7.2.2 Discrete movements 123

A Experimental equipment 125
A.1 Objectives 125
A.2 Mechanical design: the manipulandum 125
A.2.1 Abstract 125
A.2.2 Introduction 126
A.2.3 Methods 127
A.2.3.1 Instrumented device 127
A.2.3.2 Signal processing 127
A.2.3.3 Data acquisition 129
A.2.3.4 Experimental procedure 129
A.2.4 Results 131
A.2.5 Discussion and conclusion 132
A.3 Implementation 133
A.3.1 Hardware 133
A.3.2 Software 135
A.3.3 Parabolic flights logistics and mechanics 140
A.3.3.1 Campaign organization 140
A.3.3.2 Parabolic flight manœvre 141
A.4 Future improvements 143

B A model of the upper limb **145**
B.1 Problem statement 145
B.2 Resolution with Lagrange's equations 145
B.2.1 Kinematics 147
B.2.2 Dynamics 147
B.2.2.1 Forces due to gravity 148
B.2.2.2 Moments of inertia 148
B.2.3 Kinetic energy 149
B.2.4 Lagrangian formulation 150
B.2.4.1 Left hand side: kinetic energy 150
B.2.4.2 Right hand side: generalized forces 151
B.3 The equations of motion 151
B.4 Finding the normal modes 151
B.4.1 Assumption of small oscillations 151
B.5 Resolution of the equations 153
B.5.1 Reduction of the system 153
B.5.2 Simulations 154
B.6 The spherical pendulum 156

References **159**

List of figures **176**

List of tables **178**

Index **179**

Chapter 1

Introduction

> If you want to inspire confidence, give plenty of statistics. It does not matter that they should be accurate, or even intelligible, as long as there is enough of them.
>
> Lewis Carroll

1.1 Background

On a sunny afternoon, you have invited some of your friends to a barbecue. You are standing next to a table on which two orange juice cans are placed among a variety of salads and empty glasses. Your wife asks you to serve your guests with some juice. You turn your hand toward one of the two similar boxes in order to grasp it. Surprisingly, your hand moves jerky upwards with the can compressed within your fingers. You realize that the box is empty. Then, you reorient your reaching movement toward the second can. When you try to lift the object, your fingers slip on its damp surface. Reactively, you strengthen your grasp to lift the can, and start shaking to enhance the flavor. Finally, you open the container and carefully pour the juice in the first glass.

This scenario illustrates the complexity of a simple task we perform every day that is controlled by the brain. In order to be successful in such common activities, the brain must coordinate a set of computational processes that generates and controls behaviour, *i.e.* the sequence of actions that a control system produces. Actions result from actuators, like hands, that exert influence on the world, by altering its state. Output from computational processes in the brain causes actuators to generate forces that move arms, legs, hands and eyes. In addition, the brain has also the task to coordinate all these actuators in time and space to accomplish goals, *i.e.* a desired state of the world that behaviour is designed to achieve or maintain. In order to reach the main goal, one must decompose its objective in sub-goals, which in turn, will be detailed in lower level, shorter time scale sub-goals. At each level of decomposition, a goal from a higher level causes behaviour consisting of actions designed to achieve lower level goals, like a recursive process. Eventually, at the lowest level, neural impulses are delivered to muscles that act on the world. Elementary movements developped by plans may consist of activities such as reaching and grasping and usually last a few seconds. They must be further decomposed by brain structures into sequences of desired limb motions (sub-goals) lasting a few hundreds milliseconds. Desired trajectories of limbs and fingers (aiming to the juice can) are further decomposed into sequences of desired forces, velocities and positions of muscles lasting a few tens of milliseconds (apply appropriate grasping force). These are finally transformed into trains of impulses to muscles that last a few milliseconds. Stelmach (1982) described behaviour as a hierarchical model where the upper levels of the nervous system provide the fundamental ideas for the output, and where lower levels fill in the details along the messages paths.

However, in essence, the world is uncertain: unexpected events may occur, like the action of gusty wind on a tennis ball. Consequently, mistakes in the motor program can be generated because the plans are not adequate anymore. Hopefully, there is also a sensory processing hierarchy that runs parallel to this behavioural structure to operate on signals from biological sensors monitoring the world (otoliths, skin mechanoreceptors, muscle spindles, vision, etc.). At each level, feedback from sensory processing is integrated with commands from higher levels to modify behaviour so as to successfully accomplish high level goals, despite unforeseen events in the world. For most levels of behaviour, the interaction between goals and feedback occurs naturally, without conscious thought or apparent effort. The secret of generating complex sensory-interactive goal-directed behaviour lies in structuring computational modules into a hierarchical architecture such that each level decomposes its task into more details and about an order of magnitude shorter before passing it to the level below. This concept is commonly used in the Computer Science community as an efficient algorithm design paradigm and is named “Divide and Conquer”.

In this work, we investigate how the brain controls very simple manipulation tasks, when fundamental parameters of the environment are altered. More specifically, we designed a set of experiments to further understand how a priori knowledge of the world and sensory information - mainly provided by vision, proprioception and tactile afferents - interact in computational brain structures to accomplish motor actions.

1.2 Control theory

Once a goal - a desired state - has been chosen by the brain, some internal mechanisms must compute a *reference trajectory*, or a series of states along a time line. The transition between each state is ensured by actions. A *state* is a set of dynamic properties of a system at a point in time (position, momentum, energy, ...). An *action* is the output of an actuator that causes motion, exerts force or transmits energy. System control theory provides a framework to design processes that achieve this goal (Grodins, 1963). In that context, the model of a system can be considered as a box with inputs and outputs (Fig. 1.1 A). An action applied at the input causes some resulting state at the output. Many other factors like internal dynamics of the system, disturbances, interaction with other systems enter in the game to predict the right output. Disturbances are commonly represented as a noise (unpredictable) input. A system model is usually described by a set of differential equations that predict how this system will respond to a given input. The general form of a system model is:

$$\frac{dx}{dt} = f(x, u, \eta) \tag{1.1}$$

where f is a function that defines how the system state x changes over time in response to both its internal dynamics and the input control actions u. A noise factor η is introduced to account for events that occur in the system that are not represented accurately in the function f. Dually, the inverse system model predicts the required action for a desired state (Fig. 1.1 B).

There are two basic approaches to control system design: feedback and feedforward. Feedback compares the state of the system with the desired goal state and triggers actions to reduce the difference between desired and actual states. Feedforward uses a model of the system to predict what actions are required to achieve the desired goal. These two model structures are described in the following sections.

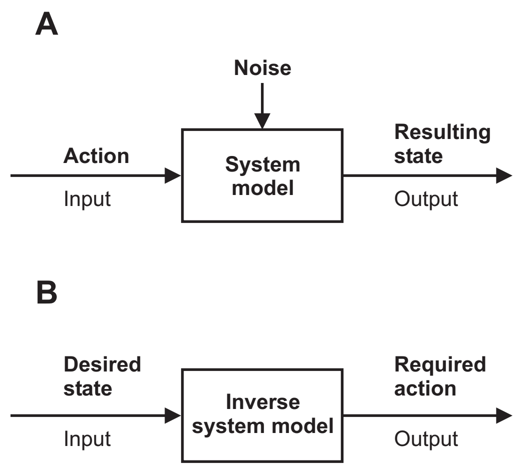

Figure 1.1: (A) Action applied to the system results in a state. (B) A desired state applied to an inverse system model computes the action required to achieve that desired state.

1.2.1 Feedback control

A feedback control produces reactive behaviour to sensory information with actions designed to reduce errors between observed and desired states. The strategy of feedback control is (Fig. 1.2):

1. Monitor the system.
2. Process the sensed data $y(t)$ to estimate the state of the system $x^*(t)$.
3. Compare the estimated state $x^*(t)$ with the desired state $x_d(t)$ and compute an error between both states.
4. Compute the feedback compensation required to reduce the error.
5. Output the command $u(t)$ to the actuators and go back to (1).

1.2.2 Feedforward control

Whereas feedback is reactive, feedforward control produces anticipatory behaviour by using an inverse model of the world to predict what actions are required to achieve the goal state. Assuming that a model of the world as described in Figure 1.1 A is available, the feedforward strategy is (Figure 1.3):

1. Invert the world model.

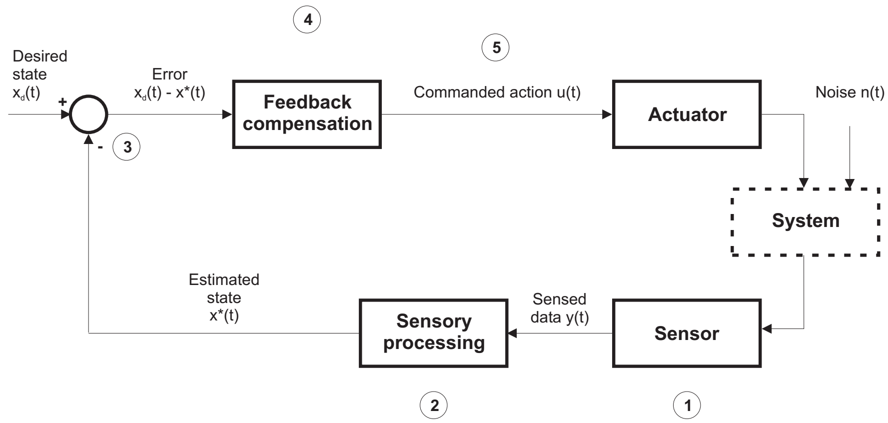

Figure 1.2: A feedback control system processes sensory information to adjust its actions.

2. Input the desired state to the inverse model and compute the required control action.

3. Output the control action to the actuator as a feedforward command and go to step (1).

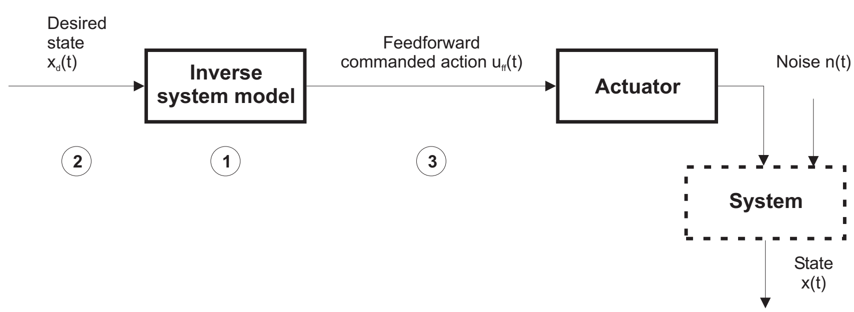

Figure 1.3: A feedforward control system predicts a required action to reach a specific state.

Intrinsically, feedforward control has an advantage over feedback control in that it anticipates the future and takes actions before errors have time to grow up. However, some important issues must be considered. First, the world can never be modeled exactly, leading to imprecise computed inverse world models. As a consequence, the required control action will never be calculated exactly. Perhaps even greater problems are associated with inverting the world model itself, to implement a controller. For instance, systems may have redundant degrees of freedom like the human body: it is possible to reach the same glass by combining forces and torques on limbs and joints an infinite different number of ways (Bernstein, 1967; Lashley, 1930). Attempts to circumvent the need to explicitly invert the world model have led to a variety of techniques that generate inverse models implicitly (neural networks, fuzzy logics, etc.). Interestingly, drawbacks present in one approach can successfully be bypassed by advantages of the other, and vice-versa.

1.2.3 Hybrid feedforward/feedback control

Combining feedback and feedforward architectures together allows to take benefit of both approaches. First, feedback control can compensate for errors. It is therefore relatively insensitive to the accuracy of the system model. Importantly, there is always some form of delays in a control feedback loop. For example, there are physical and computational delays. Physical delays may be the time between an action is commanded to the system and when a change occurs or simply inherent to the sensors. Computational delays reflect the amount of processing required in the loop to calculate the commanded action from the sensed data. The sum of all these delays can be modeled as a single delay Δt. To avoid instabilities when delays are not negligible, predictive filtering that anticipates future state of the system can be envisaged. However, feedback compensation can only take place after an error has been detected, which, in some situations, can be too late. On the other hand, the strength of feedforward systems is that it can anticipate what control action will be needed for the system to move toward the goal without waiting for feedback. Of course, if the inverse model is incomplete, incorrect or out-of-date, the feedforward control may not produce the adequate action.

For illustrative purpose, let us formalize the processes that take place in the brain when transporting the juice carton initially held, from one point to a target position in space (Fig. 1.5). First, a desired hand trajectory (1) is sent to an inverse model of the arm (a controller) that issues a motor command (2). It is essential to safely keep the object within the grasp and, the prehension force has to be tuned in real-time during the ongoing movement. Therefore, an efference copy of the arm motor command is provided to a forward model (3) that predicts an arm trajectory (4). Given that predicted arm trajectory, the constraints induced by the acceleration of the object at the end-effector can be calculated, and the required grasping force can be anticipated (5). Sensory inflows (6) coming from vision and skin mechanoreceptors for instance, are pro-

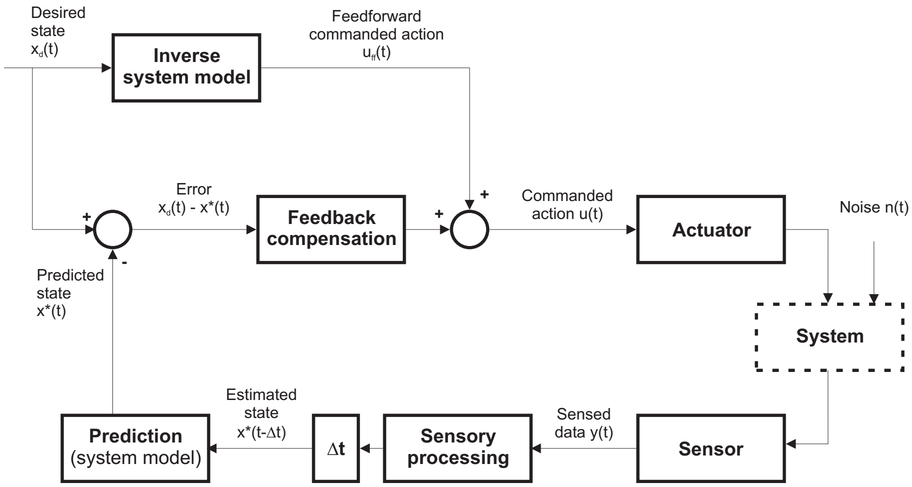

Figure 1.4: Delays inherent to feedback control and inaccuracies in direct and inverse world models can be compensated for by using a combined approach.

cessed, to predict after some delay the estimated final state (7). By comparing the desired and estimated states, an error signal can be issued to correct the movement and update the various models (8).

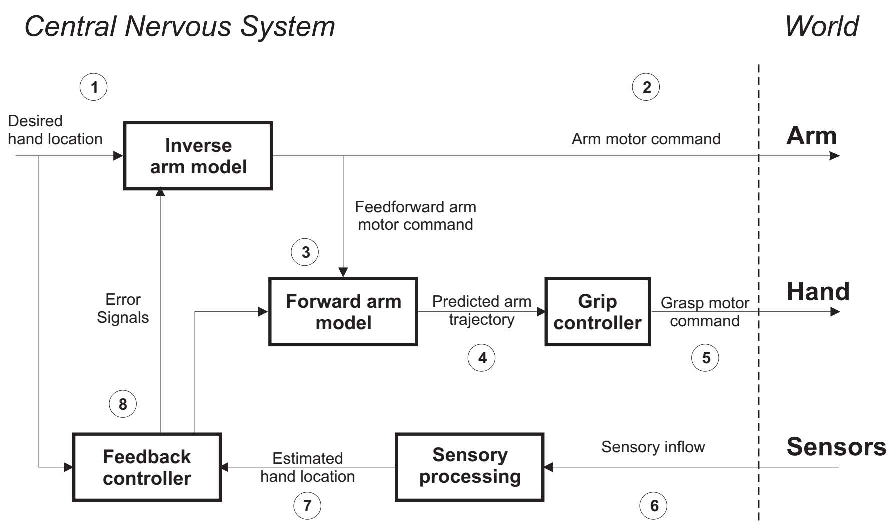

Figure 1.5: Illustration of feedback and feedforward approaches with the introductory example.

By collaborating, feedback and feedforward controls can achieve the best features of both. Feedforward anticipates what actions will be necessary to produce the desired results. Feedback corrects for errors caused by noise or inaccuracies in the inverse model.

1.2.4 Motor planning

In order to generate anticipatory actions leading to long-term goals in the distant future, planning is also required. This process must select the best trajectory through the state space that minimizes some cost function (*e.g.* energy expenditure) and respect some other criteria (*e.g.* anatomical constraints). This process can be done offline: a precomputed set of actions can be loaded when necessary. Feedforward and planning are closely related in the sense that both controls accept a desired state and generate a series of actions to achieve the final goal. However, while feedforward modules predict one action at a time, the planner initializes a series of pairs of desired results associated with planned actions. To be complete, the planning module must be appended upstream from the hybrid feedback-feedforward architecture. The accomplishment of a desired goal in the future $(t+T)$ requires the planner to hypothesize a set of required actions and evaluate the resulting consequences, through a system model, also taking into account constraints and a cost function. When the task is initiated, the plan outputs at each step the desired state $x_d(t)$ and the associated feedforward command $u_{ff}(t)$ (Figure 1.6).

In a dynamic unpredictable environment, the state of the system may change at any time. Consequently, the series of planned actions could not be adapted anymore to the current situation and replanning must be invoked. However, very rapid perturbations occur frequently in a system. For that reason, a new computation of the whole planning process could be too expensive. Hopefully, feedbacks from sensors can modify planned actions in shorter time windows, making possible to achieve the goal even if the world model used in planning was imprecise or became obsolete. A trade-off can be made between frequent replanning and feedback compensation. On the one hand, replanning requires updating the system model, generating a set of hypothesized plans, evaluating each hypothesis and selecting the best. On the other hand, feedback compensation only computes an error between desired and predicted states, and thus, requires less computation. Actually, during the interval required for replanning, several feedback cycles can be executed to provide high bandwidth response to unexpected events.

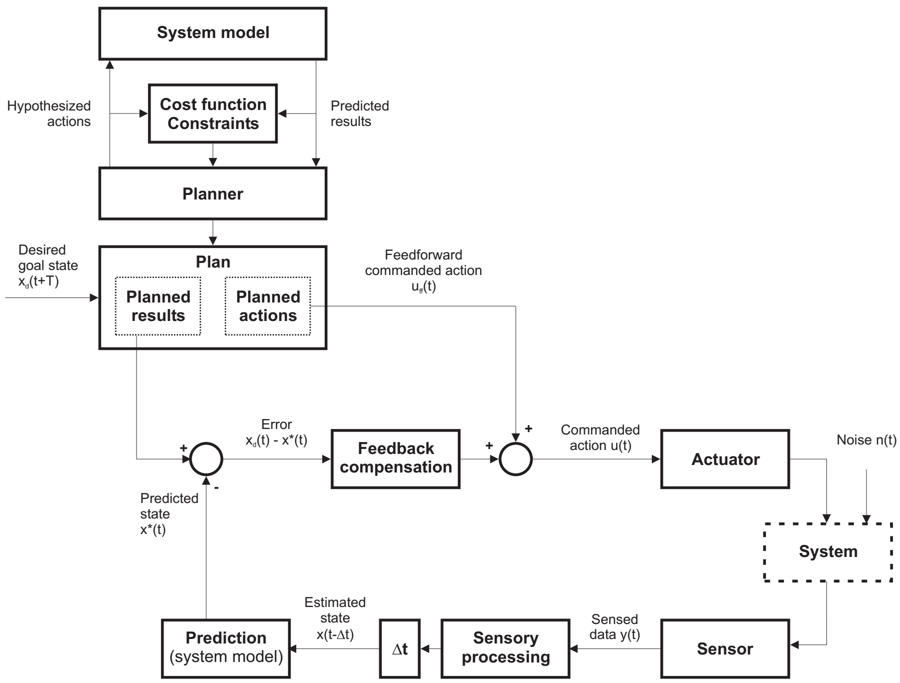

Figure 1.6: Planning module loads a pair of planned actions required to achieve planned results. This process can be performed offline; only the transitions between states are done online.

In the next section, we jump from theoretical concepts presented here to experimental evidences that similar control processes - called ***internal models*** - are utilized by the brain to control all our movements. In this light, the main objective of the present work was to further understand how the central nervous system (CNS) controls these internal models when deep alterations of the environment biases both planning process and biological sensors. We focused on a restricted set of tasks but which are fundamental in everyday life: dexterous manipulations.

1.3 Experimental evidence of internal models

Interactions with our close environment most probably passes through dexterous object manipulation and more generally, through hand actions, with the assistance of eye movements. Back to the introductory example, the brain has to compute an optimal trajectory to reach the juice can. Many steps are required from planning to final adjustments through potential corrections. First, the brain has to solve computational issues related to planning. Given the goal - to reach and grasp the object - the appropriate arm and hand movements have to be selected among an infinite number of possible combinations (Bernstein, 1967; Jordan and Wolpert, 1999). In this step, past experiences as well as visual and haptic information about the object must be taken into account to adjust the optimal grasping force. Indeed, in order to move a hand-held object without dropping it, one must apply sufficient normal force, called *grip force* (GF), to counteract the destabilizing tangential forces, called *load forces* (LF), through the action of friction. While the LF clearly depends on physical parameters like gravity, mass and the acceleration induced to the object, an adequate GF is more complicated to estimate. In the planning process, the brain must have an estimation of LF (Flanagan and Wing, 1993, 1995; Johansson and Westling, 1984) but also of friction between the fingers and the object. Moreover, two equivalent objects in term of mass will not be lifted with the same GF if their shapes are different (Gordon et al., 1993). load force Then, each intended action to accomplish the goal will have a consequence in term of predictive state. Once the planner has initialized this series of couples, typically during the reaction time period (Dubrowski et al., 2000), movement can actually start.

While all happened very well until contact occurred between the hand and the box, a wrong prediction about the state of the juice can led to errors in GF. Indeed, our individual had previously lifted similar objects many times and pre-programmed a GF that was not adapted for an empty can. Sensory feedback could be used to correct for the errors caused by this inappropriate motor command by evaluating the discrepancy between desired and actual states. Then, a complete replanning had to be initialized to grasp the other carton, taking into account a different initial configuration of the upper limb. This time, a correct LF was predicted but more condensation than expected on the box led to a wrong evaluation of fingers/object friction. Because of sensorimotor delays inherent to the feedback loop (about 60 ms), inaccuracies arose through slips of the object at the fingertips, while skin mechanoreceptors informed the Central Nervous System (CNS) that a problem occurred. These signals generated a reflex response in GF in a time window sufficiently short to reestablish a stable grasp (Johansson and Westling, 1984, 1987, 1988; Johansson et al., 1992a,b).

1.3.1 Planning

It is self evident that planning a goal-directed arm movement requires knowledge both about the location to reach and about the state of the motor apparatus, prior to movement onset. First, reaching at a visual target requires transformation of visual information about target position with respect to the line of sight, into a reference frame suitable for the planning of hand movement (*i.e.* body-centred). This problem is classically decomposed in steps that respectively provide target position information in an eye, head, and ultimately body frame of reference (Desmurget et al., 1998; Soechting and Flanders, 1992).

The first information corresponds to the angle separating the target and the line of sight. The reliability of this retinal signal is constrained by the spatial anisotropy of the retina and visual system. Indeed, because of the gradient of visual acuity, the encoding of a target location with respect to the line of sight degrades when the stimulus falls in the peripheral visual field (Westheimer, 1984). Despite this limitation, which characterizes signals related to the position of gaze as well, it is the peripheral part of the retina which is most often involved in the initial localization of a visual target (Biguer et al., 1982). Moreover, it was also shown that accurate encoding of target location requires extraretinal signals as well, which may appear paradoxical as the foveal signals define a null information from an analytical point of view. Actually, this paradox may be explained by the fact that retinal and extraretinal signals do not simply add but also interact with each other (Blouin et al., 1995; Prablanc et al., 1986). In addition to the knowledge about eye position, the transformation of retinal signals into a body-centred representation must also incorporate head position. It is known that proprioceptive input is essential in providing head-to-trunk information (Cohen, 1961; de Jong et al., 1977).

The second information - state of the motor apparatus - must also be available to the nervous system in order to plan a goal-directed hand movement. Implication of information about the initial hand configuration in motor programming is demonstrated by studies manipulating the information available prior to movement onset (Rossetti et al., 1995) and in deafferented patients (Ghez et al., 1995).

Altogether, the elimination or the alteration of visual and sensory information about the limb prior to movement clearly affects pointing accuracy, providing converging evidence that defining the state of the effector prior to motion is a necessary step of movement planning.

It is well agreed that despite the infinite number of possible trajectories that arm and hand could follow to reach a target, humans show highly stereotyped movements (Jordan and Wolpert, 1999). For instance, despite variations in movement directions, speed and location, the hand trajectories tend to follow roughly a straight line in space and present a bell-shaped velocity profile (Flash and Hogan, 1985; Morasso, 1981). However, the mechanisms that allow the planner to select the most reliable trajectories are still under debate. The main hypothesis is that rather than describing the kinematics of a movement directly, the behaviours result from the evaluation of a cost function penelizing some task parameters. The appropriate trajectory is the one that minimizes the cost function. Many possible cost functions have been examined for point-to-point movements (Nelson, 1983). They can be classified according to the criteria underlying their definition, either kinematic or dynamic. For example, it has been proposed that the squared jerk (third position derivative) is minimized over the movement (Flash and Hogan, 1985; Hogan, 1984). If $x(t)$ denotes position over time, the kinematic-based cost function is:

$$J = \int_0^T \left(\frac{d^3x}{dt^3} \right)^2 dt \tag{1.2}$$

where T is the duration of the movement. Intuitively, this corresponds to maximize smoothness by penalizing high derivatives. Lacquaniti et al. (1983) observed a relationship between path curvature and hand angular velocity during drawing and scribbling. This was generalized as the two-thirds power law (Viviani and Flash, 1995; Viviani and Schneider, 1991). Subsequently, it has been shown that this power law was a particular case of minimum jerk and could be a by-product of the limb's damping properties (Schaal and Sternad, 2001). On the other hand, dynamic based cost functions depend on the dynamics of the arm. The proposed models include a cost function like torque change, muscle tension or motor command (Nakano et al., 1999; Uno et al., 1989). There is a critical difference between the two classes of models. Since the specification of a movement in kinematic models involve the specification of positions and velocities of the arm over time, an additional process is required to compute the appropriate motor commands in the brain. In contrast, dynamic-based models compute more direct solutions in term of motor commands, although it is unlikely that a torque derivative is internally represented as is.

Interestingly, Harris and Wolpert (1998) proposed a new approach to bypass limitations present both in kinematic and dynamic models: the minimum variance theory of motor planning. The authors proposed that minimizing the variability of the arm's position in presence of biological noise is the underlying determinant of trajectory planning. On the one hand, noise is integrated over the movement duration, leading to final errors. On the other hand, the amplitude of noise in the neural control signal is proportional to the mean level of the signal. Therefore a signal-dependent noise inherently imposes a trade-off between movement duration and terminal accuracy: the longer the movement and the stronger the signals required to drive the arm, the noisier the control signal. Harris and Wolpert (1998) suggested that the feedforward sequence of neural commands are selected so as to minimize the final positional variance while keeping the duration to the minimum compatible with the accuracy constraints of a particular path. This approach has several advantages. First, this theory for arm movements also generalizes to rapid eye movements (saccades). Second, after adaptation of the motor system, profiles are insensitive to a change of dynamic parameters: the initial bell-shaped velocity profile can be recovered (Goodbody and Wolpert, 1999; Lackner and Dizio, 1998; Sainburg et al., 1995; Shadmehr and Mussa-Ivaldi, 1994). Third, it provides more a direct cost function, and avoid the need for the CNS to compute complex signals. Lastly, smoothness becomes a consequence of an optimal trajectory since an abrupt change of position would require a large driving force and hence, errors.

A common behavioural characteristic of many species including humans is the ability to generate rhythmic motor patterns of activities, which are ubiquitous in nature. Some rhythmic activities, like locomotion, are energy-greedy and are sensitive to dynamic constraints induced by the environment. If walking is viewed as a force-driven harmonic oscillator, it requires a periodic forcing actuation to sustain its oscillations against gravitational, damping and stiffness forces which tend to diminish the oscillations. In such systems, a particular frequency - the resonant frequency - is critical: it requires the minimum force to maintain the oscillations and hence, the minimal muscle activity. For instance, Wagenaar and van Emmerik (2000) showed that the preferred movement frequency of the arms can be predicted by the resonant frequency of the arm. When interacting with the environment, the preferred oscillatory movements are not simply dictated by the central nervous system but are constrained by the dynamics of the system as well (Hatsopoulos and Warren Jr, 1996; Kugler and Turvey, 1987). Hatsopoulos and Warren Jr (1996) asked subjects to oscillate their forearms in the vertical plane at their preferred frequency under conditions of added mass and external spring loading. The results showed that the preferred frequency matched the resonant frequency of the muscle-limb system under each condition. In addition, whereas the internal joint stiffness was modulated so that it corresponded to the impedance of the external springs, it was unaffected by added mass. These observations are consistent with an autonomous oscillator model that incorporates information about the dynamics of the periphery. oscillators

Interestingly, a physiologically plausible link has been demonstrated between macroscopic rhythmic movements and some specific neural networks at the spinal level called Central Pattern Generators (CPG) (Marder and Calabrese, 1996). The most fundamental CPG consists of two groups of neurons with mutual inhibitory connections (Brown, 1911) that generate antiphase oscillations in their electrical activity, which alternately drive a pair of antagonist muscular groups, to induce periodic motion. There is growing evidence that CPG provide motor commands required for rhythmic activities in both invertebrates and vertebrates (Delcomyn, 1980), including humans (Zehr et al., 2004). Hence, frequency may be a critical parameter to predict efficient rhythmic movements of biological systems obeying the biophysical laws governing oscillations (Holt, 1990).

1.3.2 Feedback control

The existence of feedback is obvious in a daily context. For instance, when we experience a first contact with a new object, we adopt a probing strategy to allow a stronger weighting on information that come from skin mechanoreceptors (Johansson and Westling, 1987). Without feedback mechanisms, we would have been had to internalize a perfect model of the world, which is unfeasible given all its uncertainties.

Many real-world tasks involve moving one or both hands to targets in the environment. Once the target is reached, we may choose to perform a number of actions (touch, grasp, pinch, etc.) but the most basic task involves vision to move the limb to a target.

A classical view of reaching movements consists of two phases: a fast initial phase that is primarily ballistic, and a slower adjustment phase under the guidance of sensory feedback (Jeannerod, 1988). Two basic observations, one computational and one empirical, seem to lend support to this view. First, the minimum delay needed for sensory information to affect the physical movement of the hand (approximately 80-100 ms) would seem to render feedback useless for the short duration reaching movements, which are on the order of 350-750 ms. Second, the fast and slow phases appear clearly in the transport kinematics of the hand, which show an initial bell-shaped velocity profile followed by an extended tail in the final phase of movements, when the hand is near the target, often with a number of re-accelerations.

The role of feedback in the slow phase of the movements is clearly demonstrated. For over a century, researchers have been interested in the central processing that must occur as part of movement planning and how much of this processing occurs on-line (Woodworth, 1899). In other words, how much of movement is open-loop control and how much feedback is used to carry out the movement in closed-loop control (See Starkes et al. (2002) for a review)? A frequently used paradigm consists in comparing terminal accuracy of goal-directed arm movements performed with different types of visual feedback (*e.g.* no feedback, feedback during either the first or last portion of the trajectory, feedback during entire trajectory). Using such a paradigm, a number of studies reported that directional accuracy of rapid arm movements was greater when the hand could only be seen early in the trajectory than when visual feedback was not available (Abahnini and Proteau, 1999; Blouin et al., 1993). Authors of these studies concluded that visual feedback of the moving limb can be processed online and rapidly to optimise directional accuracy (Saunders and Knill, 2003).

In real movement however, vision is often assisted by other source of information like proprioceptive sensory information coming from receptors in the muscles, skin, and joints. These multiple sources are combined to provide a single optimal estimate of the quantity. For example, we can both see and feel

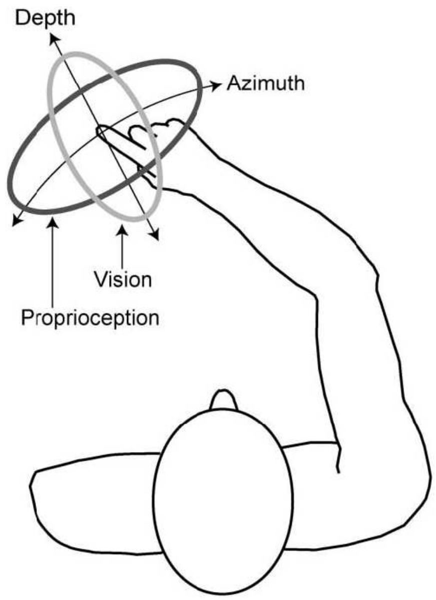

Figure 1.7: Direction-dependent precision of visual and proprioceptive localization.

where our hands are, and this information is integrated to generate a single estimate of where the hand is in space. An interesting study (van Beers et al., 2002) demonstrated that the relative weighting of visual and proprioceptive information depend upon the direction of movement: in the depth direction, the estimate of hand position relied more on proprioception than on vision, while the reverse is true for the azimuthal direction (Fig. 1.7). This suggests that a larger reliance on proprioception is actually very common in everyday life.

1.3.3 Forward models

When the environment exhibits stable dynamic properties, predictive control mechanisms can be exploited. The main advantage of feedforward control lies in the fact that it can anticipate the required control without waiting for feedback information. This implies the existence of efference copies and forward models in the brain. However, the use of forward models is less easy to demonstrate than feedback control. The development of virtual reality and closed-loop experimental set-ups coupled with psychophysical, electrophysiological and imagery techniques have considerably strengthened evidence of such predictive models in humans. In addition, for many years, the animal literature has also reported clear evidence of the involvement of the cerebellum in forward models. In the next section, we review important experiments that demonstrate different kinds of forward models. forward model

The anticipatory adjustments of grip force (GF) with load during object manipulation has been extensively investigated to provide evidence of predictive forward models (Davidson and Wolpert, 2004; Flanagan and Wing, 1997; Johansson and Cole, 1994; Kawato, 1999). For instance, when the load at the fingertips periodically varies according to a self-generated action such as shaking the juice carton, GF increases and decreases in parallel with load force (LF) with no delay (Flanagan and Wing, 1995) (Fig. 1.8). Sensory detection (about 80 ms) of the load is too slow to account for this increased GF, which therefore relies on predictive processes.

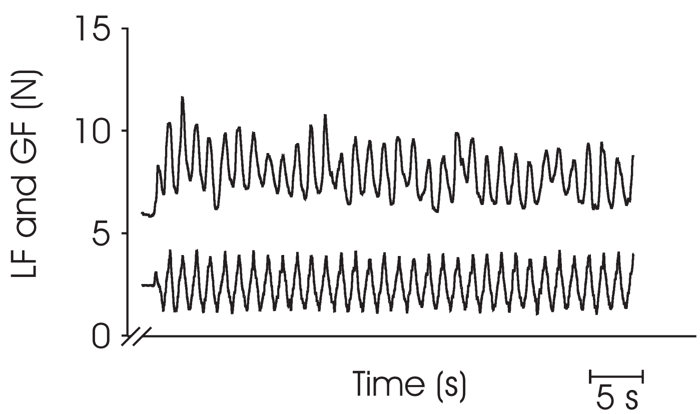

Figure 1.8: Modulation of grip force (upper trace) with load force (lower trace) in vertical rhythmic movements. Adapted from Witney et al. (2004).

Forward models must also be adapted to follow changes in the environments. These updates are mainly possible through feedbacks. Interestingly, deafferented patients lack feedback and are therefore unable to rely on error signals to learn and maintain a forward model for a novel object. Nowak et al. (2004a) asked such a patient to make point-to-point reaching movements with a hand-held object. The authors showed that the GF profile was not predictive anymore, which is consistent with an inability to predict the LF.

Interestingly, neurophysiological studies suggest that forward models of object and arm dynamics are stored in the cerebellum (Kawato et al., 2003). Single-cell recordings in monkeys suggest that the cerebellum plays an important role in predictive motion planning (Dugas and Smith, 1992; Espinoza and Smith, 1990; Smith, 1990). More specifically, an anticipatory discharge of Purkinje cells has been shown to parallel a preparatory grip force increase that preceded the onset of predictable load perturbations. This preparatory activation developed during the first trials and started earlier as a function of practice (Dugas and Smith, 1992; Smith, 1996). single-cell

1.3.3.1 Arm dynamic models

It is agreed that internal models of arm dynamics play a critical role in many movements like reaching (Atkeson, 1989; Shadmehr and Mussa-Ivaldi, 1994), or catching (McIntyre et al., 2001a; Zago and Lacquaniti, 2005). However, many parts of our body are coordinated to achieve a common goal. Hence, specific behaviours of say eyes, posture and grip force must have access to a forward model of the arm dynamics in order to predict consequences of coordinated actions on the environment.

Recordings of the muscular activities constitute a good indication of motor commands sent to the arm. Gribble et al. (2002) showed that, prior to movement onset, the EMG activity during fast point-to-point arm movements reflected the subsequent amplitude. This result indicates that inertial properties of the upper limb are taken into account before any possible return of feedback information. Similarly, Flanagan and Lolley (2001) have shown that when sliding an object across a friction-less surface to targets located in different locations, subjects varied the forces they applied normal to the surface in anticipation of direction dependent changes in initial hand accelerations. This means that forward models of the arm incorporate its anisotropy, so that subjects can move with an optimized muscular activity, without waiting for feedback. The brain selects and tunes the parameters of the adequate forward model during the planning stage of the task.

There is also evidence that the saccadic eye movement system has access to a forward model of arm dynamics (Lazzari et al., 1997; Vercher et al., 1997). When participants were asked to track their unseen arm position, they executed saccades to a location that predicted the position of their hand 196 ms in the future (Ariff et al., 2002). Even when the arm's dynamic was altered by applying various force fields, the eyes learned to make accurate predictive saccades when the externally imposed arm dynamics was eventually predictable

(Nanayakkara and Shadmehr, 2003).

The above studies suggest that at least the grip force control system and vision both have access to an adaptable internal model of arm dynamics. However, at this time, it is not clear whether this reflects a global access to a common module or multiple representations within each motor system (Davidson et al., 2005).

1.3.3.2 Object dynamic models

Beside reliable internal representations of our body segments, our brain must also contain information about controlled systems in order to be successful in interactions with the external world. Indeed, we do not manipulate an orange and an egg with the same caution. When lifting an object initially stationary, we rapidly learn to adjust GF to overcome the LF that depends both on the object's weight and on the combined effect of the acceleration and mass (Johansson and Westling, 1988). Moreover, when transporting an object, Saels et al. (1999) showed that subjects also take into account the friction at the grasp interface to control the movement as reflected in the subsequent acceleration. However, the parallel coordination between GF and LF is not innate but results from a long learning process that lasts around three years, as was evaluated in children (Forssberg et al., 1991). Then, a memory of appropriate force scaling is maintained and can be recalled later based on visual cues (Gordon et al., 1991, 1992, 1993). This memory is highly flexible: it generalizes between hands (Gordon et al., 1994) and takes advantage of previous trials with separate objects to tune the GF with the combined object (Davidson and Wolpert, 2004; Haruno et al., 2001).

Given that flexibility, it might be expected that explicit knowledge of a simple change in object dynamics could be used to update the internal model. Nowak and Hermsdorfer (2003) addressed this issue by asking subjects (1) to lift a cup full of water with a precision grip, (2) to drink half its content with a straw and (3) to lift the cup again. The maximum grip force rate provides a reliable estimate of the anticipated weight. It was surprising that, despite possessing explicit knowledge the cup was lighter after drinking, maximum grip force rate (green trace in Figure 1.9) did not reduce for the lighter cup and the object was accelerated (red trace in Figure 1.9) as if a heavier object, still full of water, was expected. In contrast, implicit knowledge of a relationship between two previously experienced objects can be used to form a new forward model (Davidson and Wolpert, 2004; Haruno et al., 2001).

There is also evidence that forward models of external complex tools are

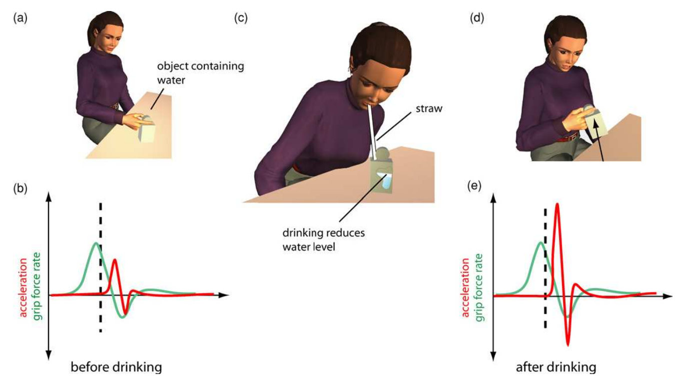

Figure 1.9: Prediction of GF is not adjusted even with explicit knowledge of a change in object properties. The GF rate before (b) and after drinking (e) did not change while acceleration was larger for the lighter glass.

used in arm control (Descoins et al., 2006; Dingwell et al., 2004; Mehta and Schaal, 2002). Previous experiments artificially manipulated different parameters like inertia, stiffness and damping of the arm (Dizio and Lackner, 1995; Flanagan et al., 2003; Shadmehr and Mussa-Ivaldi, 1994). After some adaptation, subjects regained their original smooth movements despite the perturbations. Such events constitute parametric change to the controlled system because they do not alter the fundamental structure of the arm (*e.g.* number of joints). Since the equations of motion remain unchanged excepted for values of some parameters, the same kinematics can be achieved by adjusting forces and torques. However, we often need to control motion of an object: we do not adopt the same kinematics when transporting an empty and a full glass of water. In that case, new state variables must be considered like position and velocity of the arm-object entity. Such tasks constitute deep, structural perturbations to the system: new equations must be defined and solved. Importantly, there is no direct muscle activation of the object itself: its motion can only be controlled indirectly through interactions with the dynamics of the object itself. Dingwell et al. (2004) showed that subjects were able to learn new kinematics that generalizes the minimum jerk principle (Flash and Hogan, 1985) by refining the mapping between the motor commands and the motion of the object, principally through visual sensory inflows.

1.3.3.3 Sensorimotor memory

Next to object-specific forward models, another source of information comes into the game. It has been shown that previous trials (*e.g.* object lift) also in-

fluence the current trial when visual cues are not reliable during sequential lifts (Jenmalm and Johansson, 1997) or when unpredictable viscous force fields are applied on the arm (Scheidt et al., 2001). The strongest weight was attributed to the most recent preceding trial and decayed rapidly (Witney et al., 2001). This effect has been termed "sensorimotor memory" and dominates object-specific memory in circumstances when the environment is less predictable.
This control mechanism is sometimes called a "look-up" table: it associates an output value to each visited state (Raibert, 1978). However, this becomes often practically unrealistic if we consider a broad class of movements. This is nicely illustrated by considering the following example (Wolpert and Ghahramani, 2000). If we consider the 600 or so muscles in the human body as being, for extreme simplicity, either contracted or relaxed, this leads to 2^{600} possible motor activations, which is more than the number of atoms in the universe. This clearly prohibits a simple look-up table from motor activations to sensory feedback and vice versa. However, it can be very efficient for specific behaviour. Taken together, these studies showed that according to the context, the adjustment of grip force can result from a forward model or a simpler, more volatile, sensory memory of past sensations (Nowak et al., 2004c; Quaney et al., 2003; Witney et al., 2001).

1.3.3.4 Learning

Internal models of object and arm dynamics are capable of adapting to unusual and even novel force profiles. This behaviour has been demonstrated by applying the following paradigm. Subjects are trained on a task in natural conditions (PRE). Then, they achieve the same task but when unpredictable changes in the dynamic properties of their arm or object occur (PER). Finally, participants are asked to carry on the trials but when the perturbations have been reset to normal (POST). For example, by using a robot to generate a force field acting on the hand, subjects initially showed trajectories that deviate from their normal paths and velocity profiles (Lackner and Dizio, 1994; Shadmehr and Mussa-Ivaldi, 1994). Then, they were able to adapt and move naturally in more or less time, depending on the task. This is interpreted as the adaptation of the parameters of the inverse model to take into account novel dynamics. Interestingly, the first trials in the POST condition showed a mirror effect, namely initial kinematic deviations in the other direction, which further demonstrates the acquisition of new predictive mechanisms.

Underlying mechanisms in the updating of internal models were addressed by many studies. Generalization experiments have investigated the structure of internal models. When subjects are trained for a particular task under altered dynamic environment, the question arises as to whether participants will be able to achieve this task in a different part of the workspace. If generalization was perfect, then new trajectories should be controlled perfectly from the beginning. In contrast, the performance of subjects experiencing the new environment in the different part of the workspace should be as poor as those with no prior training if generalization does not hold. Experimental data suggest an intermediate generalization level between a perfect inverse dynamic model of the system and a pure look-up table (Conditt et al., 1997; Ghahramani et al., 1996; Goodbody and Wolpert, 1998; Imamizu et al., 1995; Sainburg et al., 1995). Therefore, because a sole internal model with imperfect generalization capability cannot deal with a huge range of behavioural situations, the need for a modular approach has been proposed. In that framework, different modules compete for workspace memory during learning process especially for events closely related in time (Shadmehr and Brashers-Krug, 1997; Shadmehr and Holcomb, 1999).

Given the context, the appropriate module must be selected by the CNS. The Bayesian formalism has been proposed to estimate the probability of each context and compute a weighted combination of the most probable modules. According to Wolpert and Ghahramani (2000), the probability can be factored into the likelihood and the prior. The likelihood of a particular context quantifies the probability of the current sensory feedback, given that context. A forward model is then used to predict the sensory feedback from the movement. The discrepancy between the predicted and actual sensory feedbacks is inversely related to the likelihood. Wolpert and Kawato (1998) proposed a modular architecture in which multiple predictive models each tuned to a particular context, operate in parallel. This array of models acts as a set of hypothesis testers. The prior contains information about the structured way a context changes over time and how likely a context is before a movement. Bayes rules optimally combine the likelihood and the prior so as to generate a probability for each context (Davidson and Wolpert, 2004; Kording and Wolpert, 2004). Hence, multiple internal models can be regarded conceptually as motor primitives (building blocks) that are statistically combined according to their relevance.

1.4 Role of gravity in motor control

Catching a ball, playing tennis, moving an outstretched limb to reach an object, or simply manipulate an object are all activities influenced by the omnipresence of gravitational acceleration at the surface of the Earth. The ball will accelerate downwards and bounce with the same angle as the incident angle. Moving our arm vertically upwards requires more driving torque at the shoulder joint than downwards, especially when we hold a massive object. Therefore, when planning any action, our CNS must somehow have knowledge about gravity to optimize the control of our movements.

There is considerable evidence that the CNS takes advantage of gravity to plan optimal movements. Upward arm movements are more curved than downwards, between the same two points (Atkeson and Hollerbach, 1985). The CNS chooses different hand paths for the two directions. If gravity was a disturbing factor, rather than an explicit parameter in the internal model of trajectory planning, we would expect that performing point-to-point movements in microgravity would result in symmetric paths up and down. However, this directional difference persists in 0 g environment (Papaxanthis et al., 1998). This constitutes the first evidence that gravitational forces are integrated in the planning process. Other evidence of the importance of gravity in internal models comes from a mass discrimination experiment conducted in weightlessness. On the Earth, the weight of an object is strictly coupled to its mass. Therefore, an estimation of its mass can be performed in static condition, simply by holding the object. In microgravity, subjects poorly perceived masses of different objects that presented the same external features (size, shape) (Ross et al., 1984; Ross and Reschke, 1982; Ross et al., 1986). The authors concluded that internal models of mass and weight are indeed coupled in the brain.

Grip force modulation has also been studied in 0, 1 and 1.8 g (parabolic flights) to investigate whether people adjust their grasp according to novel gravity environments. While experienced participants presented linear GF-LF relationships from the very first exposure to each gravity level tested, several practice parabolas were needed for novice subjects to adjust their behaviour to the novel conditions (Augurelle et al., 2003) (Fig. 1.10).

There are however definite limits to this adaptation. For example, McIntyre et al. (2001b) have shown that predictive modules are tuned for the effect of gravity. When catching a ball falling vertically, people normally generate accurately timed anticipatory responses to intercept the object. In the 0 g environment, in contrast, anticipatory responses occurred too early, indicating

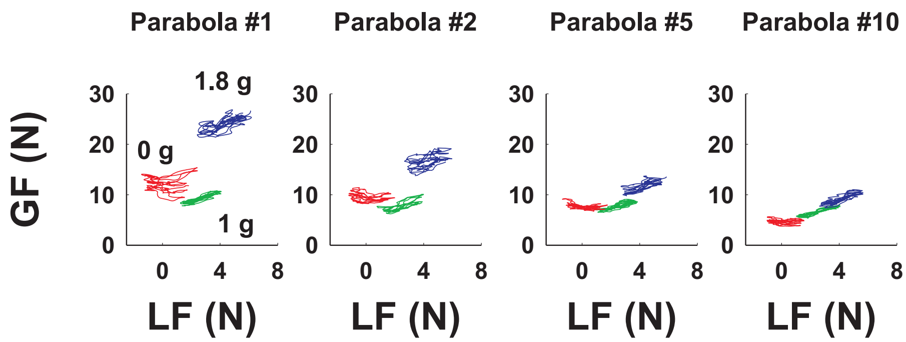

Figure 1.10: The GF-LF relationship measured during six cycles under three gravity levels in the first, second, fifth and tenth parabolas for a non-experienced subject. The GF progressively scaled with the LF in unknown gravity environments. Adapted from Augurelle et al. (2003).

that the CNS employs a second order internal model of gravity to estimate the time-to-contact which is inappropriate in a weightlessness environment (Fig. 1.11). As subjects spent more time in 0 g, the anticipatory responses slowly improved but never reached the performances achieved in 1 g, suggesting a heavy bias to terrestrial gravity. Interestingly, Indovina et al. (2005) showed that the internal model calculating the effects of gravity on seen objects is stored in the vestibular cortex and is activated by visual motion that appears to be coherent with natural gravity (g). In contrast, subjects relied more on visual motion areas to estimate time-to-contact when object acceleration was the same but opposite to that of gravity ($-g$).

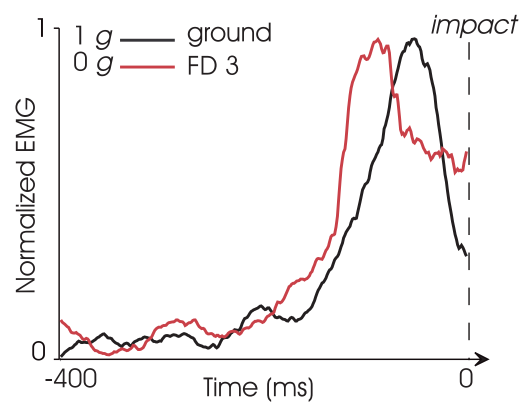

Figure 1.11: The effect of gravity is still internalized to synchronize a ball catching action in microgravity.

1.5 Parabolic flights manœuvres

Conditions of altered and particularly microgravity provides a unique method to decouple mass and weight in a manner that is completely novel to a novice subject. In 0 g, the arm and the manipulated object will have mass but no weight. Therefore, this provides a context to investigate working and adaptation of internal models where the usual relationships between variables are profoundly modified. Interestingly, the terrestrial environment allows simulation of various aspects of this approach. First, adding a mass on the object increases its inertia **and** its weight while removing gravity does not affect its inertial component:

$$F = mg + ma = m(g + a) \tag{1.3}$$

Indeed, in 0 g, the gravitational term disappears ($mg = 0$) and the residual force exerted by an object on the fingertips only depends on its mass and on the induced acceleration. Second, applying a mass-less external force allows the exploration of new force fields. However, the added force can be sensed through contact with the limb. In addition, the vestibular system remains unaffected. While otolithic otoliths organs sense linear acceleration and are hence sensitive to gravitational acceleration, semi-circular canals sense angular acceleration and function in 0 g as they do on Earth (Merfeld et al., 1999). Third, experiments performed in a centrifugal room constitute a better approximation of increased gravitational force. Nevertheless, coriolis effects add a parasite force field. Similarly, underwater manipulations, while reducing actual load through buoyancy, suffer from increased viscosity that resist movements of the limb. Finally, virtual reality coupled with haptic devices has provided valuable results (Senot et al., 2005; Zago et al., 2004). However, forces do not apply on the object itself but instead, present visually arbitrary experimental contexts. Altogether, these manipulations can change the intensity and direction of the gravitational force but are unable to remove the gravitational reference from the picture. Thus micro- and hypergravity environments afford a unique method to investigate the working of internal models when manipulating objects.

The near-weightless environment of space opens up a multitude of possibilities for basic and applied research. Among various possibilities to generate microgravity, parabolic flights offer a good compromise between duration of exposure and flexibility of experiments. The remaining part of this section is devoted to the description of low gravity platforms with a special emphasis on parabolic flights. parabolic flight

The state of free-fall is obtained in a vehicle subject to the only force of gravity, the sum of all other forces being zero. In an external inertial reference frame, no inertial forces are applied to the vehicle, which consequently falls freely. In a non-inertial reference frame attached to the free-falling vehicle, inertial forces exist but they locally balance the force of gravity. Whatever the view, the force of gravity is never canceled.

The term microgravity is also used because weightlessness in a spaceship is not perfect. Gravity decreases 1 ppm for every 3 m increase in height from the Earth surface, which results in some inaccuracies in the assumption that gravity is locally the same, from a mathematical point of view. Moreover, though very thin, there is some air (even at the level of the orbit), which causes deceleration due to friction.

European involvement in low gravity research began approximately 30 years ago with various types of low gravity platforms. The drop tower "Bremen" (Zarm, Germany) features a 110 meter high drop chamber with a diameter of 3.5 m with an attainable residual pressure in the chamber of 1 Pa within 2.5 hours. The chamber is standing inside a concrete building, which protects it from wind perturbations. The experiments are accommodated in a pressurized capsule elevated to the release platform. The drop is initiated by opening a suspension device, which generates very limited perturbations to the capsule. A free-fall duration of 4.7 seconds with residual accelerations lower than 10^{-5} g is thus achieved. Deceleration occurs in an 8 m deep tank filled with polystyrene pellets. The deceleration levels do not exceed 50 g. Two to three drops can be performed in a day. Sounding Rockets provide weightlessness to their payload with experiments during the unpowered flight phase. They provide microgravity in the range 3 to 13 minutes. All sounding rockets for microgravity research are launched from Esrange in northern Sweden. Unmanned recoverable capsules of the Foton type were introduced in 1985 by the Soviet Union. These capsules are launched into near-circular, low earth orbit by a Soyuz rocket, providing researchers with gravity levels less than 10^{-5} g for missions lasting approximately 2 weeks. Parabolic flights are used to conduct short-term microgravity scientific and technological investigations, to test instrumentation prior to deployment in space, to validate operational and experimental procedures, and to train astronauts for a future space flight. Such flights are conducted on specially-configured aircraft, and provide a period of up to 20 seconds of reduced gravity or weightlessness. Parabolic flights are the only sub-orbital carrier to provide the opportunity to carry out medical experiments on human subjects under conditions of weightlessness, complementing studies conducted in space, and on the ground (*e.g.* immersion, bed-rest) under simulated weightlessness conditions. parabolic flight The assembly of the International Space Station (ISS) started in November 1998 with the launch of the first Station element, the Zarya module into orbit, and will continue throughout the next five years. Once the Station is complete, currently planned for 2010 with the reflights of the NASA spacecraft, it will offer an extensive range of facilities in a unique environment that cannot be found on Earth, and will enable mankind to continue to learn how to live and work in space for long periods.

Table 1.1 compares these techniques in term of quality and duration of microgravity, volume of payload and possibility of human intervention.

Table 1.1: Comparison between microgravity platforms.

Platform	μ-g level (g)	Duration	V (m^3)	Control
Drop towers	10^{-3} - 10^{-6}	< 5 s	< 1	indirect
Parabolic flights	10^{-2} - 10^{-3}	20-25 s	> 10	direct
Sounding rockets	10^{-4} - 10^{-5}	5 - 13 min	< 1	indirect
Recoverable capsules	$\leq 10^{-5}$	weeks	> 1	indirect
ISS	10^{-2} - 10^{-5}	weeks - years	> 1	direct

1.6 Content of the thesis

This thesis is devoted to further understand the role of internal models in object manipulations when the gravitational environment is dramatically altered. In addition, the importance of vision as a potential source of information in adaptation is also investigated. This work is organized into 7 sections. Two appendices provide supplementary information on the experimental equipment (A) and on developments of models of the upper limb (B).

The Introduction provided a theoretical framework in which internal models are described. We focused on experimental evidence to illustrate that these concepts are applicable to the neural control of movement. We emphasized the importance of gravity in these models and motivated why its alteration provides a valuable tool to better understand mechanisms of internal models.

Many natural human movements include rhythmic activities like walking, shewing and swimming. Some of them require much more muscular force than others. For instance, it is harder to manipulate a heavy hammer than just moving the upper limb. From mechanics, it is known that driving a system at a pace close to its resonant frequency is efficient, the transfer of energy with the environment being optimal. In other words, at that particular frequency, the actuation needed to generate a given amplitude of oscillation is minimal. Interestingly, neuronal circuits - known as central pattern generators - generate rhythmic patterns of activities in invertevrates and, to some extent in humans as well. Chapter 2 examines whether those central pattern generators can be involved in driving efficient rhythmic movements of the upper limb, by investigating the ability of participants to tune their movement pace according to changes in ambient gravity.

Chapter 3 examines the coupling between grip force and load force during rhythmic movements of a hand-held load in altered gravity. In a previous study, it was shown that this modulation was rapidly acquired and presented a strong linear relationship (Augurelle et al., 2003). In this chapter 2, we specifically address the issue whether similar load forces at the fingertips but generated with different combinations of acceleration, object mass and gravity lead to the same grip force. Moreover, by adding a mass on the forearm while keeping the load force constant, the arm motor command needed to be adapted but not the grip force. Hence, we investigate whether grip force commands are biased by the motor commands sent to the arm.

Chapter 4 follows from observations raised in the previous study. The forward internal model invoked to modulate grip force takes into account the dynamic characteristics of the upper limb, the object and the environment to predict the object's acceleration and, in turn, the load force acting on the fingertips. Whereas the local physical effects induced by gravity and acceleration can be identical at the fingertips, does it mean that we take equivalently into account the gravitational and inertial components of the load to predict the grip force?

Chapters 5 and 6 switch to a discrete collision task. We showed that grip force is adjusted in anticipation of load forces when cyclically moving hand-held objects (Chapters 3 and 4). In contrast, in random discrete movements, (1) pre-programming is necessary and (2) since prediction may not be correct, feedforward control may be supplemented by feedback control. In order to dissociate the two forms of control, we studied up and down collisions, randomly interleaved. In such cases where load duration is reduced, prediction becomes more critical as the time available for sensory feedback is too short to allow a feedback loop to operate. In Chapter 5, we characterize this task in the normal Earth gravity field by analysing simultaneously various motor systems (hand, arm, gaze). Finally, in Chapter 6, we test the same paradigm but in altered gravity. Since the motor plants must integrate the influence of gravity, we verify whether the oculomotor strategy observed in 1 g also holds in new gravity fields. Taken together, the obtained results will give more insights into how the Central Nervous System controls grip force and, more generally, gaze and arm movements during a task that involves transport of an object and high impact loads.

1.7 List of publications

1.7.1 Journal articles

Augurelle AS, Penta M, **White O**, Thonnard JL. The effect of a change in gravity on the dynamics of prehension. *Exp Brain Res.* 148 (2003), 533-540.

White O, McIntyre J, Augurelle AS, Thonnard JL. Do novel gravitational environments alter the grip-force/load-force coupling at the fingertips? *Exp Brain Res.* 163(3) (2005), 324-34.

White O, Lefevre P, Thonnard JL. Eye-hand coordination in controlled collisions in altered gravity. *Comput Methods Biomech Biomed Engin Supp* 1 : 281 (2005).

Ronsse R, **White O**, Lefevre P. Computation of gaze orientation under unrestrained head movements. *J Neurosci Methods.* 159, 158-169.

1.7.2 Journal articles submitted and in preparation

White O, Wing A, Bracewell M, Thonnard JL, Lefevre P. Grip-load force coupling and gaze-hand coordination in high impact loads. *Submitted to Journal of Neurophysiology.*

White O, Wing A, Bracewell M, Lefevre P, Thonnard JL. Predictive grip for high impact loads in altered gravity. *Submitted to Neuroscience.*

White O, Bleyenheuft Y, Lefevre P, Ronsse R, Smith A, Thonnard JL. Altered gravity highlights Central Pattern Generators mechanisms. *Submitted to Experimental Brain Research.*

White O, Thonnard JL, Lefevre P, McIntyre J. The Grip force controller differentiates the dynamic sources of the load. *In preparation.*

White O, Penta M, Thonnard JL. A new device to measure the three dimensional forces and torques in precision grip tasks. *Submitted to Journal of Medical Engineering and Technology.*

1.7.3 Conference abstracts

Augurelle AS, Penta M, **White O**, Thonnard JL. (2001) The effect of a change in gravity on the dynamics of prehension. Eurohaptics. Birmingham, UK.

Augurelle AS, Penta M, **White O**, Thonnard JL. (2001) The effect of a change in gravity on the dynamics of prehension. Fourth Annual Meeting of the Belgian Society For Neuroscience. Brussels, Belgium.

White O, Blohm G, Thonnard JL, Lefevre P. (2004) Accurate visual feedback enhances learning of manipulation in altered gravity. Society for Neuroscience 34th annual meeting. San Diego CA, USA.

White O, Lefevre P, Ykman N, Wing A, Thonnard JL. (2005) Controlled collisions in altered gravitational fields. The Society for the Neural Control of Movement. Key Biscayne FL, USA.

White O, Lefevre P, Thonnard. (2005) Eye-hand coordination in controlled collisions in altered gravity. Société de Biomécanique. Brussels, Belgium.

White O, Lefevre P, Ykman N, Wing A, Thonnard JL. (2005) Controlled collisions in altered gravitational fields. ESA International Society of Gravitational Physiology (ISGP). Cologne, Germany. Young Researchers Best Presentation Award.

White O, Wing A, Lefevre P, Thonnard JL. (2006) Predictive grip for high impact loads in altered gravity fields. Society for Neuroscience 36th annual meeting. Atlanta GA, USA.

White O, Wing A, Lefevre P, Thonnard JL. (2006) Eye-hand coordination in predictive grip for high impacts loads in altered gravity fields. 9th ESA Workshop on Advanced Space Technologies for Robotics and Automation. Noordwijk, The Netherlands.

White O, Wing A, Lefevre P, Thonnard JL. (2006) Predictive grip for high impact loads in altered gravity fields. First Annual Symposium of the IEEE/EMBS Benelux Chapter. Brussels, Belgium.

White O. (2007) Dexterous manipulations in altered gravity. Invited talk. University of Wales. Bangor, UK.

Chapter 2

Altered gravity highlights Central Pattern Generators mechanisms

> The mind can proceed only so far upon what it knows and can prove. There comes a point where the mind takes a higher plane of knowledge, but can never prove how it got there. All great discoveries have involved such a leap.
>
> Albert Einstein

2.1 Abstract

In many non-primate species, rhythmic patterns of activity such as locomotion or respiration are generated by neural networks at the spinal level called Central Pattern Generators (CPG). Under normal gravitational conditions, the energy efficiency and the robustness of human rhythmic movements are due to the ability of CPG to drive the system at a pace close to its resonant frequency. This property can be compared to oscillators running at resonant frequency, for which the transfer of energy with the environment is optimal. However, the flexibility of the CPG to adapt the frequency of rhythmic movements to new gravitational conditions has never been studied. Here, we show that the

frequency of a rhythmic movement of the arm is systematically influenced by the different gravitational conditions created in parabolic flights as predicted by a pendulum model. The period of the arm movement is shortened with increasing gravity level. In weightlessness, however, the period is highly dependent on instructions given to the participants, suggesting a lesser influence of resonant frequency. Our results demonstrate that the innate modulation of rhythmic movements by CPG is highly flexible across gravitational contexts which suggests the involvement of CPG mechanisms in the achievement of efficient rhythmic arm movements. Our contribution is of major interest for the study of human rhythmic activities both in a normal Earth environment and during microgravity conditions in space.

2.2 Introduction

The most fundamental central pattern generators (CPG) consists of two groups of neurons with mutual inhibitory connections (Brown, 1911). These inhibitory connections generate antiphase oscillations in the electrical activity of the two groups of neurons, which alternately drive a pair of antagonist muscular groups (e.g. flexors-extensors), to induce periodic motion. There is growing evidence for the involvement of CPG during walking or arm swinging in mammals (Burke, 2001), including humans (Marder, 2000) although rhythmic movements in man involve higher brain centres (Iwasaki and Zheng, 2006; Marder, 2000). Recent insights suggest that the concept of CPG, as well established for human locomotion, applies to the arm as well (Dietz, 2002; Zehr et al., 2004).

Some rhythmic activities, like locomotion, are energy-greedy and are sensitive to dynamic constraints induced by the environment. If walking is viewed as a force-driven harmonic oscillator, it requires a periodic forcing actuation to sustain its oscillations against gravitational, damping and stiffness forces which tend to diminish the oscillations. In such systems, a particular frequency - the resonant frequency - is critical: it requires the minimum force to maintain the oscillations and hence, the minimal muscle activity. When interacting with the environment, the preferred oscillatory movements are not simply dictated by the central nervous system but are constrained by the dynamics of the system as well (Hatsopoulos, 1996; Kugler and Turvey, 1987). For instance, a giraffe moves with a much slower pace than small mammals, because the former have very long legs. In another context, Neil Armstrong walked on the Moon in 1969 at a much slower velocity than he certainly does on the Earth because gravitational attraction on the Moon is decreased by a factor of 6. From the neuronal control viewpoint, one functional benefit of modulating the CPG frequency with sensory feedback is that it enables a system to exploit the resonant properties of the musculoskeletal dynamics (Hatsopoulos, 1996; Hatsopoulos and Warren Jr, 1996; Iwasaki and Zheng, 2006; Williams and Deweerth, 2007).

Muscle activities are calibrated to take into account the existence of gravitational attraction, based on a lifetime of experience in a normal 1 g environment (Papaxanthis et al., 1998). Indeed, more effort is required to move an outstretched limb upward than downward. The changes of motor performance in altered gravity (Bock, 1998) must somehow be compensated through adaptive control, which is more or less time consuming, depending on the context (Lackner and DiZio, 1996).

In this study, we investigate whether human subjects are able to sustain rhythmic movements in different gravity environments. We hypothesize that if the movements are effectively driven by the CPG, the self-generated pace should vary through the different gravity fields. Indeed, since neuronal control systems cooperate with the physical constraints imposed by the dynamics of the body and the surrounding environment, we expect that a change of gravity would induce a change of frequency in order to approach the resonant frequency to perform efficient rhythmic movements. However, in 0 g, since gravity cannot assist the rhythmic movement anymore, the question remains open as to how subjects will adapt their periodic pattern.

2.3 Methods

2.3.1 Participants

Twelve right-handed volunteers participated in the study. Their health was assessed by their individual National Centres for Aerospace Medicine as meeting the requirement ("Jar Class II") for parabolic flight. No participant reported sensory or motor deficits and they had all normal or corrected to normal vision. All participants gave their informed consent to participate in this study and the procedures were approved by the European Space Agency Safety Committee and by the local ethics committee.

2.3.2 Experimental procedure

Subjects were successively confronted with periods of normal gravity (1 g), hypergravity (1.8 g) and microgravity (0 g) during parabolic flights (Fig. 2.1 A). They were asked to perform rhythmic arm movements around two virtual obstacles situated three meters in front of them following an "infinity-shaped" trajectory with a hand-held instrumented object (Fig. 2.1 B). The first group of 6 participants (Self-paced) were instructed to perform the movement at a self-generated pace. The second group of 6 subjects (Metronome Paced) followed the rhythm dictated by a metronome (1 cycle every 1.5 seconds).

2.3.3 Equipment

A video-based device (OptoTrak 3020 system, Northern Digital) recorded the position of three infrared-light-emitting diodes (IREDs) on the hand-held object (82 mm diameter, 30 mm wide, 212 g mass) and on the subject's head with a resolution of 0.1 mm within the working environment. We also measured the horizontal distance between the head and the object. A three dimensional accelerometer fixed on the floor of the aircraft recorded its acceleration along its fore-aft axis, its lateral axis and the axis normal to the floor. The two synchronized acquisition systems (OptoTrak and accelerometers) recorded parameters at a sampling rate of 200 Hz.

2.3.4 Manipulation of the gravitational context

The experiments took place in the Airbus A300 ZEROg aircraft on six flights out of Bordeaux (France) spread out over the 35th and the 38th ESA Campaigns. A total of 180 parabolas were performed (2 campaigns $\times$ 3 flight days $\times$ 30 parabolas per flight). From a steady horizontal flight (1 g), the aircraft gradually pulled up its nose and started climbing at an angle of approximately 45 degrees for about 20 seconds, during which the aircraft experiences an acceleration of around 1.8 times the gravity level at the surface of the Earth (g = 9.81 m.s^{-2}). The engine thrust is then reduced to the minimum required to compensate for air-drag, and the aircraft then follows a free-fall ballistic trajectory (a parabola) lasting an additional 20 seconds, during which weightlessness is achieved. At the end of this period, the aircraft must pull out of the parabolic arc, a manœuvre which gives rise to another 20-second period of 1.8 g, after which it returns to normal flight attitude (1 g), before the next parabola. During the parabolas, the resultant g vector was always directed to the floor of the aircraft, lateral and forward/backward components were in the range 10^{-3} g and were negligible. Two participants were tested on each flight, during the first and the second blocks of fifteen parabolas.

2.3.5 Pendulum model

The horizontal and vertical components of the trajectory are phase-coupled by a factor of 2 in order to ensure closure of the paths. Since gravity only influences vertical movements, we used a pendulum under the influence of both gravity and a torsional spring oscillating about some angular equilibrium in a vertical plane. Assuming small angles θ, the linearized equation of motion for the pendulum will be used:

$$ml^2\ddot{\theta} + mgl\theta\cos\bar{\theta} + k\theta = 0 \tag{2.1}$$

where m and l are the equivalent mass and length of the pendulum respectively, g is the ambient gravitational acceleration, $\bar{\theta}$ is the elevation angle of the equilibrium position ($l = 0.3$ m, $\theta = 1.2$ rad). Moreover, a restoring torque (angular stiffness k) proportional to the angular displacement θ was implemented to bring the pendulum back to its rest position. We can rearrange Eq. 2.1 to get rid of the explicit mass dependency and redefine k by unit of mass ($k = 7.9$ Nmkg^{-1}rad^{-1}):

$$\ddot{\theta} = -\frac{g\cos\bar{\theta}}{l}\theta - \frac{k}{l^2}\theta \tag{2.2}$$

This second-order differential equation can be solved analytically and the pulsation ω follows:

$$\omega = \sqrt{\frac{g\cos\bar{\theta}}{l} + \frac{k}{l^2}} \tag{2.3}$$

Since $\omega = \frac{2\pi}{T}$, the period T is simply given by:

$$T = 2\pi\sqrt{\frac{l}{g\cos\bar{\theta} + \frac{k}{l}}} \tag{2.4}$$

This simple model catches the relationship between gravity and the period: the larger the gravity, the shorter the period.

2.3.6 Data analysis

We calculated the period of the rhythmic movement as the time elapsed between two successive crossings of the centre of the path, as defined by the average horizontal and vertical positions (see red dot on Figure 2.1 B). Since data were not normally distributed, a nonparametric Kruskal-Wallis ANOVA on ranks was used to test the effect of gravity and repetition of parabolas within each group. Significance across conditions was assessed with Dunn's post hoc comparisons (alpha level was $p < 0.05$). Since no effect was found across parabolas, we pooled data together in each condition of gravity.

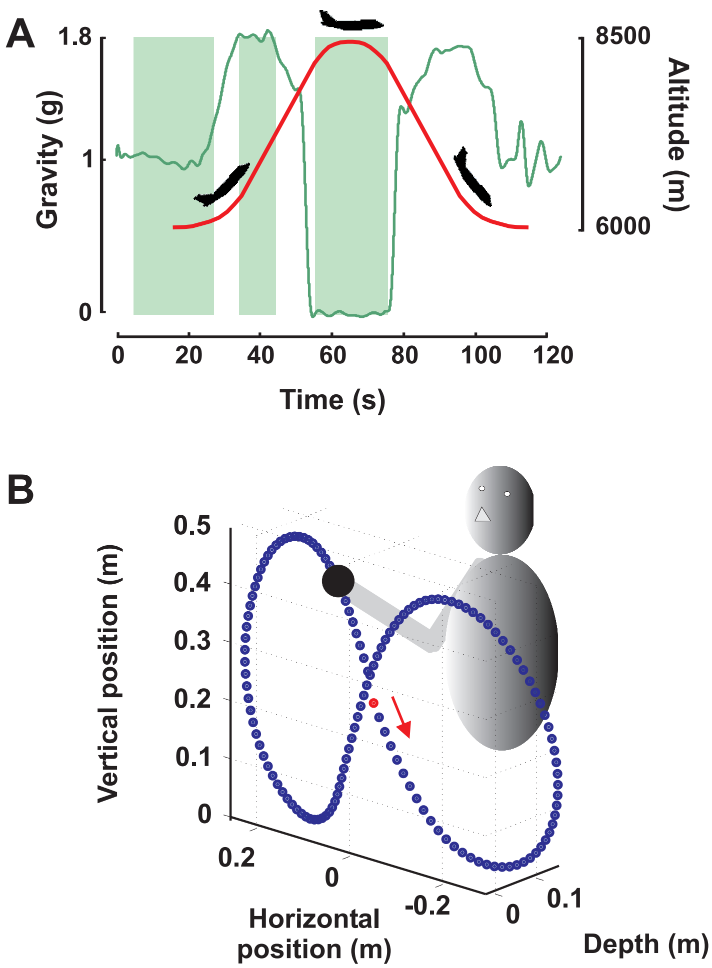

Figure 2.1: Parabolic flight manœuvre and typical trajectory performed by the participants. (A) A single parabolic flight profile generated a sequence of stable episodes of normal (1 g), hyper- (1.8 g) and micro- (0 g) gravity of about 20 seconds each. Gravity level relative to Earth is shown on the left Y-axis (green plot) and flight altitude is reported on the right Y-axis (red plot), both as a function of time. (B) The blue dots represent the object position sampled every 50 ms. The arrow marks the path to follow.

2.4 Results

Figure 2.2 A illustrates the average of the period measured in the two groups of volunteers as a function of gravity level. We examine first the trials executed in the non-zero gravity environments.

In the Self-paced group (Fig. 2.2 A, black circles), we observed that the period in 1 g was reduced in 1.8 g ($p < 0.001$). This influence of gravity on the period was also observed in the gravity scaling of the average period measured during the transition phases (0.5 and 1.5 g). Our data strongly suggest an influence of gravity on the rhythm naturally adopted by the subjects We tested whether these data would be compatible with a pendulum model, characterized by its length, an average angular elevation and a feedback component (see Methods for details). Figure 2.2 A clearly shows that the simulation of the pendulum (dashed line) is very close to the experimental data.

In the Metronome Paced group (Fig. 2.2 A, open circles), when compared to Self-paced, the period of movement in all gravity fields was longer, as dictated by the metronome ($p < 0.001$). Unexpectedly, despite the fact that the cycle frequency was imposed in this condition, the period was still modulated by the gravitational context ($p < 0.001$) and performances degraded with increasing gravity, which suggest a rather low level of control.

Interestingly, the pendulum model used in the Self-paced condition was compatible with this longer period in the Metronome paced group by increasing only the length of the pendulum by 4 cm. Therefore, with the same equation, the pendulum pace was adapted to a slower resonant frequency. Remarkably, we also found that the subjects of this group performed the movements further apart their body by 5 ± 0.1 cm (mean $\pm$ s.e.m., $p < 0.001$). This adaptation allowed participants to follow the imposed rhythm and to perform the movement at a pace close to the resonant frequency.

In the particular case of weightlessness in both groups, although all subjects sustained a rhythmic movement from the very first cycle, the periods in 0 g did not follow the trend observed in other gravitational levels and thus the pendulum model did not fit the data (Fig. 2.2 A).

2.5 Discussion

Experimental and theoretical studies suggest that biological rhythmic movements converge to the resonant frequency of a mechanical system, through sensory feedback. This property, called resonance tuning, has been evidenced

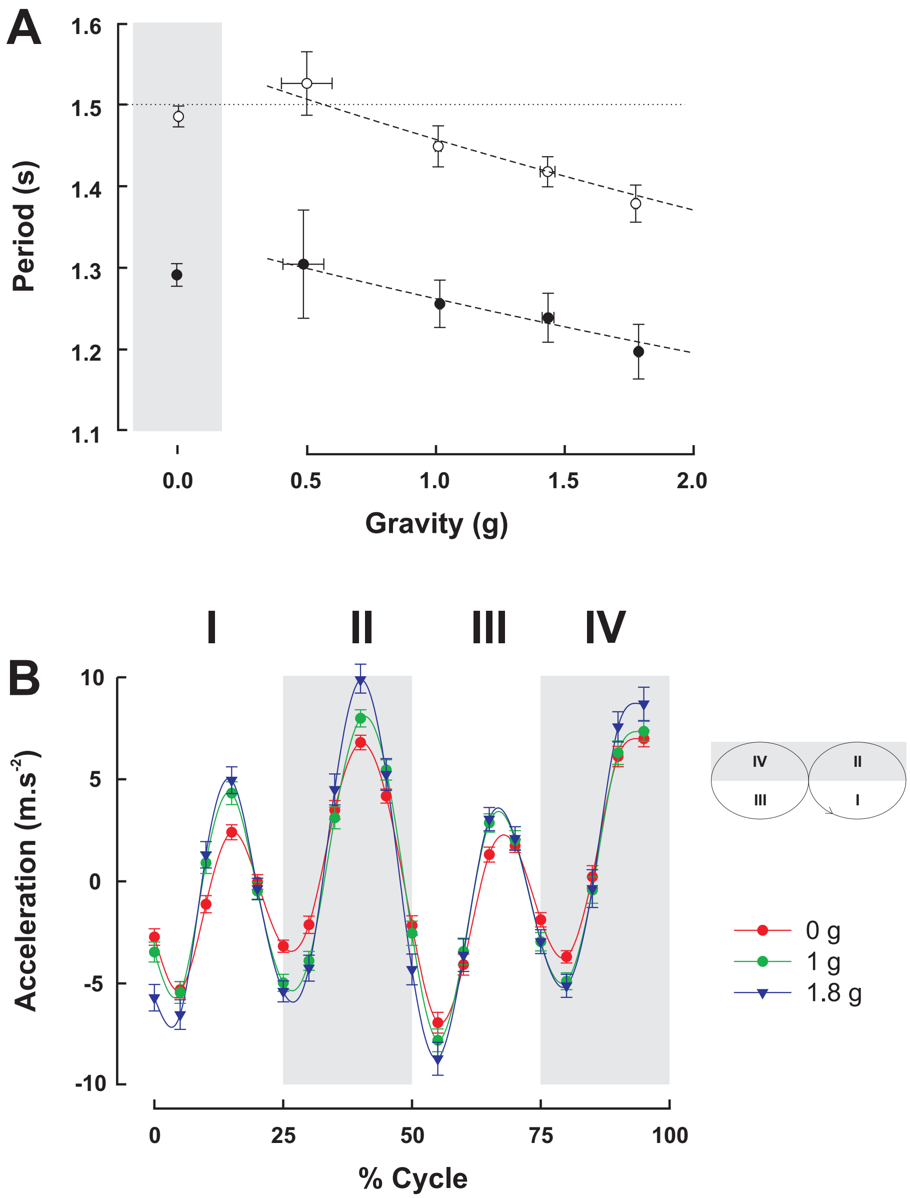

Figure 2.2: Period as a function of gravity (Earth gravity is 1 g). The circles are the mean periods adopted by the participants in the Self-paced group (filled circles, $N = 4497$) and in the Metronome paced group (open circles, $N = 3551$) for 0, 0.5, 1, 1.5 and 1.8 g. The dotted line indicates the target rhythm for the Metronome paced group. The thin curve is the pendulum model fit calculated using a Predictor-Corrector method with Runge-Kutta of order four as the predictor. Error bars represent 95% Confidence Interval on both axes.

in swimming in jellyfish and scallops (Demont, 1990) but also in leg and arm swinging in humans (Abe and Yamada, 2003; Holt, 1990). Moving at the resonant frequency offers several advantages including maximization of the movement amplitude and predictability as well as minimization of the degrees of freedom, the variability, and the energy associated with the movement (Goodman et al., 2000; Holt et al., 1995). Our data strongly suggest a similar functional role of the CPG in arm human rhythmic movements in non-zero gravity fields.

However, another strategy was observed in microgravity since the model did not fit the data anymore. Actually, without an initial force, the pendulum cannot initiate any movement at all. Therefore, the CPG could not take advantage of gravity to drive the arm at the resonant frequency anymore. Consequently, observations in microgravity might reflect different strategies according to which group participants belong.

In the Metronome Paced group, microgravity was the only condition where volunteers successfully followed the metronome, suggesting a higher level control with lesser influence from an endogenous rhythm given by the CPG. Interestingly, the patterns of acceleration differed slightly across the gravity levels and could be the sign of a different strategy in microgravity (Fig. 2.2 B). Indeed, in 0 g, subjects significantly smoothed the acceleration profile of the hand-held object ($p<0.05$) compared to 1 and 1.8 g. The larger the acceleration, the larger the forces and torques generated at the fingertips and at the joints and, consequently, the larger the energy required to perform the movement. Therefore, minimizing extreme values of acceleration in 0 g could have been a strategy to optimise the energy cost (Nelson, 1983). This process could be responsible for the classically observed slowing of movement in weightlessness (Berger et al., 1997; McIntyre et al., 2001b; Mechtcheriakov et al., 2002).

Altogether, behaviour in microgravity is different from that in non-zero gravity fields. Indeed, activities in hypergravity can be inferred from normal Earth gravity by applying a gain on calibrated actions in 1 g whereas microgravity behaviour follows from intrinsically very different rules, since mass and weight become structurally decoupled.

Recently, rhythmic movements have been shown to be performed with better performance than discrete aiming tasks (Miall and Ivry, 2004; Smits-Engelsman et al., 2006). Theoretically, since the human body is a redundant system (Bernstein, 1967), the programming of a movement as a whole (global optimum) should be more efficient than sequentially optimising sub-movements (sum of local optima). These global optima are furthermore able to adapt to different conditions. By considering together the system and its environment, the central nervous system can estimate another dynamic property - the resonant frequency - which is crucial in performing efficient and robust rhythmic movements (Marder and Goaillard, 2006). Hence, voluntary commands or supraspinal inputs can set the frequency of oscillation at a given level. In addition, cycle-to-cycle variations can be induced by modulating the activity in the oscillator interneurones. This flexible mechanism ensures stable performance, despite large fluctuations in the external environment. By allowing for plasticity, the programs implemented by neural control circuits can be parameterised instead of providing single purpose hard-wired circuits and are thus much more useful to the organism (Katz, 1995).

In this context of altered gravity environment, our results provide interesting insights into the role of CPG in regulating rhythmic arm movements. We show that gravity is an essential parameter that is profoundly integrated in our central nervous system when tuning the frequency of periodic actions to resonance in order to sustain competitive movements. The systematic aspect of this adaptation, especially when the rhythm is imposed by a metronome, supports the hypothesis that CPG contribute to drive the rhythmic arm movements efficiently except in 0 g, where a higher level strategy takes place.

Chapter 3

Do novel gravitational environments alter the grip force/load force coupling at the fingertips?

> Do not put your faith in what statistics say until you have carefully considered what they do not say.
>
> William W. Watt

3.1 Abstract

In this experiment we examined the coupling between grip force and load force observed during cyclic vertical arm movements with a hand-held object, performed in different gravitational environments. Six subjects highly experienced in parabolic flight participated in this study. They had to continuously move a cylindrical object up and down in the different gravity fields (1 g, 1.8 g and 0 g) induced by parabolic flights. The imposed movement frequency was 1 Hz, the object mass was either 200 or 400 g, the amplitude of movement was either 20 or 40 cm and an additional mass of 200 g could be wound around the forearm. Each subject performed the task during 15 consecutive parabolas.

The coordination between the grip force normal to the surface and the tangential load force was examined in nine loading conditions. We observed that the same normal grip force was used for equivalent loads generated by changes of mass, gravity or acceleration despite the fact that these loads required different motor commands to move the arm. Moreover, our results suggest that the gravitational and inertial components of the load are treated adequately and independently by the internal models used to predictively control the required grip force. These results indicate that the forward internal models used to control precision grip take into account the dynamic characteristics of the upper limb, the object and the environment to predict the object's acceleration and, in turn, the load force acting at the fingertips.

3.2 Introduction

To lift an object aloft, the grip force applied normal to the object's sides (hereafter referred to as the "normal grip force") must be sufficient to counteract both the gravitational and the inertial components of the tangential load force acting on the fingertips (Johansson and Westling, 1984). A tight temporal coupling between the normal grip force and the tangential load force has been documented in a large variety of tasks engaging different kinds of objects, grips, loads or modes of transport (Flanagan and Tresilian, 1994; Flanagan et al., 1999a,b; Gysin et al., 2003; Jenmalm and Johansson, 1997; Johansson and Westling, 1984). All studies to date seem to confirm that adjustments of the normal grip force anticipate tangential load changes when the movement is self produced, provided that the physical properties of the object are predictable (Flanagan and Wing, 1993, 1995). There is increasing evidence in the literature that the CNS acquires neural mechanisms called "internal models" that can simulate the behaviour of our body and of the environment (Flanagan and Johansson, 2002; McIntyre et al., 2001a; Wolpert et al., 1995). The principle is that during object manipulation, these internal models would predict future accelerations of the arm by using a copy of the motor command that produces the intended arm movement (Flanagan and Wing, 1997; Kawato, 1999). From this prediction, and from visual or haptic information about the object's weight, the total tangential load force can be estimated and an appropriate normal grip force can be programmed in a feedforward manner. The loads experienced at the hand could be thus derived from the arm motor commands. Flanagan and Wing (1997) showed that normal grip force was modulated in phase with, and thus anticipated, the tangential load when moving not only inertial but also viscous and elastic loads. These results suggest that the commands for normal grip force are not simplistically linked to the commands for arm movement but are, instead, based on an internal model of the motor apparatus and external load.

In a previous study in parabolic flight, we measured how subjects adjusted the normal grip force to changes in gravity that modified the relationship between arm movement and load force (Augurelle et al., 2003). We observed that after adaptation (five trials for novice subjects) the normal grip force increased adequately in hypergravity (1.8 g) in order to maintain the same safety margin as on the ground, even though the arm was nearly two times heavier. Hermsdorfer et al. (1999, 2000) showed that the predictive coupling between grip and load forces persisted even during transitions between gravity levels induced by parabolic flights.

In the current experiment we took this study a step further by asking two questions. First, by modifying gravitational and inertial components of the load acting on the arm, it was possible to require different arm motor commands to accomplish the same movement. The weight of the arm was altered either by placing an external mass (200 g) around the wrist or by moving the arm in three gravity fields (1 g, 0 g or 1.8 g) induced by parabolic flight. In the former case, both the gravitational torque at the joints (an increase of about 10%) and the inertia of the arm were modified whereas in the latter case, inertial torques remained unchanged. W also asked subjects to cyclically move hand-held objects of two different masses (200 g or 400 g) over two different distances (20 cm or 40 cm) in the three gravitational conditions. We asked two main questions concerning the control of normal grip force in these circumstances. First, would the subject exert a higher or smaller normal grip force for equivalent tangential loads at the fingers if the effort required to move the upper limb increased or decreased? Second, are gravitational and inertial components of the load force treated adequately and independently by the internal models used to predictively control the required grip force?

3.3 Methods

3.3.1 Subjects

Six right-handed subjects (30-48 years old) participated in the study. They were examined in a Center for Aerospace Medicine in order to qualify for parabolic flights (medical examination type “JAR class II”). No subject reported sensory or motor deficits. They were all accustomed to parabolic flights and all had previously flown between 300 and 2000 parabolas. All participants gave their informed consent to participate in the study, and the procedures were approved by the European Space Agency Safety Committee and by the local ethics committee.

Table 3.1: Mean acceleration for all parabolic manœuvres along the three axes and in the three gravity phases.

Axis	Gravity		
	0 g	1 g	1.8 g
Fore-aft	0.01 ± 0.002	-0.03 ± 0.010	-0.07 ± 0.019
Lateral	0.00 ± 0.005	0.01 ± 0.004	0.01 ± 0.005
Normal	0.01 ± 0.020	1.00 ± 0.029	1.76 ± 0.095

3.3.2 Parabolic flights

The flights originated in Bordeaux (France) using the Airbus A300 ZEROg aircraft. A single parabolic flight profile generates a sequence of episodes of hyper- (1.8 g), micro- (0 g), and hyper- (1.8 g) gravity of about 20 seconds duration each (see also Augurelle et al. (2003)). Thirty parabolas were performed in each of the three flights, organized as six groups of five parabolas with 2-minute pauses of 1 g flight between each parabola plus an extra 5 to 8 minutes between each group. A three-dimensional accelerometer fixed on the floor of the aircraft recorded its acceleration along its fore-aft axis, its lateral axis and normal to the floor. Table 3.1 reports the mean accelerations for all parabolic maneuvers (n = 6 subjects × 15 parabolas = 90) along the three axes and in the three stable gravity phases.

3.3.3 Apparatus

Grip versus load force coupling was examined while holding a cylindrical object (80 mm diameter, 30 mm width, 200/400 g mass) during cyclic vertical arm movements (Fig. 3.1). The instrumented object was equipped with two brass circular grip surfaces (40 mm diameter) placed on two parallel lightweight force/torque sensors (Mini40 F/T transducer, ATI industrial automation, NC). Each sensor measured the three force (F_x, F_y, F_z) components around the corresponding axes passing through the center of the corresponding grasp surface (Fig. 3.1 A). Sensing ranges for F_x, F_y and F_z were ±40, ±40 and ±120 N with 0.02, 0.02, and 0.06 N resolution respectively.

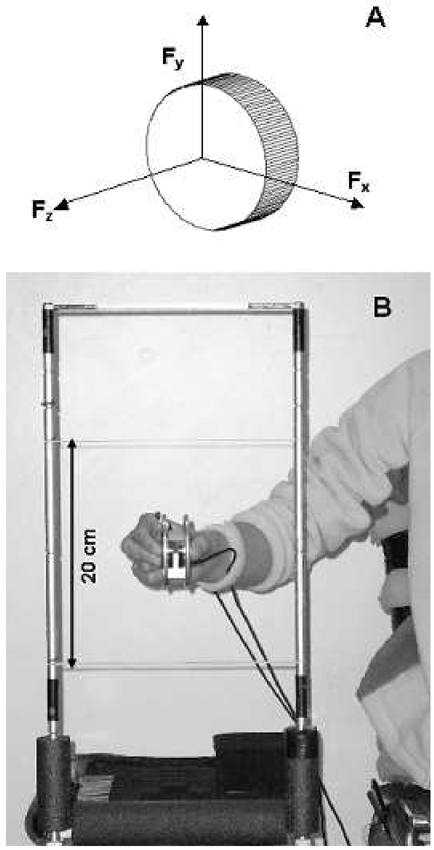

Figure 3.1: (A) Reference frames for forces (F_x, F_y, F_z) measured by the force sensor placed under each grip surface. (B) Schematic view of the apparatus held between the thumb on one side and the index and middle fingers on the other side in the 200 g configuration. Arm displacement was limited by two rubber bands spaced 40 cm apart.

3.3.4 Experimental procedure

The same procedure as in our previous experiment was followed (Augurelle et al., 2003). At a signal from the experimenter, the instrumented object was grasped between the thumb on one side and the index and middle fingers on the other side at about the center of the grasp surfaces. The fingers were aligned along the X-axis in order to place the Y-axis in the upward direction (Fig. 3.1 A). The subjects were instructed to perform cyclic vertical arm movements at a frequency of 1 Hz, aided by a metronome. The amplitudes of the oscillations were maintained by lightly constraining the movement within two parallel rubber bands spaced either 20 cm or 40 cm apart, which indicated the endpoints of the movement (Fig. 3.1 B). Subjects performed the upper limb displacement with unconstrained shoulder and elbow movements. They were instructed to maintain the Y-axis of the object in a vertical orientation without tilting in any direction.

The experiment was first carried out at 1 g on the ground before the flight in order to train the subjects on the task. Then the experiment was performed at 0 g, 1 g and 1.8 g during the three parabolic flight days. Each subject performed the task over 15 complete parabolas in the aircraft at a constant frequency of 1 Hz. In the five first trials (T1-T5), the task was performed with a 400 g mass displaced by a distance of 20 cm ("400g20cm"). In the second series of five trials (T6-T10), the mass was reduced by half and the amplitude of movement was doubled ("200g40cm"). As the frequency of movement was kept the same (1 Hz), the acceleration was also twice as great, resulting in an equivalent inertial load but an increased gravitational load. In the last five trials (T11-T15), the 40 cm movement was performed with the 200 g mass but a ballast brace of 200 g was placed around the wrist of the subject ("ballast40cm"). In this case the inertial and gravitational components of the load were the same as in the "200g40cm" case, but increased for the arm. Table 3.2 shows that among the nine loading conditions (3 gravity fields $\times$ 3 loadings), four levels of equivalent tangential load force acting on the fingertips could be reproduced while the upper limb underwent different loading and gravity environments. For simplicity sake, 2 g is reported in Table 3.2 instead of 1.8 g.

The subjects grasped the instrumented object and performed the cyclic movement during the 1 g phase of the flight, starting approximately 30 seconds before the start of the 1.8 g phase. The movement was performed throughout the entire parabola (1.8 g, 0 g, 1.8 g) and continued 30 seconds after the return to the 1 g phase.

3.3.5 Data processing

The signals from the force transducers, the 3D accelerometers and the metronome were digitized on-line at 200 Hz with a 12-bit 6071E analog-to-digital converter in a PXI chassis (National Instruments©, Austin, TX). After analog-to-digital conversion, the signals were further low-pass filtered with a fourth-order, zero phase-lag Butterworth filter having a cut-off frequency of 15 Hz.

The force applied normal to each grasp surface was calculated as $-F_z$ (Fig.

Table 3.2: The four levels (L) of equivalent tangential load forces. Gravity: gravitation in g ($g = 9.81$ m.s^{-2}); Mass: mass of the object in kg; Dist: object displacement in cm; Ballast: presence (+) or absence (−) of the 200 g mass on the arm; a: object acceleration; GL: gravitational load; IL: inertial load; LF: sum of GL and IL

Cond	L	Gravity	Mass	Dist	Ballast	GL	IL	LF
1	1	2	0.4	20	−	$2m2g$	$2ma$	$2m(2g + a)$
2	2	2	0.2	40	−	$m2g$	$m2a$	$2m(g + a)$
3		2	0.2	40	+	$m2g$	$m2a$	
4		1	0.4	20	−	$2mg$	$2ma$	
5	3	1	0.2	40	−	mg	$m2a$	$m(g + 2a)$
6		1	0.2	40	+	mg	$m2a$	
7	4	0	0.4	20	−	0	$2ma$	$2ma$
8		0	0.2	40	−	0	$m2a$	
9		0	0.2	40	+	0	$m2a$	

3.1 A). The total normal grip force (GF) was calculated as the average of the normal grip forces applied by the thumb and the fingers on each transducer. The magnitude of the tangential load force (LF) was computed as:

$$LF = \sqrt{F_x^2 + F_y^2} \tag{3.1}$$

where F_x and F_y are the horizontal and vertical components of the tangential load, respectively. During the one-second baseline, the device laid with its Y-axis vertically. The artificial bias due to the mass of the two brass surfaces covering the transducers was subtracted from F_y prior to the calculation of LF. The total tangential load force acting on the object was calculated as the sum of the tangential load force measured by the two force transducers. The ratio GF/LF between the normal and the tangential load forces was computed as well.

In preliminary inspections of force traces as a function of time we noted a potential asymmetry in the grip force and load force profiles as a function of the direction of movement. Forces near the bottom of the movement exhibited a sharper, higher peak with respect to the mean than for the upper part of the trajectory. To quantify this effect, an index of asymmetry was computed for F_y and F_n according to:

$$|F_{down} - F_{mean}| - |F_{mean} - F_{up}| \tag{3.2}$$

where F_{down} and F_{up} are the forces measured in the lower and upper parts of the trajectory, respectively.

The analysis of the force measurements was performed cycle by cycle. Seven contiguous cycles of movement were analysed in each parabola (n = 15 parabolas $\times$ 5 subjects $\times$ 7 cycles = 525) during the steady state portions of each gravitational phase (1 g, 1.8 g and 0 g). For each cycle the following values were calculated: the maximum, the minimum and the average values for F_y, LF, GF, GF/LF and the asymmetry index for F_y and GF. A linear regression between F_y and GF was evaluated across the seven cycles. Absolute values of F_y were computed prior to the regression to take into account only the magnitude of the force. A cross-correlation between GF and LF series was calculated for each trial to determine the phase lag at which the maximal correlation between the two series was obtained. A negative phase lag indicated that the correlation was maximal when the normal force anticipated the load change.

3.3.6 Inertial and gravitational components of the load

The prediction of a sufficient normal grip force depends on (1) the ability to adjust the mean level of the normal grip force to the object's weight and on (2) the ability to modulate the normal grip force with the load force due to the object's acceleration. The vertical load force F_y can be divided into the sum of two components, inertial and gravitational:

$$F_y = F_g + F_i \tag{3.3}$$

where $F_g = mg$ and $F_i = ma(t)$. If hypotheses about grip force modulation hold true, grip force should be proportional to load force F_y, whatever the source of the load:

$$GF = kF_y + c \tag{3.4}$$

To a first-order approximation, and ignoring horizontal forces for cyclic movements in the up/down direction, grip force can be described as a linear function of the gravitational and inertial components of the vertical force load:

$$GF = k_g F_g + k_i F_i + c \tag{3.5}$$

If Equation 3.4 holds, k_g should therefore be equal to k_i. To test this hypothesis we estimated k_g and k_i as follows. For each subject and each loading condition we computed the average GF and F_y. The factor k_g was computed as the slope of the best-fit (least-squares) line passing through the three pairs of points for each of the 3 gravitational levels. Then for each gravitational level and each loading condition k_i was computed as the slope of the best-fit line passing through all sampled data pairs of GF and F_y.

3.3.7 Statistical analysis

A three-way analysis of variance for repeated measures was performed on measurements of load force to compare the four levels of equivalent load and to test for effects of loading condition (factor 1: “400g20cm”, “200g40cm” and “ballast40cm”), gravity (factor 2: 1 g, 1.8 g and 0 g) and learning across the five trials (factor 3). A Tukey pairwise multiple comparison procedure was used to determine which treatments were significantly different. The same structure of analysis was carried out on measurements of grip force to test for the influence of the loading condition, gravity and inter-trial learning on grip force/load force modulation. All the statistical analyses were conducted with Statistica 6.0 (StatSoft Inc.).

3.4 Results

Figure 3.2 presents seven contiguous cycles of movement obtained in each stable phase of a parabola (1 g, 1.8 g and 0 g) while oscillating a 200 g mass on a distance of 40 cm at a frequency of 1 Hz. The vertical aircraft acceleration was constant in each gravitational phase (Fig. 3.2 A).

3.4.1 Description of the task across gravitational fields

Description of the task in 1 g

When moving the object up and down at 1 g, the tangential load force (LF) was primarily due to its vertical component (F_y) because its horizontal component (F_x) was close to zero throughout the cycle. Tangential load force LF fluctuated around the object weight, proportional to the vertical acceleration of the arm. It reached a maximum at the bottom of the trajectory when the gravity and the vertical components of the object's acceleration acted in the same direction. It was minimal when the object's vertical acceleration was opposite to that of gravity. The normal grip force (GF) oscillated continuously in

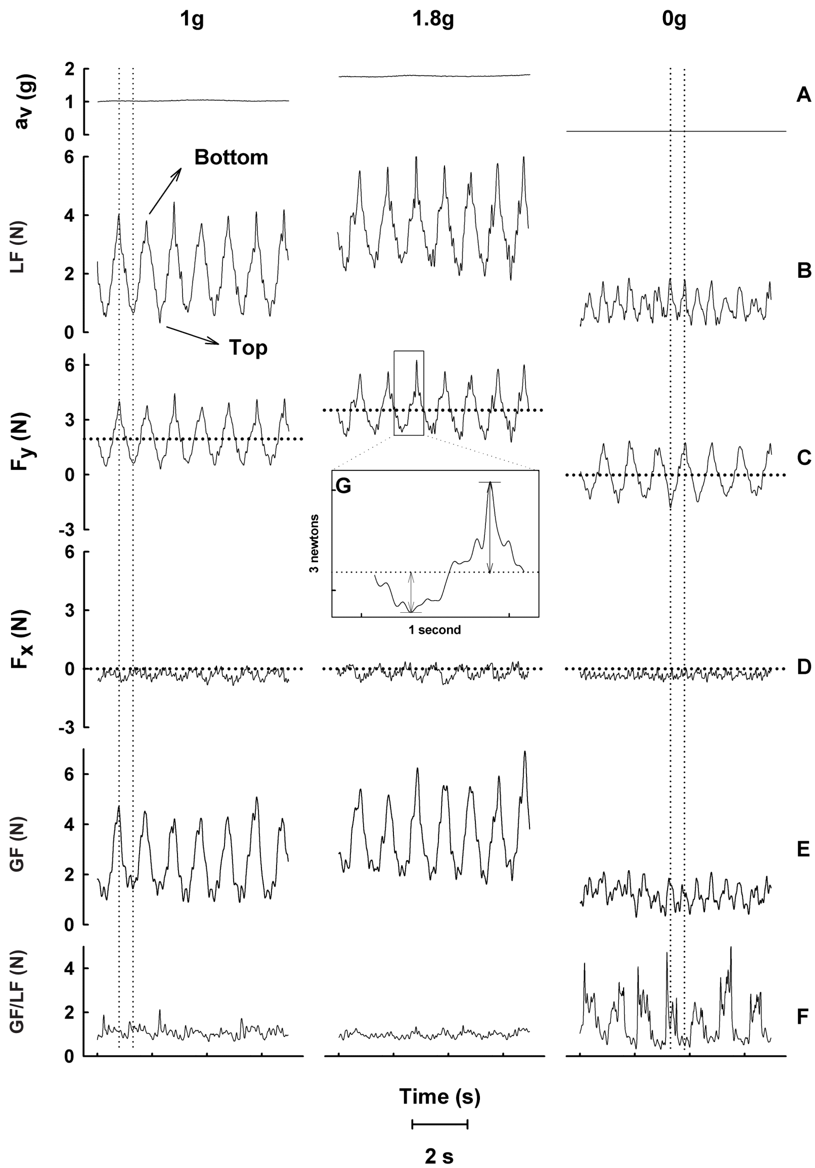

Figure 3.2: Single records of 7 typical cycles of movement in the stable period of each gravitational phase while oscillating a 200 g load a distance of 40 cm at a frequency of 1 Hz. Displayed over time are: (A) the vertical aircraft acceleration (a_v), (B) the tangential load force (LF), (C) the vertical (F_y) and horizontal (F_x) components of the tangential load force, (E) the normal grip force (GF) and (F) the force ratio (GF/LF). The vertical dotted lines show the coordination between F_y and GF. The inset (G) illustrates the asymmetry index on one particular cycle in 1.8 g.

parallel with the load fluctuation (F_y) (vertical dotted lines) so that the force ratio (GF/LF) was quite constant across the cycles.

Description of the task in 1.8 g

In hypergravity (1.8 g), LF was also principally due to its vertical component F_y (F_x remained close to zero). The mean LF increased because the object weight was nearly doubled. The normal grip force (GF) varied in parallel with the load fluctuation (LF) giving a nearly constant force ratio (GF/LF) across the cycles, the same as in 1 g.

Description of the task in 0 g

In microgravity (0 g), the object had to be actively accelerated twice (upwards and downwards) because gravity no longer accelerated the object downwards. In this way, the tangential load force LF reached a maximum in both the upper and lower parts of the arm trajectory. Subjects increased normal grip force (GF) in anticipation of the peaks of load both at the top and at the bottom of the trajectory so that the force ratio reached minimum values at these times (vertical dotted lines) comparable with what occurs in the 1 and 1.8 g gravity. In microgravity, LF was periodically close to 0 N leading to higher values in the GF/LF ratio, when the object was at the top of the trajectory. Note that in the three gravitational conditions, F_x did not oscillate around 0 N but around a negative value indicating a tangential stress in the antero-posterior direction. This means that the movement was not perfectly vertical in the sagittal plane but slightly curved.

3.4.2 Cross Correlation analysis

A cross-correlation between the tangential and normal forces was carried out for each of the fifteen trials performed in each level of gravity. The maximum correlation was 0.89 ± 0.05 both at 1 g and 1.8 g and 0.66 ± 0.12 at 0 g. The maximum correlation occurred at time lags of 2 ± 15 ms, -618 ms, 7 ± 20 ms at 1 g, 1.8 g and 0 g, respectively.

3.4.3 Comparison between the levels of force

Four statistically different levels ($p < 0.001$) of mean tangential load force LF emerged among the nine loading-gravity combinations, corresponding to the four levels predicted on theoretical grounds (Table 3.2). Within each of these levels, the mean LF were not significantly different ($p > 0.05$). The same analysis applied to the vertical component (F_y) of the load force gave the same results. Describing load force in terms of LF is most appropriate, because it is the net tangential load that should determine the grip force. However, the directional characteristic of the load force is lost. In the following we consider only the vertical component F_y because this quantity reflects the direction of the force in the upward and downward directions, making it easier to grasp the differing effects on grip force. This simplification is justified because F_x is insignificantly large compared to F_y.

Level 1 forces (mean $F_y = 7.06 \pm 0.01$ N) were generated when moving 400 g at 1.8 g a distance of 20 cm (Fig. 3.3 A). Level 2 forces (mean $F_y = 3.68 \pm 0.01$ N) were generated either by moving 200 g at 1.8 g a distance of 40 cm with or without an additional mass on the wrist or by moving 400 g at 1 g a distance of 20 cm. Note however that with the 400 g mass, the mean F_y and its maximum (Fig. 3.3 A and B) were higher than in the other two conditions ($p < 0.001$). This is due to the fact that the mass of the hand-held object was doubled while the hypergravity (1.8 g) was not twice normal gravity (1 g). Level 3 forces (mean $F_y = 1.96 \pm 0.01$ N) were obtained with 200 g moved at 1 g with or without the ballast on the wrist. Finally, level 4 forces occurred at 0 g in any of the three loading conditions (mean $F_y = 0 \pm 0.01$ N). The peak F_y reached greater extrema with respect to the mean value with the 400 g mass than with 200 g ($p < 0.001$) (Fig. 3.3 B).

The normal grip force (GF) was measured at each level of load to test whether the same normal grip force was used for equivalent levels of load (Fig. 3.3 C-D) and to test whether the same force ratio (GF/LF) was maintained when the level of load changed (Fig. 3.3 E-F). Within each level, the normal grip forces applied for the different load conditions were the same (Fig. 3.3 C-D). In this way, similar force ratios were maintained inside each of the four levels (Fig. 3.3 E-F). Note however the higher values of the mean ratio in Level 4 due to higher values in the GF/LF ratio at the upper part of the trajectory (see Fig. 3.2 F, 0 g).

When comparing across the four levels of load in Figure 3.3 F, an interesting finding was that the subjects used the same GF/LF ratio for the nine combinations when the load reached a maximum *i.e.* at the bottom of the arm trajectory. This ratio is low and highly reproducible for each subject. The GF/LF ratio when the load reached a minimum was higher and more variable because the subjects did not release their grip as much as they might have

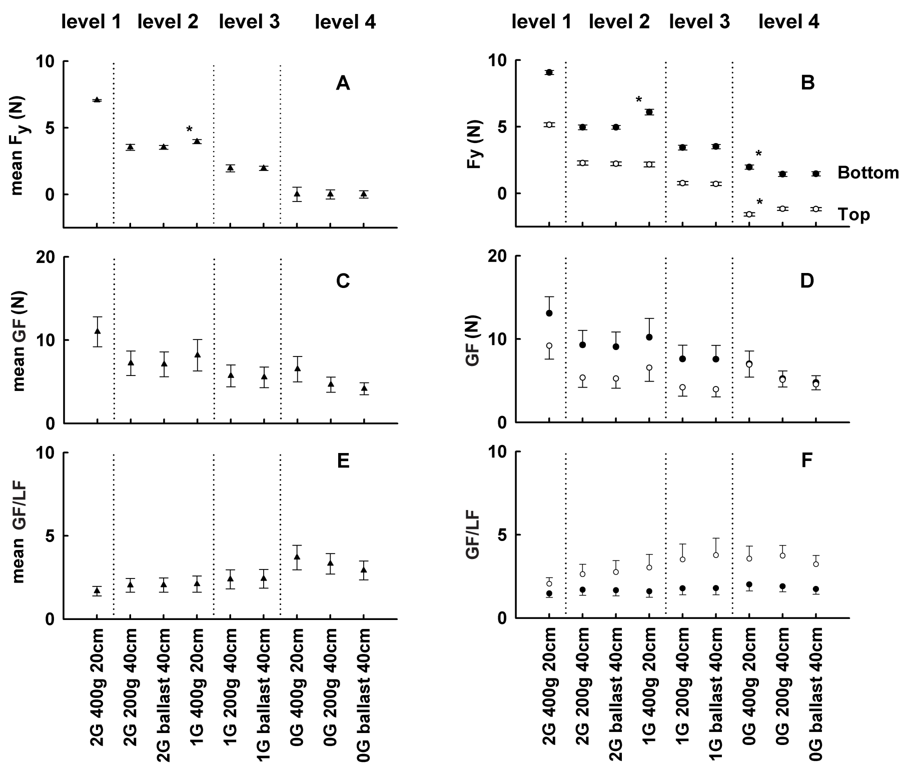

Figure 3.3: The means and standard errors of the parameters are plotted for each load condition for all subjects and trials. The *left* graphs present the mean magnitude (triangles) of (A) the vertical tangential load force, (C) the normal grip force and (E) the force ratio. The right graphs present the values at the top (*open circles*) and at the bottom (*filled circles*) of (B) vertical tangential load force, (D) the normal grip force, and (F) the force ratio. Vertical dotted lines delimit the four levels of equivalent load. Asterisks signal a significant difference ($p < 0.05$) between load conditions within each level.

while still maintaining an adequate safety margin to avoid accidental slip.

3.4.4 Adaptation to inertial and gravitational components of the load

Figure 3.4 A shows a typical scatter plot of F_n as a function of the load F_y while moving a 400 g mass in the three gravitational environments. According to Equations 3.5, the gravitational gain (k_g) is given by the slope of the linear regression (dashed line) calculated between the three means of F_y and its corresponding GF in 0 g, 1 g and 1.8 g. The inertial gain (k_i) is given by the slope of each regression line (solid line) calculated between F_y and GF within each gravity field. Figure 3.4 B shows the gravitational (right panel) and the inertial (left panel) gains for each loading condition. Loading conditions did not modify the gravitational gain ($p > 0.05$). The inertial gain was smaller in 0 g whatever the loading condition ($p < 0.001$) and was smaller with the 400 g mass whatever the gravity field ($p = 0.002$).

3.4.5 Asymmetry in load and normal grip forces

Figure 3.2 G (inset) highlights the asymmetry between the maximum and the minimum of F_y. The asymmetry index (Equation 3.2) is displayed on Figure 3.5 A for F_y (open symbols) and GF (closed symbols) in the three gravity fields. All the values are positive, which means that the amplitudes of peak forces were always larger at the bottom of the trajectory, *i.e.* for maximal tangential load forces (in the presence of gravity). Moreover, when compared to 1 g, this asymmetry was significantly lower for both LF and GF in 1.8 g ($p < 0.015$) but only for GF in 0 g ($p < 0.003$). Figure 3.5 B shows that the asymmetry for GF does not change across trials in 1 g and 1.8 g but significantly decreases in microgravity ($p < 0.025$).

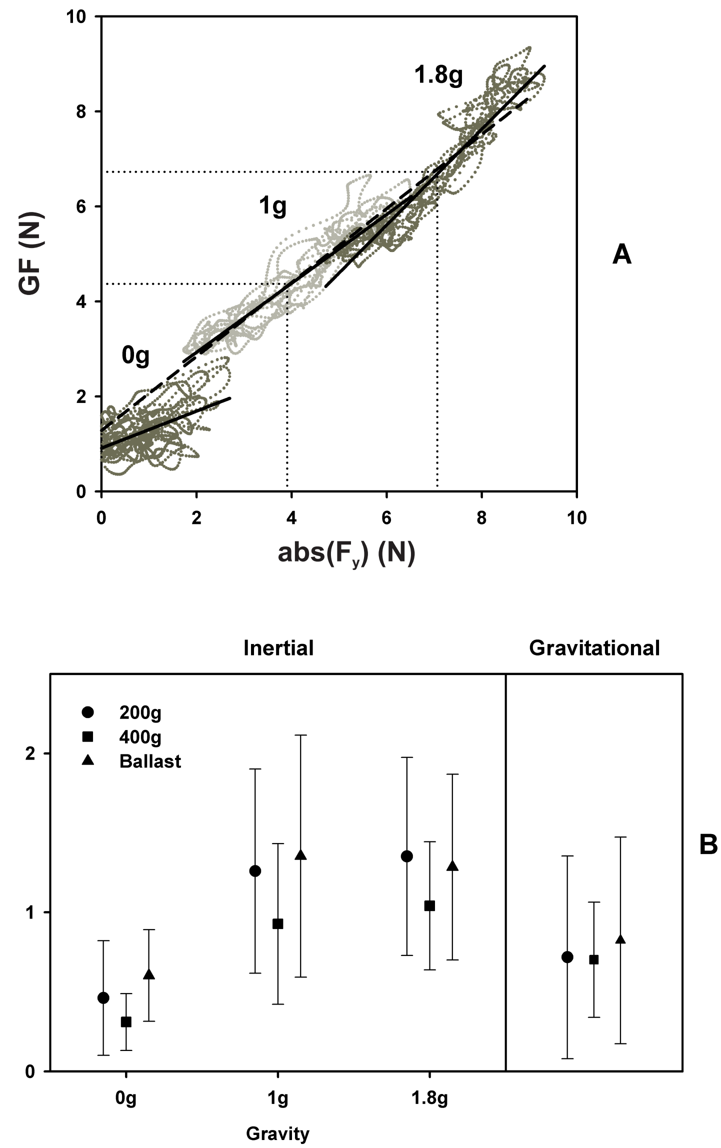

Figure 3.4: (A) Typical trace of the gravitational and inertial gains of GF as a function of the load F_y while moving a 400 g mass in the three gravitational environments. (B) Gravitational (*right panel*) and inertial (*left panel*) gains for each loading condition. Error bars represent SD.

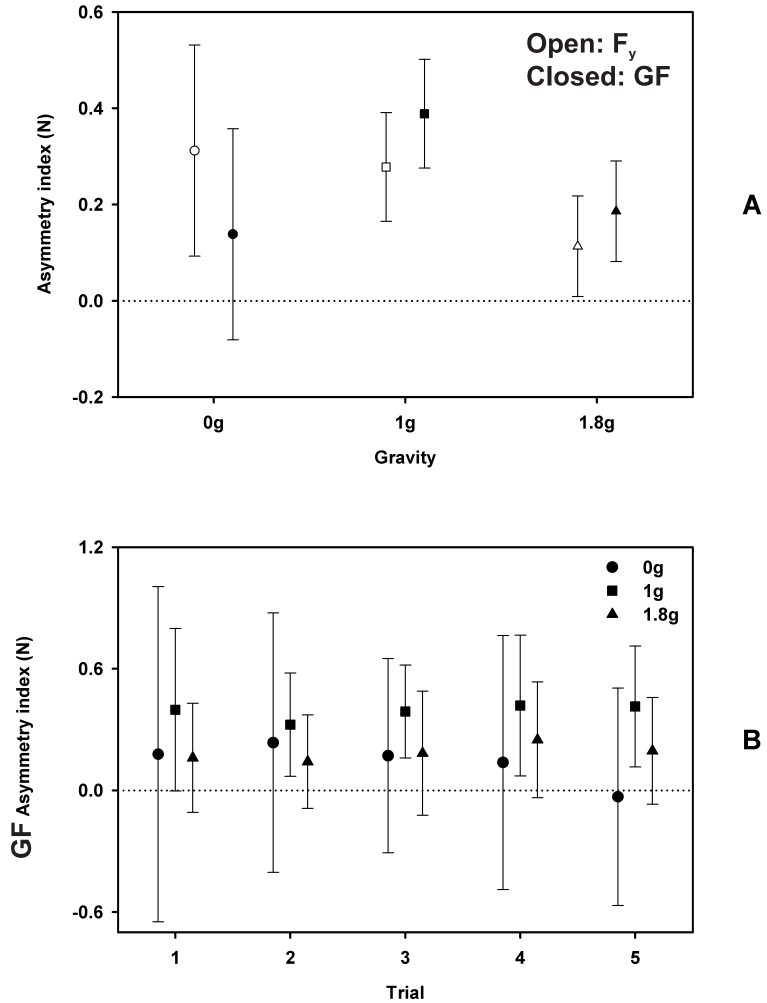

Figure 3.5: (A) Asymmetry index for F_y (*open circles*) and GF (*filled circles*) for each gravitational conditions. (B) The GF asymmetry index for 0 g (circles), 1 g (squares) and 1.8 g (triangles) is plotted in function of the trials. Error bars represent SD.

3.5 Discussion

In this experiment we examined the relationship between normal grip force (GF) and vertical component of the tangential load force (F_y) while moving an object up and down in different gravitational environments. Through a variety of test conditions we varied independently the inertial and gravitational components of the forces acting on the upper limb. On the one hand, we modified the inertial components by varying the mass of the load or the mass of the limb (ballast on the forearm). On the other hand, we varied the weight of the limb and load by adding mass and by varying the effective gravitational field. In this way it was possible to generate equivalent magnitudes of loads at the fingertips while the mechanical constraints on the upper limb and thus the motor commands required to move the arm were modified. Similarly, certain trials required similar motor commands to move the arm, but different grip forces to maintain the object safely in the grasp.

3.5.1 Arm and grip force controllers are decoupled

In each loading condition, the normal grip force was modulated in phase with the load fluctuations, confirming previous results obtained in similar paradigms performed on Earth and in parabolic flight (Augurelle et al., 2003; Flanagan and Wing, 1993, 1997; Flanagan et al., 1999a,b; Hermsdorfer et al., 2000). In microgravity, normal grip force increased at the top of the arm trajectory to prevent slip as the object was pushed downwards. The main finding was that the magnitude of the normal grip force was adequately adjusted for each maximum of load to maintain the same minimum ratio between the normal grip force and the tangential load force (GF/LF) in the nine loading combinations (Fig. 3.3 F, black circles). The subjects were able to maintain this optimum ratio in different contexts of mass, gravity and upper limb accelerations. For equivalent loads at the fingertips at 1 g or 1.8 g, the subjects used the same normal grip force despite the fact that it required more force to displace the arm in hypergravity. These results show that normal grip force is not related to the muscle commands to the upper limb in a simplistic manner. Normal grip force is adjusted appropriately to the tangential load forces applied to the fingertips, rather than being tuned to the overall load applied to the limb.

In the experiments reported here, control of normal grip force was very stable from one parabola to the next, starting from the very first parabola. We observed no systematic evolution of the grip force as a function of trial within each loading condition. This indicates that grip force was appropriate immediately from the first trial after either a change of gravity or a change of the inertial load on the upper limb. These observations from the experienced subjects used in the current study are compatible with our previous experiment in which significant evidence of adaptation to varying gravitational levels was observed only in those subjects who were faced with altered gravity for the first time (Augurelle et al., 2003).

The two results above further extend the general framework in which the grip-force/load-force coordination is observed. Not only does this coupling reflect a general control strategy for any particular grip or mode of transport (Flanagan and Tresilian, 1994; Gysin et al., 2003) but we have also shown that this strategy is used in different environmental (*i.e.* gravitoinertial) contexts. The similar force ratios observed in the nine loading combinations indicate that dynamic constraints such as gravitational force and inertial resistance of the arm and object were well taken into account in the control of precision grip. The precise temporal coupling between the normal grip force and the tangential load force also shows that the load was predicted correctly and that the normal grip force was calculated in a feedforward manner based on this prediction. This suggests that the forward model predicting the load can be adjusted to account for various physical contexts. In other words, subjects were able to identify the environmental context and select the appropriate motor program.

In a modular approach to the problems of motor control, it has been proposed that the brain contains multiple controllers (inverse models) associated with their corresponding predictor (forward models), with each of them suitable for one or small set of contexts (Blakemore et al., 1998; Wolpert and Kawato, 1998). Based on several contextual cues such as experience from previous manipulations of the object and based on visual and tactile information about the object's physical properties, subjects can pre-select an appropriate module for, say, displacing a 400 g object a distance of 20 cm in hypergravity. The selected controller will issue the motor command and the corresponding forward model will predict its sensory consequences. If the prediction is good, the module will continue to be used. When the context estimate is wrong, the prediction will be poor and another module will be selected (Kawato, 1999; Wolpert and Kawato, 1998). This model fits well with our results. In this experiment, the six subjects were familiar with parabolic flights and were trained to perform the manipulative task on Earth. In flight, the nine loading conditions were thus different combinations of known environments and previously manipulated objects. The modular model of motor control also assumes that separate internal models learned for different contexts can be mixed to cope with a given task

(Flanagan et al., 1999b; Wolpert and Kawato, 1998). It is likely that having learned the task in 1 g before the flight, and being already familiar with the different gravity fields in parabolic flight, the subjects could more easily execute the task after just a few trials.

3.5.2 Interaction between gravity and inertia to predict GF

By decoupling the usual link present on Earth between gravity and inertia, we investigated whether the internal model could take into account this separation in order to adjust the normal grip force. Although we observed overall that grip force followed load force with a more or less common relationship (data points in scatter plots of grip force versus load force fall more-or-less along the same line within and across gravitational levels, see Fig. 3.4) we noted subtle differences in the gain of the grip-force/load-force relationships between different loading conditions. On the one hand, we found that the gravitational gain (k_g, Eq. 3.5) did not vary across loading conditions. That is, for both hand-held loads and with or without extra weight on the arm, subjects were able to adjust their normal grip force to gravity, with the same gain. On the Earth, we easily adjust our normal grip force proportional to the mass held. A pure change of gravity (no movement of the arm) induces a change of tangential load force felt by the fingertips just like that produced by a modification of mass on Earth. Therefore, subjects could easily select the appropriate model based on experience in 1 g to predict the correct extent of GF modulation with gravitational load.

On the other hand, we showed that the inertial gain was influenced by gravity and loading conditions. The inertial gain k_i was systematically smaller for the 400 g object than for the 200 g object, whatever the gravity level. Nevertheless, the inertial gain for the 200 g load was not affected by the additional loading of the arm (ballast). Grip force was also modulated in microgravity to account for fluctuations of the inertial load but the gain was lower in microgravity than in non-zero gravity fields. It has previously been observed that increases in average grip force, either due to an increase in the frequency of oscillation or due to voluntary effort, can lead to a decrease in the inertial gain (Flanagan and Wing, 1995). This could explain the reduced inertial gain observed for 400 versus 200 g, but cannot explain the decrease of the inertial gain in microgravity. Thus, when taking into account changes in both loading and gravity, it seems that inertial and gravitational gains can be adjusted independently across conditions. This decoupling between k_g and k_i indicates that these are under high-level control and emphasizes the predictive, internal model-based character of grip force control. If the parameters of grip force modulation were based entirely on sensory feedback about the tangential force at the fingertips, it should not matter whether the source of the tangential load is gravitational or inertial; k_g and k_i should precisely co-vary. This point is further emphasized by measurements of grip-force/load-force coupling compared between novice and experienced parabolic flight subjects (Augurelle et al., 2003). Initial trials in novice subjects showed a much greater influence of gravitational than inertial load on grip force (higher k_g) during initial trials but gradually achieved a more coherent pattern of grip force regulation after practice in 0 g.

3.5.3 Asymmetrical GF and LF are pre-programmed

The results reported here showed that the load fluctuations were not symmetric around the object weight regardless of the gravitational level, as would be the case if the peaks in arm acceleration were equal and opposite at the upper and lower reversal points of the trajectory. One of two subjects showed a similar asymmetry in a related study in microgravity (Hermsdorfer et al., 2000) and asymmetry in arm kinematics has also been reported for discrete point-to-point arm movements in terms of hand-path curvature Papaxanthis et al. (1998) and in terms of the relative time taken to accelerate and decelerate the movement (Papaxanthis et al., personal communication).

One might ask what is the source of these asymmetries? Do they reflect optimization of the motor plan with respect to the dynamic constraints imposed by gravity, or is this simply an asymmetric effect of gravity on what would otherwise be a symmetrically programmed behaviour? The fact that these effects persist (at least initially) in 0 g is the key point: variations of limb kinematics and grip force tuned to the differing effects of gravity on the limb for upward and downward movements are programmed in an anticipatory manner, otherwise they would have disappeared immediately on entry into the 0 g environment.

As we show here, the predictive controller that regulates grip forces takes into account even the subtle asymmetry in kinematics and load forces associated with vertical arm movements. The results suggest two cooperative controls for these different processes which are, nevertheless, somewhat independent. On the one hand, the grip force controller seems to take into account the asymmetries in the tangential load forces for non-zero gravity fields. On the other hand, in microgravity, the grip force controller learned to apply symmetric patterns after five trials although the asymmetry in the kinematics persisted (Fig. 3.5 A and B). We can speculate that with more trials, subjects would succeed in producing symmetric patterns of kinematics and load forces in microgravity.

Although the coupling between normal grip force and the tangential load force was preserved in hyper- and microgravity, the kinematics of the arm movements seems to be influenced by the gravitational level. The results reported here showed that the load fluctuations were not symmetric around the object weight, as would be the case if the peaks in arm acceleration were equal and opposite at the top and at the bottom of the trajectory. Such perturbations in the arm movement kinematics in a new gravitational environment have been previously observed in target pointing, manual tracking (Bock, 1998) and arm movement control (Fisk et al., 1993; Hermsdorfer et al., 2000).

Overall, we have shown that the CNS predicts load force precisely enough to program grip force in a feedforward manner, despite variations in the mass of the load, the mass of the limb and the gravitational context. We conclude that the internal models used to control precision grip are sophisticated enough to take into account the differing effects of gravitational force and inertial load on the muscular effort required to move the arm and the grip force required to hold the object.

Chapter 4

The grip force controller differentiates the inertial and gravitational components of the load

> While the individual man is an insoluble puzzle, in the aggregate he becomes a mathematical certainty. You can, for example, never foretell what any one man will be up to, but you can say with precision what an average number will be up to. So says the statistician.
>
> Arthur Conan Doyle

4.1 Abstract

In everyday life, one of the most frequent activity involves accelerating and decelerating an object held in precision grip. In a broad variety of activities, human subjects scale and synchronize their grip force (GF), normal to the surface of contact of the object, in anticipation of the expected tangential load force (LF), resulting from the combination of weight and inertia. This tight

coordination between GF and LF has been shown when transporting objects, or when the load at the fingertips depends on position, velocity, acceleration and even gravity through the implementation of anticipatory mechanisms in the Central Nervous System. A few studies have qualitatively examined how we adjust the parameters - gain and offset - of this relationship between GF and LF. In this study, we manipulate combinations of mass of a hand-held object and frequency of movement to generate equivalent magnitude of LF. We show that despite the fact the same LF are generated, different GF strategies are applied at the fingertips. We conclude that since the same constraint was felt at the fingertips, peripheral biological sensors might not be sufficient to differentiate inertial from gravitational constraints. This provides clear evidence that the analysis of the origin of LF is performed in the brain, and not at the periphery.

4.2 Introduction

There is evidence that when holding an object with a precision grip, a minimal grip force (GF, normal to the contact surfaces) must be applied to prevent the object from slipping under the influence of load forces (LF, tangential to the contact surfaces). A normal force generates a proportional friction force between the fingers and the object that assists in stabilizing the grip against external constraints. Potential slips in the use of erroneous GF adjustments emphasise the need for anticipatory mechanisms that can predict the required GF as a compromise between keeping the object in hand while minimizing muscle fatigue. In everyday life, one of the most frequent activity involves accelerating and decelerating an object held in precision grip. According to Newton's second law, accelerating an object creates an inertial force. In a gravitational field, the total load force increases when an object is accelerated upwards, while it decreases when the object is accelerated downwards[1]. In a broad variety of activities, human subjects scale and synchronize their GF in anticipation of the expected LF. For instance, this tight coordination between GF and LF has been shown when transporting objects (Flanagan and Tresilian, 1994), during locomotion (Gysin et al., 2003) or when the load at the fingertips depends on position, velocity (Flanagan and Wing, 1997), acceleration (Flanagan and Wing, 1993, 1995) and even gravity (Nowak et al., 2001).

The implementation of anticipatory mechanisms in the Central Nervous System (CNS) have been demonstrated. It has been suggested that the CNS uses the motor command of the arm (an efference copy) in conjunction with

[1] In fact, on the Earth, the load force reaches zero if the downward acceleration $= g$.

an internal model of the arm, the object and the environment to anticipate the resulting LF and thereby adjusts GF appropriately (Flanagan and Wing, 1997; Kawato, 1999; Wolpert et al., 1995). By experiencing object manipulations in many contexts, we learn a set of internal models, with each of them suitable - or at least constituting a reasonable first guess - for one or a small set of contexts (Blakemore et al., 1998; Wolpert and Kawato, 1998). However, to our knowledge, only a few studies quantitatively investigated the sensitivity of these internal models of grip force to external parameters. The strong linear relationship between GF and LF was first reported in rhythmic arm movements by Flanagan and Wing (1995). These authors also evaluated the effects of frequency, surface texture and voluntary GF level on the gain and offset that describes the modulation between the two forces. In an interesting paradigm, Zatsiorsky et al. (2004) investigated the differential effects of gravity and inertia on grip forces during rhythmic manipulations of hand-held objects. They analysed the relationship between GF and LF in different conditions of masses and accelerations induced to the hand-held load. By analysing these regressions, they concluded that the controller regulates grip force in static (holding) and dynamic (moving) tasks differently.

The aim of this study is to further understand quantitatively how contextual parameters such as mass of the object and acceleration influence the grip force exerted against the load. We asked participants to perform rhythmic vertical movements at different frequencies and with several masses. First, we tested whether the combinations of mass and frequency influence the gain and offset of the GF-LF relationship, as in Zatsiorsky et al. (2004). Second, as the local effects induced by gravity and acceleration are identical - physics in an accelerating spacecraft is equivalent to physics in a gravitational field (Einstein, 1907)[1], does it mean that people adjust the grip force to gravitational and inertial forces identically? If this hypothesis holds, then participants should not exert different grip forces against equivalent load forces but generated with unequal contributions of mass and acceleration.

[1]The Equivalence Principle.

4.3 Methods

4.3.1 Subjects

Six adult subjects (25.3 years old) participated voluntarily in this study. Subjects used their preferred hand (four right- and two left-handed) and reported no previous history of neuropathies or trauma to the upper extremities.

4.3.2 Equipment

Grip force/load force coupling was studied while holding a cylindrical object with the index finger and the thumb during rhythmic vertical arm movements. The instrumented object (manipulandum) was equipped with two circular grasp surfaces placed on two parallel force sensors. The sensors measured the two tangential force components (F_x and F_y) and the normal force component (F_z) under the thumb on one side and the index finger on the opposite side. The device was the same as in White et al. (2005). The total mass of the object could be varied by inserting half-rings weighting either 8 g or 83 g. In addition to the empty manipulandum, a total of 7 combinations of 6 half-rings could generate 8 different configurations of masses (see Table 4.1 and Fig. 4.1 A-D).

Table 4.1: Detailed combinations of half-rings for the 8 masses conditions. Labels "L" and "H" refer to a light and a heavy half-ring, respectively. The mass is given in the right column in grams.

	Top half body	Bottom half body	Mass (g)
M1	Empty	Empty	235
M2	LLL	LLL	283
M3	LLL	LHL	358
M4	LHL	LHL	433
M5	LHL	HLH	508
M6	HLH	HLH	583
M7	HLH	HHH	658
M8	HHH	HHH	733

In order to avoid any rotational slip induced by a torque around the grip axis (Z-axis, normal to the contacting surface), the lower half-body was more heavily loaded than the upper half-body, when the mass configuration required an asymmetric half-rings insertion (M3, M5, M7, Table 4.1). An opaque cover around the manipulandum kept the masses interlocking and gave no cue to

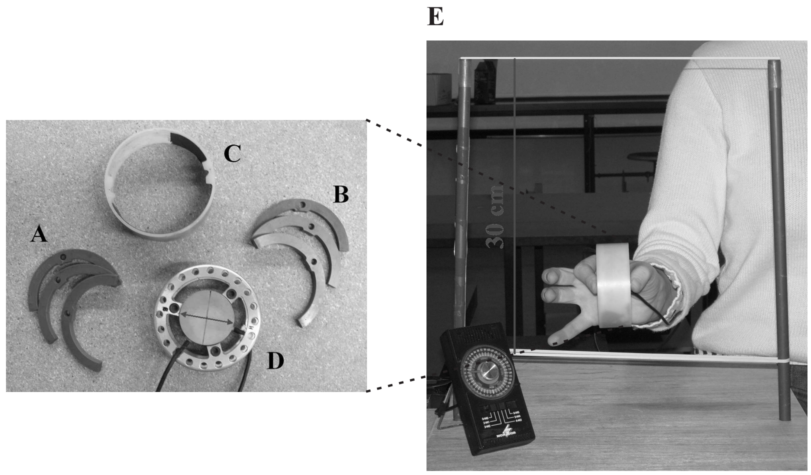

Figure 4.1: The light (A) and heavy (B) half-rings, the opaque cover (C) and the manipulandum (D) equipped with the sensors. (E) Frontal view of the apparatus held between the thumb on one side and the index on the other side. Arm displacement was limited by two elastic bands spaced 30 cm apart. The black device in the bottom-left corner is the metronome that emitted periodic tones.

the subject about the hidden distribution. The manipulandum and the opaque cover weighted 235 g together (M1 in Table 4.1).

4.3.3 Experimental procedure

Each subject was seated in a chair to start the experiment. At a signal from the experimenter, the manipulandum was grasped between the thumb and the index finger. The subjects were instructed to perform vertical rhythmic arm movements between two horizontal elastic bands 30 cm apart during 30 seconds (Fig. 4.1 E). The oscillations were timed by a metronome twice a cycle, at the two extremities of the trajectory. The subject performed the movement with the upper limb unconstrained and no indication about the magnitude of the load was provided.

A complete experimental session comprised 8 blocks, each corresponding to a certain mass (M1 to M8 in Table 4.1). During each block, the subject performed the movement at four frequencies (0.66 Hz, 1 Hz, 1.33 Hz and 1.66 Hz) during 30 seconds ($N = 8$ masses $\times$ 4 frequencies 32 conditions for a session). The frequencies were randomized in a block and blocks were randomized across the subjects. No specific instruction was provided regarding the grip force. Two subjects were tested in turn for each block to limit fatigue. For instance, subject 1 performed block M4 then subject 2 performed block M1, subject 1 performed block M3, etc.

4.3.4 Data analysis

The signals from the transducers and the metronome were digitised on-line at 400 Hz with a 12-bit 6071E analog-to-digital converter in a PXI chassis (National Instruments©, Austin, TX). The force applied normal to each grasp surface was calculated as $-F_z$. The total normal grip force (GF) was calculated as the average of the normal grip forces applied by the thumb and the index on each transducer. The magnitude of the tangential load force (LF) was computed as:

$$LF = \sqrt{(F_{x,1} + F_{x,2})^2 + (F_{y,1} + F_{y,2})^2} \tag{4.1}$$

Grip and load forces were low-pass filtered at 15 Hz (autoregressive dual pass filter). In some trials, low-frequency changes in the GF were observed. Therefore, a high-pass filter at a cutoff frequency of 0.2 Hz was passed to the raw GF and an offset was added such that the filtered force had the same means as the unfiltered data (dual pass fourth order Butterworth filter). We verified that each subjects followed the rhythm dictated by the metronome.

For each trial of 30 seconds, we computed a linear regression between GF and LF:

$$GF = \alpha LF + \beta \tag{4.2}$$

where α and β are the gain and the offset, respectively.

In addition, an iterative procedure identified a 1 N-width interval of LF across the 32 collapsed conditions, under the constraint that it maximised the number of mass/frequency combinations for the 6 subjects. The load forces varied between 0 and 18 N, across subjects and conditions. The optimal 1 N-bin LF ranged from 3.25 to 4.25 N and covered 17 combinations. Note that this interval could include LF generated by slow movements with a heavy mass as well as constraints induced by fast oscillations with a lighter weight. The second, third and eighth masses were not included in the set of equivalent LF. We also calculated the regressions between GF and LF for each of the 17 mass/frequency conditions.

The movement was modelled with a sine wave:

$$x(t) = \frac{A}{2}\sin(\omega t) = \frac{A}{2}\sin(2\pi f t) \tag{4.3}$$

where A is the amplitude and f the frequency of oscillations. The first and second derivatives give the velocity and acceleration:

$$\dot{x}(t) = \frac{A\omega}{2}\cos(\omega t) = A\pi f\cos(2\pi f t) \tag{4.4}$$

$$\ddot{x}(t) = -\frac{A\omega^2}{2}\sin(\omega t) = a(t) \tag{4.5}$$

The theoretical expression of LF is therefore given by:

$$LF(t) = mg + ma(t) = mg - 2mA\pi^2 f^2\cos(2\pi f t) \tag{4.6}$$

with a linear dependence on the mass (m) and a quadratic dependence on the frequency (f).

4.4 Results

4.4.1 Typical trials

Figure 4.2 A shows an example of GF and LF over time for a single subject oscillating a mass of 583 g (M6) at the frequency of 1.33 Hz. The LF (Fig. 4.2 A, blue trace) followed a sinusoid centred on the object's weight (about 5.7 N, red crosses). The GF (Fig. 4.2 A, green trace) was synchronized with the LF. The right panel presents eight GF-LF relationships for a given frequency of 1 Hz for a given subject (Fig. 4.2 B). On the one hand, the clouds of points seem approximately parallel. However, whereas the nearly linear relationship between the two forces was present in all conditions, we observed substantial offsets proportional to the mass being moved. In other words, the average GF exerted during the oscillations increased for heavier masses. For instance, an average LF of 2.3 N (235 g) led to an average GF of about 2 N (Fig. 4.2 B, dotted lines, red cloud) and an average LF of 5.7 N (583 g) led to an average GF of 8.5 N (Fig. 4.2 B, dashed-lines, yellow cloud).

4.4.2 Global effects of acceleration and mass

It is therefore interesting to analyze whether mass and acceleration (through the frequency of oscillations) have an influence on the parameters of the linear

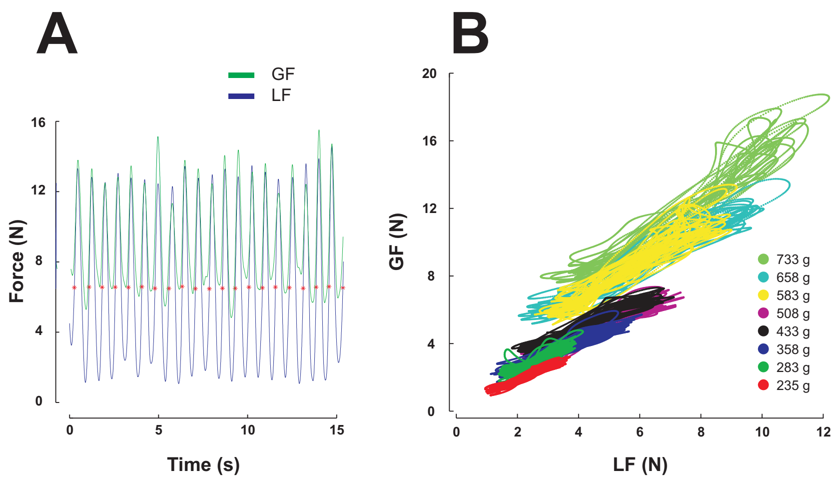

Figure 4.2: (A) Evolution of GF (green trace) and LF (blue trace) over time during oscillations at 1.33 Hz with a mass of 583 g. (B) GF-LF relationships for all masses oscillated at a frequency of 1 Hz.

regression between GF and LF. We conducted a 2-way ANOVA on the gain and offset taking the mass as the first factor and the frequency as the second factor. A Scheffé post-hoc test was assessed when necessary. Figure 4.3 presents the evolution of the gain (A) and offset (B) for the 8 masses and the 4 frequencies.

We observed that for a given mass, the gain was not influenced by frequency (Fig. 4.3 A, $p > 0.948$). In addition, the gain was also constant over the entire mass range ($p > 0.9$), except for M8 ($p < 0.001$). In contrast, the offset was influenced both by the mass and the frequency, with an interaction effect (Fig. 4.3 B): for a given mass below M5, the offsets are not different whereas they significantly diverge with frequency for masses above M5.

4.4.3 Grip force control in a given range of load force

In this section, we test how the mass of the object and the frequency of movement influence the parameters α^* and β^* of the linear regression between GF and $\overline{LF}$. The notation $\overline{LF}$ is used for load force since we assume it is constant within the interval, compared to the whole fluctuations observed during the experiment:

$$GF = \beta^* \overline{LF} + \alpha^* \tag{4.7}$$

Figure 4.4 shows that mass and movement frequencies have different effects

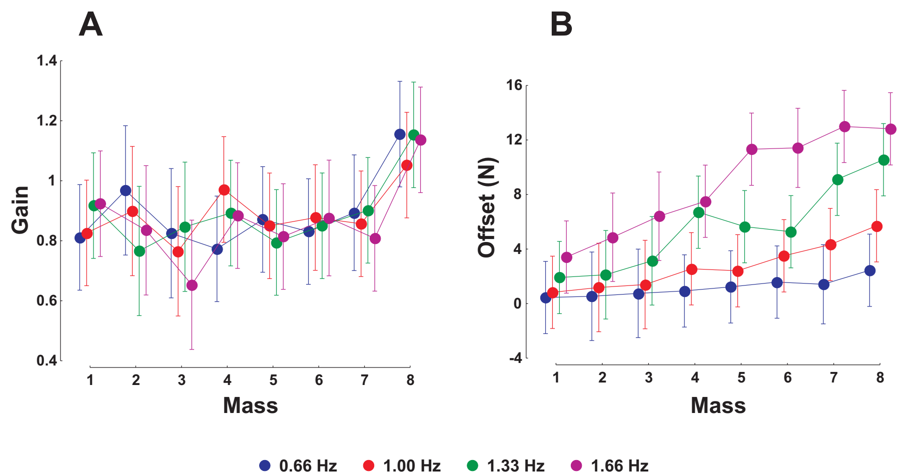

Figure 4.3: Influence of mass and frequency on the GF-LF linear regression. The gain (A) and offset (B) of the regression are presented for the 8 masses (X-axis). In each panel, the 4 plots correspond to the frequencies 0.66 Hz, 1 Hz, 1.33 Hz and 1.66 Hz.

on the regulation of GF, as demonstrated by changes in the gain α^* (Fig. 4.4 A) and the offset β^* (Fig. 4.4 B). The masses on the X-axis refer to labels in Table 4.1 and are shifted by a constant amount of 75 g. Note that M1 was discarded because all frequency conditions generated LF outside the interval (below 3.25 N).

On the one hand, for the two smaller frequencies (0.66 Hz - 1 Hz), the gain decreased significantly with the mass (Fig. 4.4 A, disk, $p < 0.03$) while the trend was not significant for faster pace (Fig. 4.4 A, triangles, $p > 0.626$). On the other hand, the mass influenced the offset in both slow and fast movements ($p < 0.001$), but equivalently as revealed by the parallel increase in the linear fit (Fig. 4.4 B, $p > 0.231$). Altogether, we show that equivalent LF does not imply similar GF. More explicitly, since we have linear co-variations of gain and offsets, we can write:

$$\begin{cases} \alpha^* = \alpha_1^* m + \alpha_2^* f + \alpha_3^* \\ \beta^* = \beta_1^* m + \beta_2^* f + \beta_3^* \end{cases} \tag{4.8}$$

By plugging the above expressions of α^* and β^* into Eq 4.7, we get a prediction of GF:

$$\widehat{GF} = (\alpha_1^* m + \alpha_2^* + f\alpha_3^*)\overline{LF} + (\beta_1^* m + \beta_2^* f + \beta_3^*) \tag{4.9}$$

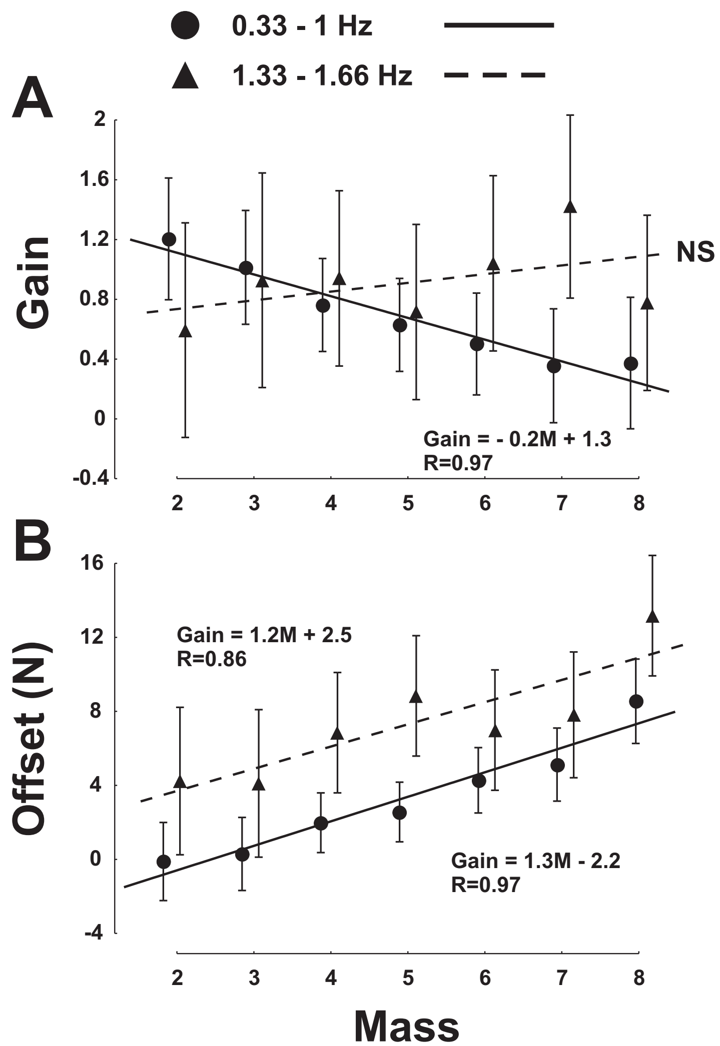

Figure 4.4: Evolution of the gain (A) and the offset (B) of the GF-LF linear relationship in function of mass (X-axis) for slower (0.66 Hz - 1 Hz, disks) and faster frequencies (1.33 Hz - 1.66 Hz, triangles). NS is Non Significant and error bars denote 95% Confidence Intervals.

Since $\overline{LF}$ can reasonably be locally approximated by the mean of the interval (3.75 N), we can rearrange the above equation to express GF in function of m and f:

$$\widehat{GF} = 8.93m + 3.76f - 2.20 \tag{4.10}$$

The regression equation through the experimental data (GF, m, f) is close to the prediction and is given below:

$$GF = 10.03m + 4.98f - 3.21 \tag{4.11}$$

4.4.4 Model prediction

It is interesting to test whether this model generalizes to other values of LF. If we explicit the time dependence of the LF by plugging Equation 4.6 in Equation 4.9, we infer the following $\widehat{GF}$:

$$\begin{aligned}\widehat{GF}(t) = (\alpha_1^* m + \alpha_2^* f + \alpha_3^*)(mg - 2mA\pi^2 f^2 \cos(2\pi f t)) + \\ (\beta_1^* m + \beta_2^* f + \beta_3^*)\end{aligned} \tag{4.12}$$

We evaluate the model for a mass of 0.358 kg displaced at a frequency of 1.33 Hz, over the same amplitude (0.3 m). This mass/frequency combination was not included to learn the model. The α_i^* and β_i^* coefficients were deduced from the regression on the experimental data (Eq. 4.8). The LF covered a broad range of forces (1 to 7 N approximately). Figure 4.5 compares real and predicted LF (upper panel) and GF (lower panel). Despite the fact LF was accurately fitted by the prediction, the GF did not catch an important offset. However, the amplitude of GF oscillations were close to the model prediction.

4.5 Discussion

In this experiment, we evaluated whether the mass and/or frequency of oscillations influence the control of GF as measured through a simple linear regression between GF and LF. We found that whatever the experimental condition, the GF was always accurately predicted by a first order model although its parameters varied with mass and acceleration. Interestingly, we also showed that for a given narrow interval of LF, participants did not adjust GF equivalently, which may reveal high level mechanisms of GF control.

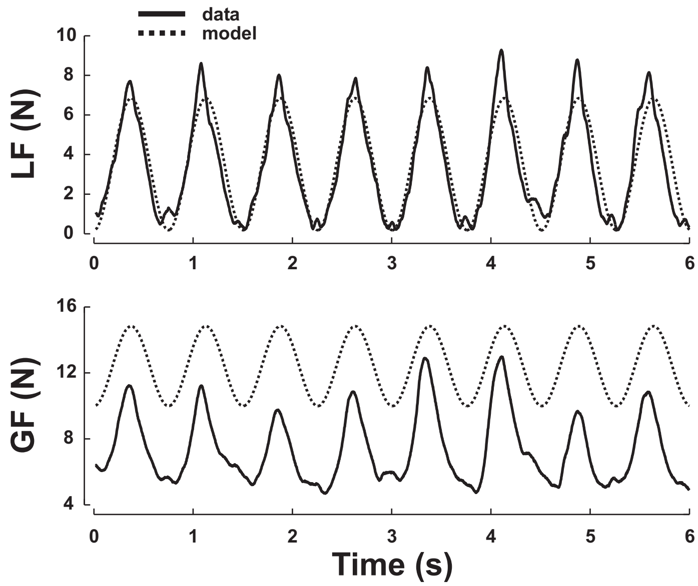

Figure 4.5: Real (solid line) and predicted (dashed line) LF (upper panel) and GF (lower panel) during the oscillations of a 0.358 kg mass displaced at a frequency of 1.33 Hz, over 0.3 m.

4.5.1 Global adjustments of the grip-load force coupling

Our data confirm that subjects modulate the GF with the LF with a high degree of precision in different loading conditions. Indeed, we found values of correlation coefficients compatible with other experiments (see for example Flanagan and Wing (1993)). We characterized the modulation between the two forces with the gain and the offset. We did not find reliable effect of mass nor frequency on the gain. In contrast, Flanagan and Wing (1995) observed that increasing the average GF, either by increasing the frequency of oscillation or due to voluntary effort, can lead to a decrease in the slope. On the other hand, Zatsiorsky et al. (2004) reported that the slopes were steeper with heavier loads and decreased with movement frequency, for all masses. Our results seem contradictory regarding this point because (1) the slope was constant up to M7 and (2) even increased for M8. Flanagan and Wing (1995) and Zatsiorsky et al. (2004) both suggest that the central controller might take into account, when determining the grip force magnitude, not only the expected LF but also its origin and whether the force is increased due to the an increase of mass or acceleration. The discontinuity in the gain between M7 and M8 could be attributed to a psychological threshold linked to the mass, independently of frequency. In sum, this suggests that GF control is under high level mechanisms.

On the other hand, our data indicate that mass and frequency contributed to increase the offset. This is consistent with the fact that when confronted with heavier loads and/or faster pace, participants increased their average GF. This strategy is implemented to reduce the higher risk of dropping the object. Interestingly, the relative difference in offsets between the four frequencies increased with the mass. Namely, doubling the mass or doubling the frequency will not result in the same shift in the average GF. This suggests that participants integrated that frequency is involved quadratically in the expression of LF (see Eq. 4.6). This strengthen the existence of contextual internal models (Davidson and Wolpert, 2004; Kawato, 1999).

In their paradigm, Zatsiorsky et al. (2004) investigated the effects of the gravitational and inertial forces on grip force by manipulating object mass and oscillation frequency. However, they did not compare how GF varied in a given range of LF.

4.5.2 Inertial and gravitational forces are independent in the CNS

We found that the controller regulates GF differently if *the same* LF is generated by different combinations of masses and accelerations (Fig. 4.4). During slower movements, the gain decreased dramatically from 1.2 (lightest mass, M2) to 0.4 (heaviest mass, M8). The offsets in slow and fast paced oscillations increased in parallel with the mass, although being shifted upwards in rapid movements. It is interesting to ask why such differences exist in the control despite similarity of LF. Our results do not support the hypothesis that this low level - or automatic - modulation is implemented in order to optimise the sensitivity of the mechanoreceptors (Edin, 2004; Johansson and Westling, 1984, 1987). Since the same constraint was felt at the fingertips, it is unlikely that peripheral biological sensors might differentiate inertial from gravitational constraints (Angelaki et al., 2004). Therefore, there is good indication that the analysis of the origin of LF must be situated at a higher level. In comparison, a sensory ambiguity also arises in identifying the actual motion associated with linear acceleration sensed by the otoliths in the inner ear (Angelaki and Dickman, 2000; Fernandez and Goldberg, 1976). These internal linear accelerometers respond identically during translational motion and gravitational acceleration. Remarkably Angelaki et al. (2004) identified motion-sensitive neurons in monkeys that provide a distributed solution to the ambiguous problem of differentiating inertial and gravitational accelerations as measured by the otoliths. This provides clear evidence that the dissociation is performed in the brain, and not at the periphery.

In the same vein, White et al. (2005) had the opportunity to perform a similar experiment in parabolic flights, when gravity could really be altered in the LF expression. They generated combinations of gravity (0 g, 1 g, 1.8 g), amplitude of oscillations (20 or 40 cm) and masses of the test object (0.2 kg or 0.4 kg) so as to induce similar LF at the fingertips. The experimental constraints allowed an investigation of only a limited number of conditions. More importantly, the microgravity (0 g) condition did not overlap with a 1 or 1.8 g environment. However, data were sufficient to clearly conclude - at least qualitatively - that inertial and gravitational forces are treated independently by the CNS. Further evidence that subjects are able to integrate the effects of gravity on the LF is provided by the tight GF/LF coupling in micro- and hypergravity when an object is held stationary (Hermsdorfer et al., 1999) or rhythmically moved vertically or horizontally (Hermsdorfer et al., 2000). In sum, we described in a simple formalism how the CNS differentiates the source of the load in order to generate the appropriate grip motor command.

Nevertheless, we have to acknowledge several limitations of our model. First, it is based on a limited range of LF. It should not be extrapolated to other values of LF. The impact of neglecting the friction coefficient might be partly responsible for the shift between predicted and actual GF, as illustrated in the last part of our results (Fig. 4.5). This parameter is largely idiosyncratic and should be adapted to each subject. In addition, a close look at the same figure reveals that load fluctuations were not symmetric around the object weight, as would be the case if the peaks in arm acceleration were equal and opposite at the upper and lower reversal points of the trajectory. This effect has been reported for discrete point-to-point arm movements in terms of hand-path curvature (Papaxanthis et al., 1998). Since this effect seemed to be pre-programmed and is really reflected in the grip profile (White et al., 2005), future improvements should take these asymmetries into account.

Chapter 5

Grip-load force coupling and gaze-hand coordination in high impact loads

> Say you were standing with one foot in the oven and one foot in an ice bucket. On average, you should be perfectly comfortable.
>
> Bobby Bragan

5.1 Abstract

The predictive basis of arm movement control is emphasised by the anticipatory nature of the adjustments of normal grip force (GF) used to stabilise an object held in precision grip against tangential load forces (LF) arising from inertia in accelerating and decelerating the object. In this study, we investigated the control of GF when participants performed a targeted tapping task with a hand-held instrumented object toward an upper or lower target. Two phases were clearly identified: the transport phase corresponded to the initial part of the movement and the collision phase covered the period around the impact. In the transport phase GF and LF were coupled in all conditions, but this was not the case at collision as revealed by a clear dissociation between the two forces. At collision, participants produced stereotyped patterns of GF in all conditions characterized by a maximum in GF shortly after contact. We demonstrated

that this maximum in GF was pre-programmed independently of the force at impact but was predicted by GF and GF rate before contact. We argue that GF at contact was kept at a lower level than after impact in order to absorb the high frequency component of the collision and that the GF maximum after impact served to stabilize hand-object posture. A detailed analysis of the oculomotor behaviour suggests that gaze was optimised to provide vision of the decelerating object in a target-centred reference frame and to allow visual feedback of the collision phase, especially in the more challenging upward trials.

5.2 Introduction

The predictive basis of upper limb movement control is emphasised by the anticipatory nature of adjustments of normal grip force (GF) used to stabilise an object held in precision grip against tangential load force (LF) arising from inertia when accelerating and decelerating the object (Flanagan and Wing, 1993, 1995; Flanagan et al., 1993; Wing, 1996). Such prediction involves a mapping between arm motor commands and hand kinematics and dynamics derived from an internal forward model (Flanagan and Wing, 1997; Wolpert et al., 1995). There is evidence for a systematic modulation of GF with various changes in LF including those dependent on position, velocity and acceleration (see for example Flanagan et al. (2003); Nowak et al. (2004b)).

Hand-held objects can be involved in collisions with target objects present in the environment. In such cases, where load duration is reduced, prediction becomes more critical as the time available for sensory feedback is very short. Several studies have addressed the control of GF in collision tasks. One study involved keeping a hand-held receptacle in position when a ball was dropped into it (Johansson and Westling, 1988). When the participant dropped the ball, an anticipatory rise in GF prior to collision was followed by an increase in GF after collision that was attributed to a reflex. However, Turrell et al. (1999) showed that the post impact response may be absent in self-produced as opposed to imposed collisions induced by hitting or receiving a pendulum bob. Delevoye-Turrell et al. (2003) suggested the importance of visual factors in determining the predictive GF in collisions. However, despite the underlying importance of vision in dexterous manipulation, to our knowledge, gaze movements strategies and GF control in collision tasks have received little experimental attention.

Gaze and hand movements in reaching are highly correlated but also largely context-dependent (see Desmurget et al. (1998) for review). Interestingly, Johansson et al. (2001) investigated the role of gaze in the control of manipulation. Subjects transported a bar to contact a target, either directly or around obstacles. They found stereotyped patterns of gaze-hand coordination that brought the eyes on key positions, such as salient obstacles or targets to which the grasped object was subsequently directed. They concluded that gaze assisted hand movement planning by marking positions on the forthcoming trajectory.

In the present study, we investigated gaze-hand coordination in a vertical collision task with stationary targets. We first addressed the question whether GF is anticipatory or reactively coupled to collision. Does the feedforward strategy of GF-LF modulation in smoothly varying LF also hold at impact? More precisely, if subjects can predict the occurrence and the amplitude of the impact, they should pre-program GF proportional to and synchronized with the collision LF. In addition, we were interested in the information provided by vision to control an action for which grasp stability is an issue. Indeed, the consequences of a wrong GF adjustment especially in upward collisions are likely to induce the drop of the object. Therefore, we might expect a more supportive strategy of gaze-hand coordination in upward compared to downward collisions. This study provides novel insights about how the brain coordinates gaze and hand movements in manipulations involving transport and impact loads.

5.3 Methods

5.3.1 Equipment

The manipulandum comprised a cylindrical instrumented object (82 mm diameter, 30 mm wide, 212 g mass) equipped with two brass circular grip surfaces (40 mm diameter) placed on two parallel lightweight force-torque sensors (Mini 40 F/T transducers, ATI Industrial Automation, NC, USA). The sensors measured the three force components (F_x, F_y, F_z) along the axes passing through the centre of the corresponding grasp surface. Sensing ranges for F_x, F_y and F_z were ±40, ±40 and ±120 N with 0.02, 0.02, and 0.06 N resolution respectively. A PXI controller (PXI-8156B) equipped with a 12-bit PXI-6071E analog-to-digital converter, external triggering facilities and a SCSI interface PXI-8210 (National Instruments, Austin, TX, USA) recorded the synchronized signals from the force sensors at a sampling rate of 1 kHz. Simultaneous two dimensional (horizontal and vertical) recordings of both eyes were made with the Chronos head mounted video-based eye tracker (Clarke et al. (2002), CHRONOS VISION GmbH, Berlin, Germany). Algorithms for the calculation of eye position were based on the determination of the centre of the pupil (see *e.g.* Zhu et al. (1999)). The recording frequency was 200 Hz. The system was linear in the horizontal and vertical plane up to $\pm 20^o$ with a resolution of the order of 5'. A second video-based device (OptoTrak 3020 system, Northern Digital, Ontario, Canada) tracked three infrared-light-emitting diodes (IREDs) on the Chronos helmet to reconstruct the gaze orientation (Ronsse et al., 2007) and three others on the hand-held device. The OptoTrak was mounted on the floor at a distance of 3 m in front of the participant, facing upward at an angle of $\pm 18^o$ relative to the floor. The positions of the IREDs were expressed in a reference frame parallel to the floor centred at the middle lens of the position sensor. The X, Y and Z axes pointed rightward, upward and toward the participant, respectively. The position of the six IREDs were sampled at a frequency of 200 Hz with a resolution of 0.1 mm within the working environment. The Chronos eye-tracker and the OptoTrak were triggered by the PXI controller.

5.3.2 Experimental procedure

Seven right-handed volunteers (22 to 48 years old, 2 female), participated in the study. No participant reported sensory or motor deficits. All participants gave their informed consent to participate in this study and the procedures were approved by the local ethics committee. The participant was secured by a seat belt on a chair. At a signal provided by the experimenter, the manipulandum was grasped between the thumb on one side and the index and middle fingers on the other side at about the centre of the grasp surfaces. The fingers were aligned so that F_y was aligned upwards with the Y-axis of the reference frame (Fig. 5.1 B). Participants performed a targeted tapping task with the manipulandum, on each trial moving from a home position up or down to tap an upper or lower target and then return back to the home position. The two circular targets (75 mm diameter), cushioned with 17 mm thick high density foam to limit the impact, were mounted 283 mm above and below the start position and parallel to the floor on two horizontal crossmembers of a rigid square frame (Fig. 5.1 A). A red mark, vertically midway between the two targets, indicated the home position. A brief auditory tone prompted movement toward the upper (high tone) or lower (low tone) target. The tone onsets occurred at random between 300 and 500 ms after completion of the previous movement. Each participant performed 5 blocks of at least 40 randomised up and down collisions.

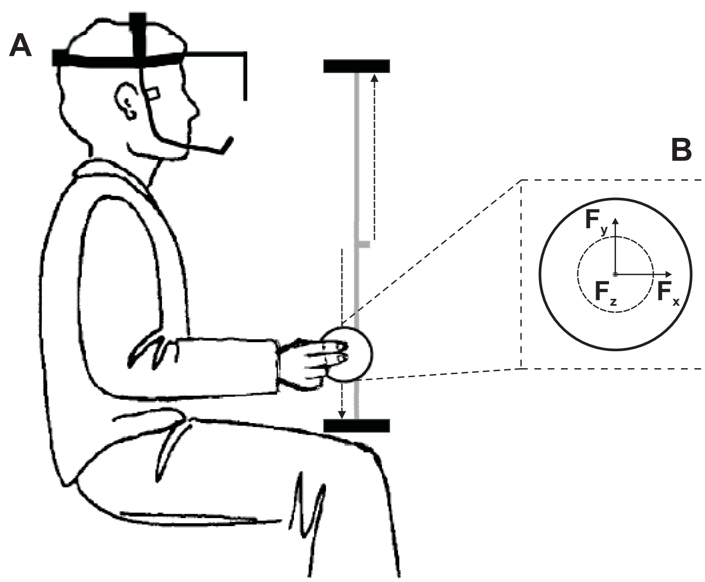

Figure 5.1: (A) Lateral view of the experimental set-up. The participant equipped with the eye tracker produced collisions between the manipulandum (circle) and two targets (black rectangles). The horizontal elastic band (grey tick on the vertical line) was equidistant from the targets and defined the hand's home position. (B) Scaled enlargement of the manipulandum (solid circle) with its 3D reference frame centred on a sensor (dotted circle).

5.3.3 Data processing

All the signals were synchronized and linearly interpolated to the same sampling rate (1 kHz). Kinematic and eye position signals were low-pass filtered using a zero-phase digital filter (autoregressive, forward and backward filter, cut-off frequency: 35 Hz). The force applied normal to each grasp surface was calculated as $-F_z$. The total normal grip force (GF) was calculated as the average of the normal grip forces applied by the thumb and the fingers on each transducer. The magnitude of the tangential load force (LF) was computed as:

$$LF = LF_1 + LF_2 \tag{5.1}$$

with:

$$LF_i = \sqrt{F_{x,i}^2 + F_{x,i}^2} \tag{5.2}$$

where $F_{x,i}$ and $F_{y,i}$ are the horizontal and vertical components of the load force of transducer i ($i = 1, 2$) respectively. The impact force was obtained by averaging values of 3 samples centred on the maximum of LF.

Saccades were detected using an acceleration threshold of 500 deg/s^2 subject to visual checking. For each trial, we determined the following timings: onset for the saccade towards the target (ST_{onset}) and time of arrival at the target (ST_{land}), and onset of the saccade from the target back to the home position (SH_{onset}) and time of arrival at the home position (SH_{land}). We computed the duration of target fixation by subtracting the time of saccade landing on the target from the time of saccade onset back to the home position ($SH_{onset} - ST_{land}$). Gaze position was reconstructed by combining independent eye-in-head and head-in-space positions following standard linear algebra operations (Ronsse et al., 2007).

The geometric centre of the manipulandum was calculated from the three IRED positions. Instantaneous velocity and acceleration were obtained using a 5-point central-difference algorithm. Hand movement onset (HO) was defined at the first sample at which the absolute acceleration exceeded 2.5 m.s^{-2}. The contact time (TC) was detected from the load force trace when the impact force sharply increased during the compression of the high density foam covering the target. Kinematic measures included both the spatial location and time of hand movement onset (HO), peak acceleration (PA) and peak velocity (PV). The grip force and load force were averaged over 10 ms centred at each of the previously mentioned times (HO, PA, PV) or over 10 ms preceding the contact (TC) to avoid artefacts. Additionally, the grip force maximum (GF_M) and its time of occurrence were measured. They corresponded to the maximum in GF occurring at least 15 ms after the contact.

A two-way analysis of variance was performed on variables of interest to test for the effects of direction (UP or DOWN) and repetition across the five blocks. Main and interaction effects were further analysed using Scheffé post hoc procedure (alpha level was $p < 0.05$). All the statistical analyses were conducted with Statistica 6.0 (StatSoft).

5.3.4 Inertial and gravitational components of the load

By Newton's second law:

$$\sum \vec{F}(t) = m\vec{a}(t) \tag{5.3}$$

During the transport of the object, this total force is the resultant of a constant gravitational term (mg) and the load force LF:

$$\sum \vec{F}(t) = m\vec{a}(t) = m\vec{g} + \vec{LF}(t) \tag{5.4}$$

By projecting the vectorial quantities on the vertical axis, we get:

$$mg + ma(t) = LF(t) \tag{5.5}$$

Therefore, upward accelerations ($a > 0$) lead to larger load forces and downward accelerations ($a < 0$) result in decreased load forces with respect to the object's weight.

5.4 Results

Illustrative collisions with the upper (left) and lower (right) target are shown in Figure 5.2.

In the upward collision, the vertical position trace increased until the manipulandum came into contact with the target at TC and then decreased about 100 ms after contact to return to the starting position. The velocity trace exhibited a single peak (PV) and a bell-shaped profile, truncated at target contact. In the collision the velocity dropped sharply to zero and was briefly negative indicating a cycle of compression and decompression of the high density foam cushioning on the target. Following hand onset (HO) the acceleration trace reached a maximum (PA) before decreasing to negative values, indicating the object was decelerated just before contact. At collision the acceleration function exhibited a large (off-scale) negative value reflecting foam compression and the early phase of decompression followed immediately by a moderate positive value, reflecting the late phase of foam decompression. This was followed by a smaller negative acceleration associated with initiation of the return movement. A final positive acceleration phase brought the movement to a halt back at the home position. The load force trace (LF) varied with acceleration in the transport phase (Eq. 5.5). In the collision, LF increased sharply to a (off-scale) value around 7 N. After passing through a negative peak terminating at end of contact the LF trace again paralleled the acceleration. With the exception of a short period of artefact immediately after the collision, the grip force (GF) increased during transport, reaching a maximum after the collision (GF_M). An upward saccade (ST_{onset} to ST_{land}) was triggered to the target near hand onset. After a period of fixation, a return saccade (SH_{onset} to SH_{land}) was executed to foveate the home position. Downward collisions mirrored upward collisions in that the vertical position trace decreased until TC and increased some 100 ms after contact to return to the starting position and the velocity, acceleration, LF and eye positions appear inverted compared to those for the upward collisions. Grip force increased prior to impact reaching a maximum shortly after impact. Note that during the transport of the object, the maximum in upward acceleration (and the downward minimum) contributed to increase (or decrease) in LF some 200 ms before contact. In both directions, there is evidence of object deceleration prior to contact.

5.4.1 Transport and collision phases

Vertical movements induce a directional bias in the load at the fingertips (see Eq. 5.5). We concentrated our analyses on the control of GF during transport and collision phases in both directions. Figure 5.3 presents the values of grip force at different epochs in the trajectory for upward and downward movements. Time zero defines the time of contact (TC). The grip force at movement onset (HO) was the same in both directions ($p > 0.133$). At peak acceleration (PA), the directional bias due to gravity induced a larger load force upwards compared to downwards ($p < 0.001$) and yielded a larger GF upwards. At peak acceleration (PA) and peak velocity (PV), which both occurred 20 ms later in downward collisions ($p < 0.001$), participants exerted a larger grip force upwards. This was also the case at contact (TC) and at grip force maximum (GF_M) ($p < 0.04$). In both upward and downward collisions, GF was noticeably elevated immediately prior to collision.

In maintaining a stable grasp throughout the movement, participants, first, had to counteract inertial forces arising from the transport of the manipu-

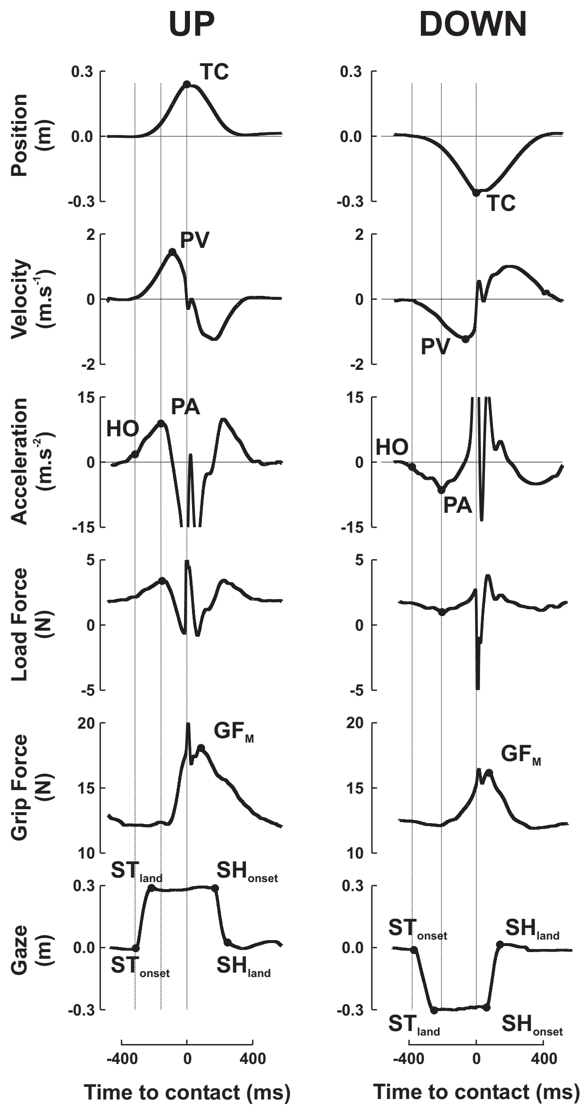

Figure 5.2: Records of a single collision upwards (left column) and downwards (right column). The following traces are shown as a function of time: the vertical position, velocity and acceleration of the object, the load force and the grip force and the vertical gaze position. The left vertical dashed line is aligned with hand onset (HO). The middle dashed line is positioned at peak acceleration (PA). The right dashed line signals the contact with the target (TC).

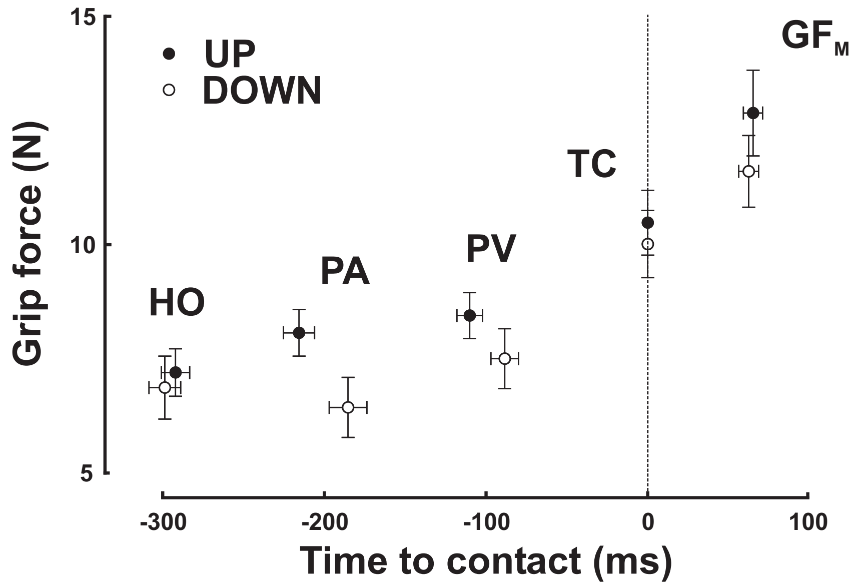

Figure 5.3: Grip force as a function of time to contact for upward (closed circles) and downward (open circles) movements. The means and 95% confidence intervals of grip force are reported at the following instants: hand onset (HO), peak acceleration (PA), peak velocity (PV), contact (TC) and grip force maximum (GF_M). The horizontal 95% confidence intervals quantify the variability in the time of occurrence of the events. The vertical line is positioned at contact (TC).

landum before the collision, and then, had to cope with the impact forces at collision. The former are relatively low forces distributed over a moderately long period of time around peak of acceleration whereas the latter have impulse characteristics with large amplitude and short duration. On the one hand, in the transport phase, participants coupled their GF with the LF at peak acceleration in upward movements ($R = 0.64$, slope $= 3.4$, $p < 0.001$). On the other hand, this GF-LF covariation was greatly reduced at impact ($R = 0.39$, slope $= 0.27$, $p < 0.001$). A similar reduction in correlation was seen between transport and collision in downward trials. Therefore, this contrasting behaviour suggests that participants adjust GF according to different rules in the transport and collision phases of the action.

5.4.2 Grip force maximum is pre-programmed

A maximum in GF was observed in both directions following impact with the same latency (mean $\pm$ SD $= 64.2 \pm 33.3$ ms, $p > 0.25$). We therefore proposed that this maximum in GF might be pre-programmed and used multiple regression to determine its correlation with the grip force at contact and first derivative of grip force at contact (prior to impact):

$$GF_M = 0.932 GF_C + 0.037 \frac{dGF_C}{dt} + 0.533 \tag{5.6}$$

where GF_M refers to the maximum GF, GF_C to the GF at contact and dGF_C/dt to the rate of change of GF at contact. We found that GF_M was well predicted by two variables calculated before the contact with the target, *i.e.* independently of the value of the collision load force. The most significant variable in Equation 5.6 (partial $R = 0.95$) was GF at contact (gain $= 0.93$). The coefficient that multiplies the first derivative of grip force at contact can be interpreted as a duration (37 ms) and contributed secondarily in Equation 5.6 (partial $R = 0.84$). Both terms contributed significantly to the prediction of GF_M ($p < 0.001$). Interestingly, despite the intensive repetition of the collision task, we observed a large variability of collision LF ($SD = 6.15$ N). Equation 5.6 shows that this variability is not taken into account in the programming of GF since the correlation of GF_M with impact LF was not statistically significant. The multiple regression analysis is illustrated in Figure 5.4 where the comparison between panels A and B confirms that data points are very well fitted by the regression plane. Altogether, these results suggest that GF_M is pre-programmed and is not a simple reaction to the collision.

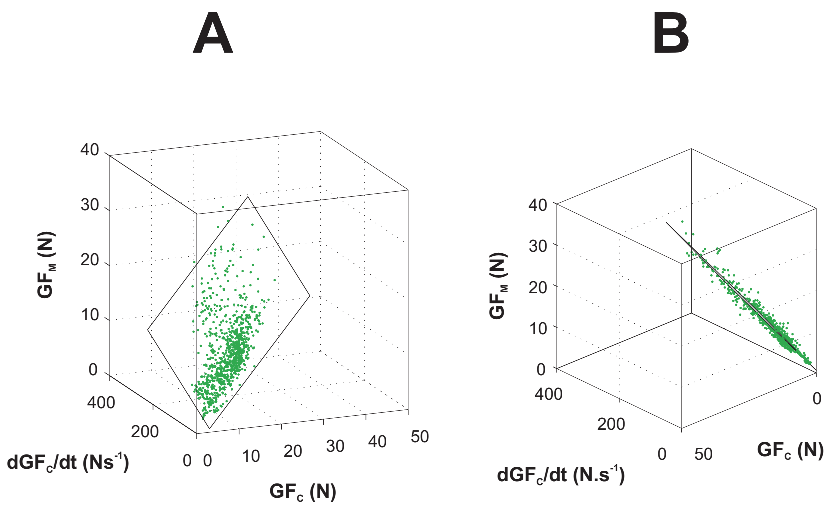

Figure 5.4: 3D plots of grip force maximum (GF_M, vertical axis) in function of grip force at contact (GF_C) and first derivative of grip force at contact (dGF_C/dt) (horizontal axes). The two plots depict the same relation but from different viewpoints to show the good fit of the regression plane (solid lines on the left plot, side view on the right plot). Partial $R = 0.95$ for GF_C and 0.84 for dGF_C/dt, both $p < 0.001$.

5.4.3 Gaze and hand coupling in the transport phase

The collision involved relatively fast movements of the hand with peak velocities around 1.4 m.s^{-1}. We did not observe any use of smooth pursuit eye movements to track the hand and object trajectory on the way to the target. We evaluated the degree to which gaze and hand actions were coupled to achieve the collision task. We calculated the correlations between gaze saccade reaction time (ST_{onset}) and specific epochs occurring in the hand trajectory (HO, PA, PV and TC). We found significant positive correlations in all cases (R ranging from 0.63 to 0.68, $p < 0.001$). In the following, we analyse gaze-hand coordination and duration of target fixation in more detail.

As a first step, we investigated hand and gaze reaction times to the auditory prompt (Fig. 5.5 A and B). We observed increased reaction times for hand onset in upward collisions (Fig. 5.5 A, $p < 0.001$). However, gaze reaction times were not influenced by the direction of movement (Fig. 5.5 B, $p > 0.642$). We defined gaze saccade latencies with respect to hand onset and peak hand acceleration:

$$\Delta_{G-HO} = R_G - R_{HO} \text{ and } \Delta_{\mathrm{G-PA}} = \mathrm{R_G} - \mathrm{R_{PA}} \tag{5.7}$$

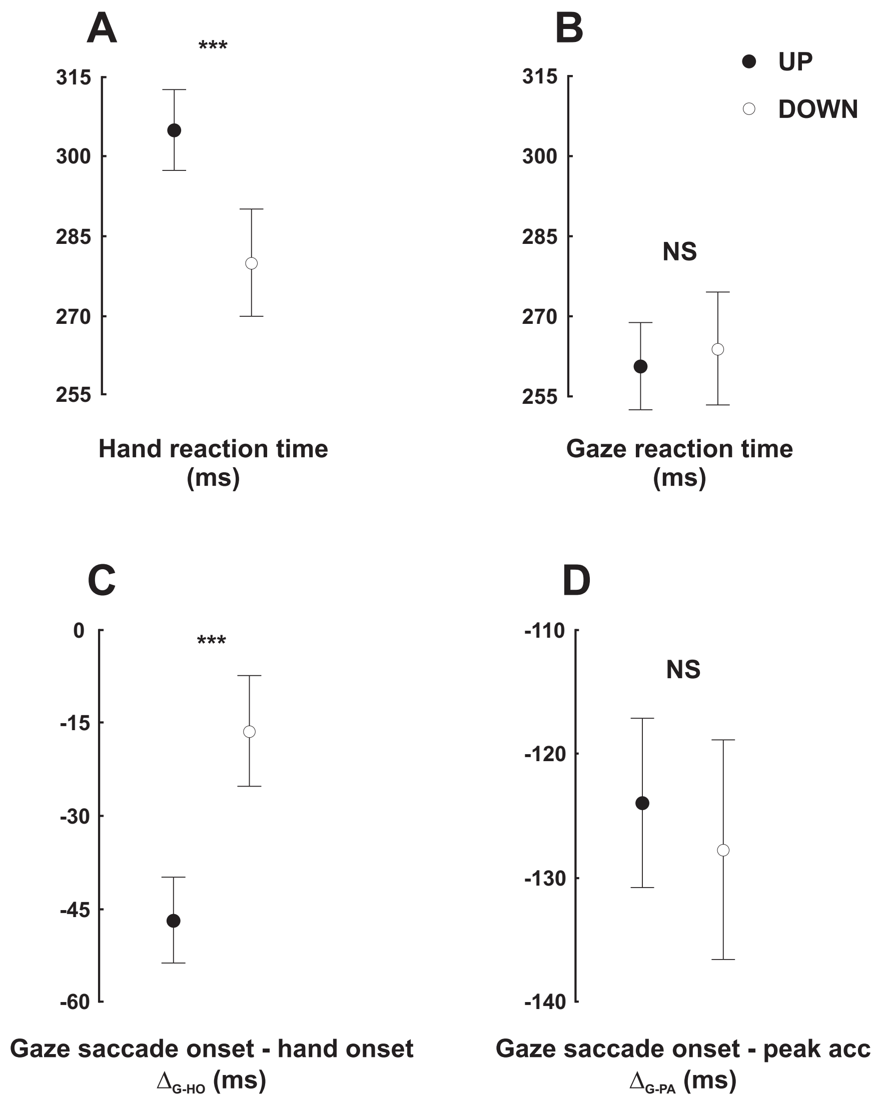

Figure 5.5: The following latency variables are presented for upward (open circles) and downward (closed circles) movements: hand reaction time (A) and gaze saccade reaction time (B), gaze leads with respect to hand onset (C) and peak acceleration (D). Error bars represent 95% CI (*** = $p < 0.001$, NS = Non Significant).

where R_G and R_{HO} stand for gaze and hand reaction times respectively and R_{PA} is the elapsed time between the tone and the instant when hand reached its peak of acceleration. In the above expression, negative Δ_{G-HO} and Δ_{G-PA} mean that gaze leads the hand and peak acceleration, respectively. We first focus on relative gaze and hand onsets (Δ_{G-HO}, Fig. 5.5 C). In both directions, gaze started to move ahead of the hand, as reflected by negative delays up to -45 ms. In addition, greater lead time for gaze (Δ_{G-HO}) was observed in upward compared to downward collision ($p < 0.001$). This direction effect is explained by the increased hand reaction times upwards (Fig. 5.5 A). Interestingly, the delays Δ_{G-PA} between peak hand acceleration and saccade onset were the same in both directions from the second block of trials (Fig. 5.5 D, $\Delta_{G-PA} = -125.4 \pm 2.7$ ms, $p > 0.402$). In the first block, delays in PA with respect to gaze onsets induced longer Δ_{G-PA} but these were similar in both directions (-170.3 ± 9.8 ms, UP and DOWN, $p > 0.925$). Importantly, this was only true with respect to PA and not to any other event in the trajectory (HO, PV, TC, GF_M, $p > 0.05$). Hence, gaze saccade onset seems to be time-locked with peak of hand acceleration, from the second block of trials (Fig 5.5 D). time-locking

5.4.4 Target fixation strategy is direction-dependent

In generating high impact loads, it seems likely that participants might seek to collect information in order to maintain control of the hand-held object. We examined target fixation and hand position as a function of time to contact. Figure 5.6 shows that the movement duration of the hand in the transport phase was significantly longer in downward collisions (Fig. 5.6, HAND, Transport phase, $p < 0.01$). It shows also that the duration of contact between the object and the target was longer for upward collisions (Fig. 5.6, HAND, Collision phase, $p < 0.001$). The duration of target fixation is also shown in Figure 5.6. Clearly, the duration of target fixation was significantly longer in upward collisions, both before and after contact (Fig. 5.6, EYE, $p < 0.001$) and did not decrease across trials ($p > 0.05$). In sum, participants used different gaze strategies in the up versus down conditions: in upward movements, (1) gaze arrived at the target more in advance of the hand contact, and (2) maintained fixation for longer; indeed gaze did not leave the target until after the hand had left.

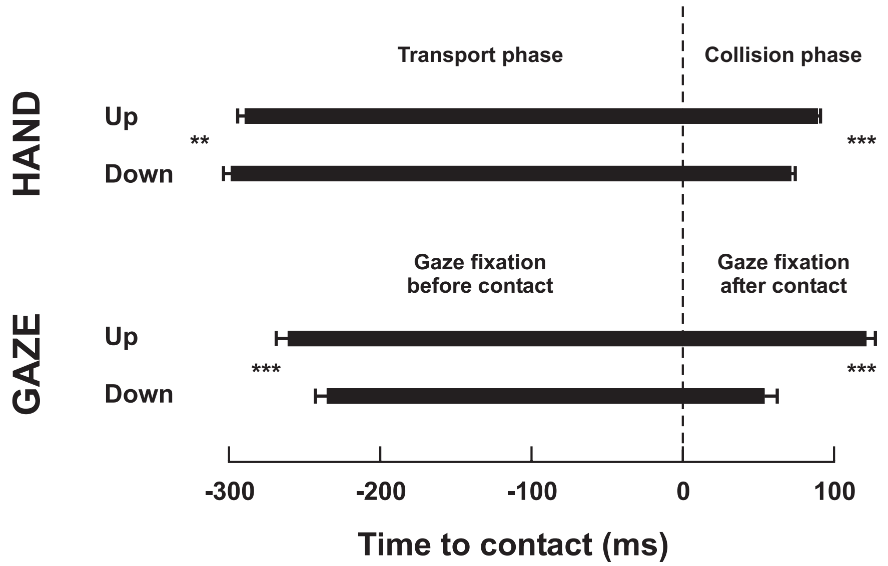

Figure 5.6: Movements durations (HAND, upper row) and duration of target fixations (GAZE, lower row) relative to contact in upward (Up) and downward (Down) movements. The vertical dashed line denotes time of contact. Error bars represent 95% CI (** $= p < 0.01$, *** $= p < 0.001$).

5.5 Discussion

Several studies have used the modulation of grip force (GF) with load force (LF) as an index of prediction in the control of voluntary movement. Various authors reported anticipatory adjustment of GF for different forms of LF including those dependent on position, velocity and acceleration, and with impulsive as well as smoothly varying profile (see for example Augurelle et al. (2003); Flanagan et al. (2003); Nowak et al. (2004b); Turrell et al. (1999)). In addition, Johansson et al. (2001) reported a coupling between gaze and hand movements in controlled hand trajectory.

We analysed the coordination between movements of a hand-held object and gaze strategy in a task that required motion planning in two distinct phases. We identified a transport phase that corresponded to the initial part of the movement and a collision phase that involved the period around the impact. Whereas the results confirmed GF-LF coupling during the transport phase in all conditions, this was not the case in the collision phase, as revealed by a clear dissociation between the two forces. At the collision, participants exhibited larger GF when colliding with the upper target and pre-programmed a maximum of GF shortly after the contact. We found that gaze led the hand and arrived at the target long before the collision. In addition, gaze saccade onset was triggered a fixed time before the peak hand acceleration in both directions. Finally, participants maintained longer fixations on the upper target, especially after the impact.

5.5.1 Grip force/load force coupling in a collision task

The primary goal of the participants was to collide with the target while keeping the object in the hand. In the transport phase, the tight coupling between GF and LF demonstrates predictive control of GF as a function of LF, whatever the direction of movement. This is in agreement with previous studies where participants adjusted their GF according to the LF in vertical point-to-point and rhythmic movements (Flanagan and Wing, 1993, 1995). In the collision phase, however, a dissociation between GF and LF contrasted with their tight coupling during transport. This suggests that the collision phase was programmed differently from the transport phase. Indeed, GF increased progressively in anticipation of the occurrence of the impact and reached a maximum after contact. This observation is in agreement with Serrien et al. (1999) who reported a ramp-like increase of GF prior to impact paralleled by an analogous build-up of EMG activity when opening a drawer to its mechanical stop. Similarly, Turrell et al. (1999) found a maximum of GF occurring around 100 ms after receiving an impact induced by a pendulum swing. In the same study, these authors reported that the maximum of GF was synchronized with the impact when actively producing a collision with a pendulum in order to generate a specific swing. This is a clear indication that the profile of GF after the impact is pre-programmed and is not a simple reflex to the collision since it was absent in specific experimental conditions, in contrast with what was reported previously when unpredictable loads were applied to a hand-held object (Johansson and Westling, 1988; Johansson et al., 1992a; Nowak and Hermsdorfer, 2006). Pre-programming of GF is also supported by the latency of the maximum GF that occurs around 65 ms, which is too short a latency to be related to the latencies typically observed for postural and grip reflex responses (Johansson and Westling, 1988; Johansson et al., 1992a). Further evidence for pre-programming of the maximum of GF is provided by our finding that GF_M can be predicted by GF and GF rate before contact (Eq. 5.6 and Fig. 5.4).

If the GF profile after impact is accepted as reflecting pre-programming in our collision task, it is interesting to ask why the maximum of GF occurs some time after impact and not at the time of collision, when the LF and the risk of slippage are the highest. To test whether there could be a functional advantage in applying a moderate GF at the time of impact, we quantified the influence of GF on the integral of the tangential constraints exerted at the fingertips after the collision, for a specific range of LF at impact. Following this analysis, we found that a larger GF at impact induced a larger integral of LF after collision (see section 5.6 and Figure 5.7 C). This can be explained by the fact that GF increases the stiffness of the contact between the hand and the manipulandum and consequently reduces the damping of the constraints induced by the collision. This hypothesis is validated quantitatively with a simplified biomechanical model in the appendix. Within this context, there is a clear functional advantage in rapidly absorbing the tangential constraints (moderate GF at contact) before increasing GF (GF_M) and stabilizing the hand posture in order to prepare the return movement. Interestingly, when participants produced collisions by hitting a pendulum (initially stationary) with a grasped object, GF and LF peaks were synchronized (Turrell et al., 1999). In that specific context, participants controlled their movement to generate targeted pendulum swings. Therefore, there was a clear advantage to maximize hand-object stiffness in order to control the transfer of kinetic energy from the hand-held object to the pendulum. Our hypothesis is further validated by Lin and Rymer (1998) who studied biomechanical properties of areflexive and reflexive muscles. Postural maintenance often requires that a perturbed joint returns to its initial position (length regulation) and that transients be quickly damped out (velocity regulation). Areflexive muscle does not satisfy the first of these requirements but is very effective at satisfying the second one. In contrast, reflexively active muscle is more effective at position regulation, but not velocity regulation because of the emergence of high stiffness. The authors suggest that the CNS regulates the system parameters as a trade-off to generate an optimal mechanical impedance and damping according to the tasks requirements. Altogether, our results are compatible with the role of feedforward processes adapted to the dynamic properties of the environment (Burdet et al., 2001; Franklin et al., 2003).

5.5.2 Gaze strategy in transport and collision phases

Although gaze strategy in daily activities is highly task-specific, a common finding is that participants control gaze shifts and fixations proactively to gather visual information for guiding movements (*e.g.*, Epelboim et al. (1997)). First, we found that in a majority of trials, gaze led the hand by 15-45 ms which is similar to other values found in the literature (Angel et al., 1970; Prablanc et al., 1979). Vision of the hand at rest prior to movement onset has been shown to greatly improve the accuracy of movement by permitting a multisensorial (proprioception and vision) representation of the movement origin that may facilitate movement planning (Bedard and Proteau, 2001; Desmurget et al., 1998; Prablanc et al., 1979). Second, gaze arrived at the target around 250 ms prior to the hand. This time differential allows the hand control system access to vision of the end-effector from a target-centred frame of reference. Behavioural and neurophysiological evidence support the notion that, under many conditions, including normal, unrestricted vision as in the current experiment, reaching movements are coded in eye-centred coordinates. The Parietal Reach Area (roughly equivalent to MIP) is involved in comparing the target and hand positions in retinal coordinates. It may be involved in computing an estimate of the state of the arm in eye-centred coordinates (Beurze et al., 2006; Buneo et al., 2002; Crawford et al., 2004). Third, we found that gaze saccade onset was time-locked time-locking with peak hand acceleration in all conditions, in agreement with previous findings reporting that the kinematics of the hand movement determines when to shift gaze between landmarks (Johansson et al., 2001; Pelz et al., 2001). Namely, despite the shifts in the occurrences of peak acceleration between up and down movements, a saccade was triggered 125 ms before PA. Given that their durations did not exceed 70 ms, gaze was already on target at the beginning of the deceleration phase of the arm movement. It is generally believed that closed-loop visual control in pointing deceleration takes place to guide the hand to the target and that the first part of the movement, when the hand is accelerating, is open-loop or preprogrammed (Neggers and Bekkering, 2002). It could be worth validating this time-locking between saccade onset and PA when the kinematics is explicitly varied, for instance by asking subjects to move at different velocities.

Gaze movements may also play a role in the control of hand movement after the target has been identified (Andersen et al., 1998; Carey, 2000). The collision phase is an event that induces dynamic instabilities. We observed contrasting strategies between the two directions: longer fixations both before and after contact with the up target. We suggest that this prolonged fixation reflects the more challenging task of controlling an upward collision (larger LF integral, $p < 0.001$) possibly coupled with a greater risk of dropping the object (Mrotek et al., 2004). Similarly, Johansson et al. (2001) found that gaze entered the target zone before target contact and exited the zone after the initial contact occurred. They hypothesized that this strategy is implemented to maintain correlation between visual and somatosensory information and efferent copy signals required for motor planning. Therefore, we suggest that closing the visuo-manual loop by increasing the fixation after contact upwards is a strategy to specifically update the sensorimotor memory. We speculate that longer fixation times after contact would be required - at least in the first trials - in a collision task where critical parameters are altered such as stiffness of target or dynamic environment in order to adjust the motor system to the new constraints.

5.6 Appendix

In the collision phase, a tangential reaction force is responsible for transient signals measured in the transducers responses. We modeled the target-object-hand system with a mass-damper-spring system. The foam covering the target (coefficient of restitution of about 0.75) and the elastic properties of the skin can be modelled by a spring with stiffness coefficient k while viscous properties of the system are modelled by a dashpot with damping factor b (Fig. 5.7 A). The equation of motion of this simple unforced system results from a second order differential equation with dependent variable y (displacement), independent variable t (time) and system parameters m (mass), b and k:

$$m\frac{d^2y}{dt^2} + b\frac{dy}{dt} + ky = 0 \tag{5.8}$$

We solved Equation 5.8 to simulate the response of this overdamped system (initial condition $y(0) = 0$ and $\frac{dy}{dt}(0) = 1$ m.s^{-1}) for different values of k and b. We then computed the integral I of the absolute resultant force during the transient (a 70-ms window):

$$I = \int \left| m\frac{d^2y}{dt^2}dt \right| \tag{5.9}$$

Figure 5.7 B shows that for a given damping factor b, the integral of restoring force increases as a function of stiffness. Moreover, the stronger the damping (large b), the larger the absorbed energy and the smaller the released constraints measured on I. By analogy, the increase of GF induced an increment of stiffness and a decrement of damping, compatible with our model (Fig. 5.7 C). From these observations, we conclude that a compromise between stiffness and damping is calculated so as to absorb high frequency vibrations in the force signal at impact while optimising stability after collision.

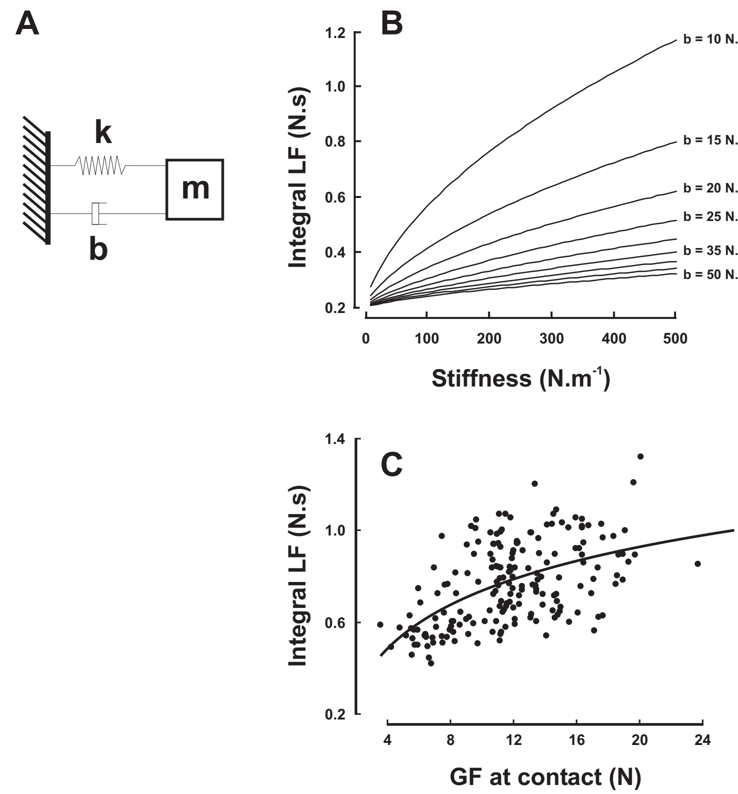

Figure 5.7: (A) A mass m (4 kg) is connected to the wall by a spring (stiffness coefficient k) and a dashpot (damping factor b). (B) Integral LF (Y axis) resulting from the simulation for initial conditions $y(0) = 0$ and $\frac{dy}{dt}(0) = 1$ m.s^{-1} for stiffness ranging from 0 to 500 N.m^{-1} (X axis) and damping factors from 10 to 50 N.s.m^{-1} (curves). (C) Data fit between GF at contact (X axis) and Integral LF (Y axis) for a restricted range of LF [19N - 29N] ($R = 0.52$, $p < 0.001$).

Chapter 6

Predictive grip for high impact loads in altered gravity

Statistics may be defined as "a body of methods for making wise decisions in the face of uncertainty".

W.A. Wallis

6.1 Abstract

In this study, we investigated the control of grip force (GF) when participants performed a targeted tapping task with a hand-held device toward an upper or lower target. The experiments were performed during parabolic flights (0, 1 and 1.8 g) where the inertial and gravitational components of the load could be separated. The task comprised a transport phase corresponding to the initial part of the movement and then a collision phase involving the period around the impact. First, we showed that GF control is anticipatory both during the transport and collision phases. There was a tight coupling between GF and load force (LF) in the transport phase. This coupling was based on predictive mechanisms and improved across parabolas. In the collision phase, there was a clear predictive control of GF that anticipated the sudden increase in LF at impact but the tight coupling between GF and LF disappeared. Second,

the microgravity condition revealed that subjects changed the mode of control of GF between the transport and the collision phases, around the time of peak hand acceleration. Third, the analysis of gaze-hand coordination revealed that the gaze generally moved ahead of the hand and that saccades were time-locked to the peak hand acceleration in all conditions, despite variability in the trajectories. Finally, the oculomotor strategy was adapted in order to provide optimal visual feedback of the controlled object around the collision, as demonstrated by longer duration of fixation in challenging conditions. In conclusion, altered gravity environments allowed to shed light on the mechanisms used by the Central Nervous System to coordinate gaze, hand and grip motor actions during a task that involves transport of an object and high impact loads.

6.2 Introduction

When we interact with our close environment, we often produce collisions between a hand-held object and the environment (*e.g.* cup - table). These activities involve first the transport of the mass and then the contact occurs. In such cases when load duration is very short as in impacts, prediction becomes critical. Several studies addressed the control of Grip Force (GF) when subjects had to cope with unpredictable or predictable collisions. In the first case, when unpredictable loads were applied to a hand-held object, an increase in GF after collision was observed and was attributed to a reflex (Johansson and Westling, 1988; Johansson et al., 1992a; Nowak et al., 2001; Turrell et al., 1999). In contrast, in self-generated impacts, although the peak GF was delayed 60 to 100 ms with respect to the collision Load Force (LF), there was clear evidence of GF pre-programming (Serrien et al., 1999; Turrell et al., 1999; White et al., submitted).

In a recent experiment, we further investigated how the Central Nervous System controls GF in a vertical collision task between a hand-held object and a target (White et al., submitted). We identified a transport phase during which LF varied smoothly with acceleration and a collision phase that involved the period around the impact. Whereas GF and LF were coupled in the transport phase in agreement with previous studies (Flanagan and Wing, 1993, 1995; Flanagan et al., 1993; Wing, 1996), this relationship disappeared in the collision phase. However, we evidenced a pre-programming of GF in the collision phase and ruled out a pure reflex mechanism. We also specifically studied the role of visual information in this task. In agreement with experiments that examined eye movements in dexterous manipulation (Johansson et al., 2001; Pelz et al., 2001), we found that gaze movements were triggered a fixed time before a precise kinematic feature in the hand trajectory, both in upward and downward movements. In addition, participants maintained longer fixation in the more challenging upward trials, where the object could drop from the grasp.

All the above experiments have been conducted in the Earth environment, where the motor system is calibrated to 1 g gravitational forces. In the present study, we extend this collision paradigm to microgravity (0 g) and hypergravity (1.8 g) to understand in greater depth how the central nervous system switches from the transport to the collision mode. A change in gravity allows to decouple the effects of acceleration (time-varying inertial force) and gravity (constant weight) on LF. Importantly, gravity affects more significantly LF during the transport phase than during the collision phase because the average level of LF is much lower in the transport phase than at impact. In new gravitational environments, we hypothesize that GF will still be pre-programmed both during the transport of the object and during the collision phase and we expect an adaptation of the feedforward GF control over trials. In addition, we test the influence of a change in the gravitational context on gaze-hand coordination by evaluating whether gaze and hand actions are coupled in the same way as they are in normal gravity. In particular, we also assess the role of visual feedback in this demanding collision task.

6.3 Methods

6.3.1 Manipulation of gravitational context

The experiments took place in the Airbus A300 ZEROg aircraft on three flights out of Bordeaux (France) during which a total of ninety parabolas were performed. A single parabolic flight profile generated a sequence of episodes of normal (1 g), hyper (1.8 g), micro (0 g), hyper (1.8 g) and normal (1 g) gravity of about 20 seconds duration each (Augurelle et al., 2003). Thirty parabolas were performed in each of the three flights blocked in three groups of ten parabolas with 2-minute pauses of 1 g flight between each parabola plus an extra 5 to 8 minutes between each block. Three participants were tested on each flight, during the first, second and third blocks of ten parabolas. A three dimensional accelerometer fixed on the floor of the aircraft recorded its acceleration along its fore-aft axis, its lateral axis and the axis normal to the floor.

6.3.2 Experimental procedure and equipment

Nine right-handed volunteers (22 to 48 years old) 3 of whom were female, participated in the study. Their health was assessed by their various National Centres for Aerospace Medicine as meeting the requirement ("Jar Class II") for parabolic flight. No participant reported sensory or motor deficits. None had previously experienced parabolic flight. All participants gave their informed consent to participate in this study and the procedures were approved both by the European Space Agency Safety Committee and by the local ethics committee. Of the nine participants, two experienced nausea during the flight and were not included in the analyses as they did not complete data collection.

The participant was secured by a seat belt on a chair. Briefly, participants grasped a test object with a precision grip and performed a targeted tapping task with the manipulandum, on each trial moving from a start position up or down to tap an upper or lower target and then return back to the start position. A series of auditory tones prompted movement towards the upper (high tone) or lower (low tone) target and occurred at random between 300 and 500 ms after completion of the previous movement. The two circular targets (75 mm diameter), cushioned with high density foam to limit the impact, were mounted 283 mm above and below the start position on two horizontal crossmember of a rigid square frame. A red mark, vertically midway between the two targets, indicated the start position (see White et al. (submitted) for details).

The cylindrical test object (82 mm diameter, 30 mm wide, 212 g mass) was equipped with two parallel force-torque sensors (40 mm diameter , Mini 40 F/T transducers, ATI Industrial Automation, NC, USA) which measured the three force components (F_x, F_y, F_z) along the axes passing through the centre of the corresponding grasp surface. A PXI controller (PXI-8156B) equipped with a 12-bit PXI-6071E analog-to-digital converter (National Instruments, Austin, TX, USA) recorded the synchronized signals from the force sensors at a sampling rate of 1 kHz. In addition, simultaneous horizontal and vertical recordings of both eyes were made with the Chronos head mounted video-based eye tracker at 200 Hz (Clarke et al. (2002), CHRONOS VISION GmbH, Berlin, Germany). A second video-based device (OptoTrak 3020 system, Northern Digital, Ontario, Canada) tracked three infrared-light-emitting diodes (IREDs) on the Chronos helmet to reconstruct the gaze orientation (Ronsse et al., 2007) and three others on the hand-held device. The positions of the six IREDs were sampled at a frequency of 200 Hz with a resolution of 0.1 mm within the working environment. The Chronos eye-tracker and the OptoTrak were triggered by the PXI controller.

The experiment was first carried out on the ground in order to train the participants. Each participant performed 5 blocks of at least 40 randomised up and down collisions. Then each participant performed the task over 10 complete parabolas in the aircraft. The data analysed corresponded to the first 1 g and 1.8 g phases, plus the 0 g phase, of each parabola.

6.3.3 Data processing

All the signals were synchronized and linearly interpolated to the same sampling rate (1 kHz). The total grip force (GF) was calculated as the average of the normal forces applied by the thumb and the fingers on each transducer. The magnitude of the tangential load force (LF) was computed as:

$$LF = LF_1 + LF_2 \tag{6.1}$$

with:

$$LF_i = \sqrt{F_{x,i}^2 + F_{x,i}^2} \tag{6.2}$$

where $F_{x,i}$ and $F_{y,i}$ are the horizontal and vertical components of the load force of transducer i ($i = 1, 2$) respectively. The impact force was obtained by averaging values of 3 samples centred on the maximum of LF.

Saccades were detected using an acceleration threshold of 500 deg/s^2 subject to visual checking. For each trial, we determined the following timings: onset for the saccade towards the target (ST_{onset}) and time of arrival at the target (ST_{land}), and onset of the saccade from the target back to the home position (SH_{onset}) and time of arrival at the home position (SH_{land}). Duration of target fixation was computed by subtracting the time of saccade landing on the target from the time of saccade onset back to the home position ($SH_{onset} - ST_{land}$). Gaze position was reconstructed by combining independent eye-in-head and head-in-space positions following standard linear algebra operations (Ronsse et al., 2007).

The geometric centre of the manipulandum was calculated from the three IRED positions. Instantaneous velocity and acceleration were obtained using a 5-point central-difference algorithm. Hand movement onset (HO) was defined at the first sample at which the absolute acceleration exceeded 2.5 m.s^{-2}. The contact time (TC) was detected from the load force trace when the impact force sharply increased during the compression of the high density foam covering the target. Kinematic measures included both the spatial location and time of hand movement onset (HO), peak acceleration (PA) and peak velocity (PV).

The grip force and load force were averaged over 10 ms centred at each of the previously mentioned times (HO, PA, PV) or over 10 ms preceding the contact (TC) to avoid artefacts. Additionally, the grip force maximum (GF_M) and its time of occurrence were measured. They corresponded to the maximum in GF occurring at least 15 ms after the contact (on average 71.8 ± 32.7 ms).

A three-way ANOVA was performed on variables of interest to test the effects of direction (UP or DOWN), gravity condition (0 g, 1 g, 1.8 g) and repetition across the ten parabolas. Main and interaction effects were further analysed using Scheffé post hoc procedure (alpha level was $p < 0.05$). All the statistical analyses were conducted with Statistica 6.0 (StatSoft).

6.3.4 Inertial and gravitational components of the load

By Newton's second law:

$$\sum \vec{F}(t) = m\vec{a}(t) \tag{6.3}$$

During the transport of the object, this total force is the resultant between a constant gravitational term (mg) and the load force LF:

$$\sum \vec{F}(t) = m\vec{a}(t) = m\vec{g} + \vec{LF}(t) \tag{6.4}$$

By projecting the vectorial quantities on the vertical axis, we get:

$$mg + ma(t) = LF(t) \tag{6.5}$$

Therefore, in 1 g and 1.8 g phases, upward accelerations ($a > 0$) lead to larger load forces and downward accelerations ($a < 0$) result in decreased load forces with respect to the object's weight. The 0 g phase is a particular case: since the gravitational component (mg) disappears, LF is now directly proportional to acceleration.

6.4 Results

Illustrative collisions with the upper (left) and lower (right) target in microgravity (0 g) are shown in Figure 6.1. In the upward collision, the vertical position trace increased until the manipulandum came into contact with the target at TC and then decreased 100 ms after contact to return to the position at the start. The velocity trace exhibited a single peak (PV) and was truncated at target contact, where the velocity dropped sharply to zero. Following HO, the acceleration trace reached a maximum (PA) before decreasing to negative values, indicating that the object was decelerated just before contact. At collision the acceleration exhibited a large (off-scale) negative value followed by fluctuations reflecting interaction with the target. Then, a smaller negative acceleration was associated with the initiation of the return movement. A final positive acceleration phase brought the movement to a halt back at the home position. The load force trace (LF) varied with acceleration in the transport phase (Eq. 6.5). In the collision, LF increased sharply to a (off-scale) value around 21 N. After passing through a negative peak terminating at end of contact, the LF trace again paralleled the acceleration. With the exception of a short period of artefact immediately after the collision, the grip force (GF) increased during transport and reached a maximum after the collision (GF_M). An upward saccade (ST_{onset} to ST_{land}) was triggered to the target near hand onset. After a period of fixation, a return saccade (SH_{onset} to SH_{land}) was executed to foveate the home position. Downward collisions mirrored upward movements in that the vertical position trace decreased until TC and increased some 100 ms after contact to return to the starting position.

Importantly, the acceleration profiles in microgravity (Fig. 6.1, acceleration) appeared symmetric between upward and downward movements. In particular, the absolute value of PA were the same (Fig. 6.1, acceleration, PA, $p > 0.999$). Consequently, the LF at PA were also equivalent in both directions (Fig. 6.1, LF, LF_{PA}, $p > 0.178$).

6.4.1 Grip force strategy in transport and collision phases

In order to ensure a stable grasp through the collision task, participants, first, had to cope with inertial forces arising from the transport of the object, and second, had to counteract the impact forces at collision. The former are relatively low forces distributed over several hundreds of milliseconds around PA. The latter have impulse characteristics with large amplitude and last an order of magnitude shorter. Figure 6.2 shows the relationship between GF and LF at PA in the transport phase (Fig. 6.2, A-B) and at impact in the collision phase (Fig. 6.2, C-D) in upward (closed disks) and downward (open disks) movements in 0, 1 and 1.8 g. A fourth factor (GF or LF) was included in the ANOVA to quantify the degree to which patterns of GF and LF were statistically similar.

In the transport phase, we observed similar PA in both directions, for a given gravity level ($p > 0.987$). Since ma and mg are additive and subtractive in upward and downward movements respectively (see Eq. 6.5), the LF at PA was larger upwards than downwards in 1 and 1.8 g (Fig. 6.2 A, 1 and

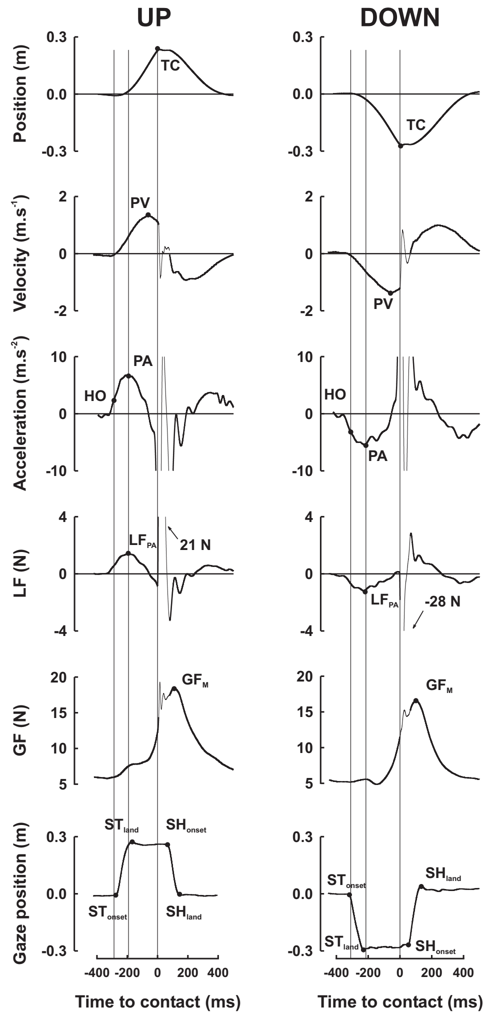

Figure 6.1: Typical collisions in microgravity. Records of a single collision upwards (left column) and downwards (right column) in 0 g. The following traces are shown as a function of time: the vertical position, the vertical velocity and the vertical acceleration of the object, the load force and the grip force, and the vertical gaze position. The left vertical thin line is aligned with hand onset (HO). The middle thin line is positioned at peak acceleration (PA). The right thin line signals the contact with the target (TC). The dimmed parts of the curves depict the transient zone. The labels PV, LF_{PA}, GF_M, $SH/T_{onset/land}$ denote peak velocity, LF at PA, GF Maximum and saccade onset/landing to/from Home or Target, respectively.

1.8 g). In contrast, in 0 g, equivalent PA and the absence of weight led to similar LF (Fig. 6.2 A, 0 g). Remarkably, we found that the effects of direction and gravity on GF at PA (Fig 6.2 B) were broadly parallel to those for LF (4-way ANOVA, $p > 0.288$). Moreover, there were reliable within-condition correlations between GF and LF at PA in every gravity fields ($R = 0.52$ to $R = 0.66$, $p < 0.001$).

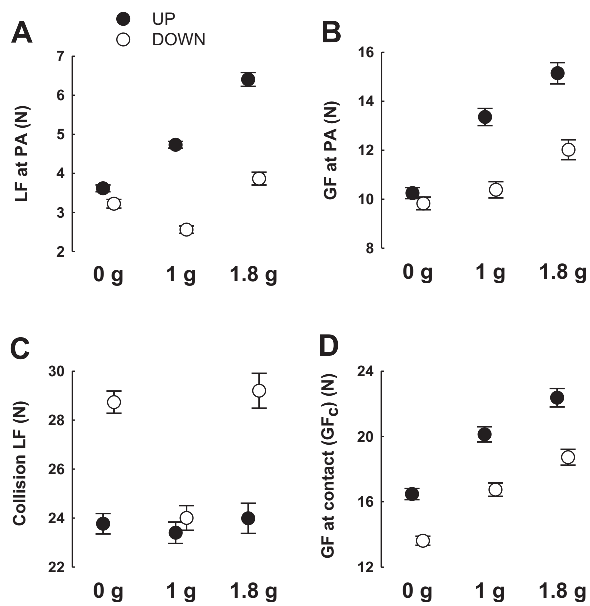

Figure 6.2: GF-LF coupling in transport and collision phases. Load force (A) and grip force (B) at peak acceleration. Collision load force (C) and grip force at contact (D). Closed and open disks represent upward and downward movements respectively, in 0, 1 and 1.8 g. Error bars represent SE.

In the collision phase (Fig. 6.2, C-D), participants produced similar impacts in both directions in 1 g ($p > 0.915$) but not in 0 and 1.8 g ($p < 0.001$) (Fig. 6.2 C). In contrast with the transport phase, there was no clear coupling between GF and LF at collision (Fig. 6.2 C-D, 4-way ANOVA, $p < 0.002$). Specifically, in 0 and 1.8 g, participants produced larger collision LF downwards but exerted larger GF upwards. The most remarkable aspect resides in the different patterns of LF across conditions (compare Fig. 6.2 A and C, 4-way ANOVA, $p < 0.002$) and the similarity in GF patterns (compare Fig. 6.2 B and D, 4-way ANOVA, $p > 0.05$) between transport and collision phases.

Finally, it is worth mentioning that in agreement with previous studies (Augurelle et al., 2003; Hermsdorfer et al., 2000), the correlation between GF and LF at PA improved across parabolas during the transport phase ($p < 0.05$). In contrast, no reliable learning was found between GF and LF at collision ($p > 0.662$).

Since the GF must counteract the constraints during both transport and collision phases in the three gravitational fields, it would be interesting to extend our analysis to other kinematic events than PA and collision.

6.4.2 Microgravity dissociates transport and collision phases

Figure 6.3 presents the values of GF at different epochs in the trajectory for upward and downward collisions in microgravity (left panel, 0 g), normal gravity (middle panel, 1 g) and hypergravity (right panel, 1.8 g). Time zero defines the time of contact (TC).

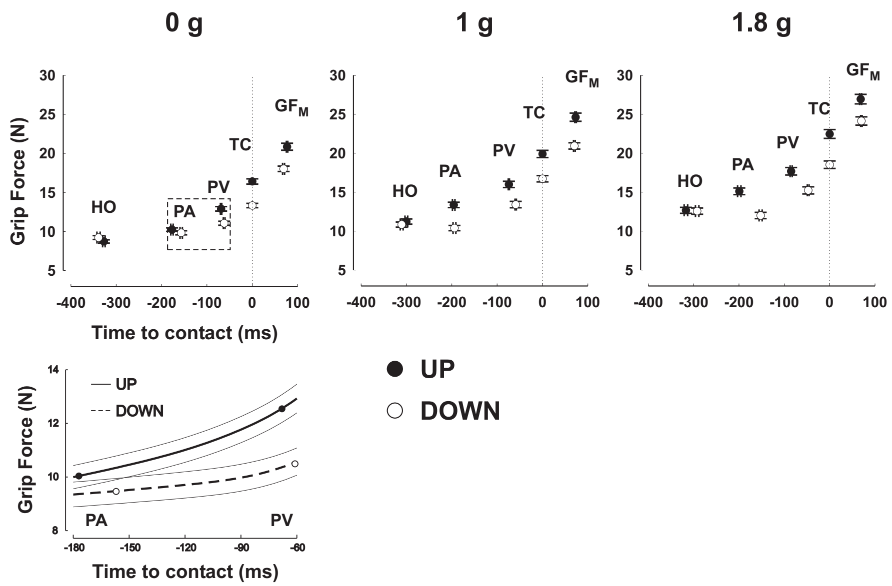

Figure 6.3: Grip force in function of time to contact in upward (closed disks) and downward (open disks) movements in 0 g (left panel), 1 g (middle panel) and 1.8 g (right panel). The means and SE of GF are reported for the following occurrences: hand onset (HO), peak acceleration (PA), peak velocity (PV), time of contact (TC) and grip force maximum (GF_M). The horizontal standard error bars quantify the variability in the time of occurrence of the events. The vertical dotted line is positioned at contact. The dashed box in the 0 g panel enlarges the GF profile averaged over 2-ms bins between PA and PV. The solid and dashed lines in the enlargement report upward and downward collisions, respectively. The thin lines around mean GF traces are 95% CI.

In 1 g (Fig. 6.3, central panel), GF at hand onset (HO) was the same in both directions ($p > 0.971$). At peak acceleration (PA), the directional bias due to gravity induced a larger LF upwards compared to downwards ($p < 0.001$) and led to proportionally larger GF upwards ($p < 0.001$). Then, participants exerted a larger GF upwards in the remaining part of the trajectory (at PV, TC and GF_M, $p < 0.001$).

The behaviour in 1.8 g (Fig. 6.3, right panel) was close to the behaviour in 1 g: GF was similar at HO ($p > 0.999$) and then remained larger upwards (GF at PA, PV, TC and GF_M: $p < 0.03$). Note that the PA occurred earlier in upward compared to downward movements ($p < 0.001$) which reflects differences in the kinematics of opposite movements.

In 0 g, participants also exerted similar GF in both directions at hand onset (Fig. 6.3, HO, left panel, $p > 0.884$). Since trajectories were symmetric, similar LF were generated in opposite movements at PA ($p > 0.178$) and GF was the same in both directions (at PA, $p > 0.959$). Interestingly, the two GF profiles diverged significantly starting from 150 ms before TC ($p < 0.05$, see enlargement in Figure 6.3). Then, the GF remained larger in upward trials (at PV, TC and GF_M: $p < 0.008$). It is also worth to report that as in 1.8 g, PA occurred later with respect to movement onset for downward movements ($p < 0.001$).

In sum, a common characteristic in the GF profile across the three gravitational fields resides in a dramatic increase of GF prior to collision with GF systematically larger in upward movements, even in microgravity. In addition, the divergence in GF after PA between up and down movements in 0 g highlights a dissociation between the transport and the collision phase.

6.4.3 Pre-programming of grip force

A maximum in grip force (GF_M) was observed in all conditions following impact. We also tested whether GF_M was pre-programmed by using a multiple linear regression to determine its correlation with the grip force at contact (GF_C) and first derivative of grip force at contact (dGF_C/dt):

$$GF_M = aGF_C + 0.037b\frac{dGF_C}{dt} + c \tag{6.6}$$

We found that GF_M was accurately predicted in all conditions by these two variables calculated before the contact ($p < 0.001$). While the coefficients depended on the condition ($a = 0.83$ to 0.89, $b = 0.03$ to 0.05 and $c = 1.92$

to 5.05), the most significant term was always proportional to GF_C (partial R ranged from $R = 0.83$ to 0.95) and the second term contributed secondarily in Equation 6.6 (partial R ranged from 0.59 to 0.81).

6.4.4 Gaze saccades onsets are time-locked to peak hand acceleration

In this section, we investigate whether the oculomotor strategy is also influenced by the experimental context by analysing gaze-hand coordination and duration of target fixation.

Firstly, we tested how gaze and hand reaction times to the prompted tone varied with direction and gravity. We observed increased hand reaction times in upward collisions in 1 and 1.8 g but also in 0 g despite the absence of gravity (Fig. 6.4 A, $p < 0.04$). For a given direction of movement, no difference was found across 0, 1 and 1.8 g (Fig. 6.4 A, $p > 0.3$). In addition, since we measured shorter gaze latencies than hand reaction times in the majority of trials, the gaze led the hand by some 80 ms on average.

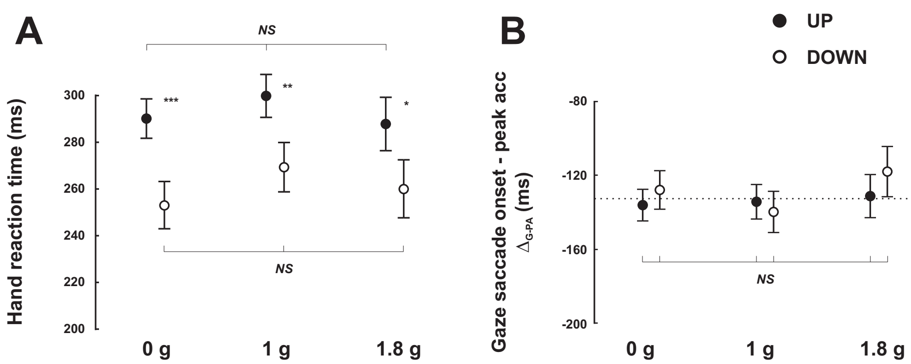

Figure 6.4: Eye-hand coordination. Hand reaction time (A) and gaze leads with respect to peak acceleration (B) in upward (closed disks) and downward (open disks) movements in 0, 1 and 1.8 g. The dashed line on D is the mean value of the corresponding latency. Error bars represent 95% CI (*** = $p < 0.001$, ** = $p < 0.01$, NS = Non Significant).

In order to examine gaze-hand coordination in greater depth, we defined saccade latencies with respect to peak hand acceleration (PA):

$$\Delta_{G-PA} = R_G - R_{PA} \tag{6.7}$$

where R_G is the gaze saccade reaction time and R_{PA} is the elapsed time between the prompted tone and the occurrence of PA. In the above expression, negative values of Δ_{G-PA} mean that the gaze initiated a saccade before the hand reached its PA. Strikingly, we observed a constant gaze lead across all conditions (Fig. 6.4 B, $\Delta_{G-PA} = 132.6 \pm 83.5$ ms, $p > 0.108$). Thus, the saccades were triggered a constant amount of time before the hand reached PA, despite variability in its occurrence. Moreover, further analyses reported that this time-locking did not hold with any other kinematic characteristics in the trajectory (HO, PV, TC or GF_M). In conclusion, the gaze moved ahead of the hand in the majority of conditions and saccades were time-locked to PA in all conditions.

When generating high impact loads, collecting information is essential to maintain a control on the hand-held object and is strengthened by the new gravity conditions. Thus we concentrated on target fixation as a function of time to contact (Fig. 6.5). Participants elicited a gaze movement to the target on average 241.1 $\pm$ 84.1 ms before the collision. In contrast, two clear effects can be highlighted in the durations of fixation after contact. First, in every gravity field, the duration of fixation after contact in upward movements was longer than downwards ($p < 0.001$). This duration increased by an equivalent amount in the three gravity levels (56 ms, $p > 0.26$). Second, for a given direction of movement, this duration of fixation was the shortest in 1 g, compared to 0 and 1.8 g ($p < 0.05$). Therefore, participants coordinated their gaze in order to allow vision of the collision: the gaze landed on the target in advance of the contact, and maintained fixation until after the impact occurred. In addition, the duration of fixation after contact increased in the more challenging conditions, in particular, in new gravity fields and in upward movements Interestingly, this duration of fixation did not decrease with repetition of the task ($p > 0.05$). Altogether, we showed that the oculomotor strategy was influenced by the experimental context.

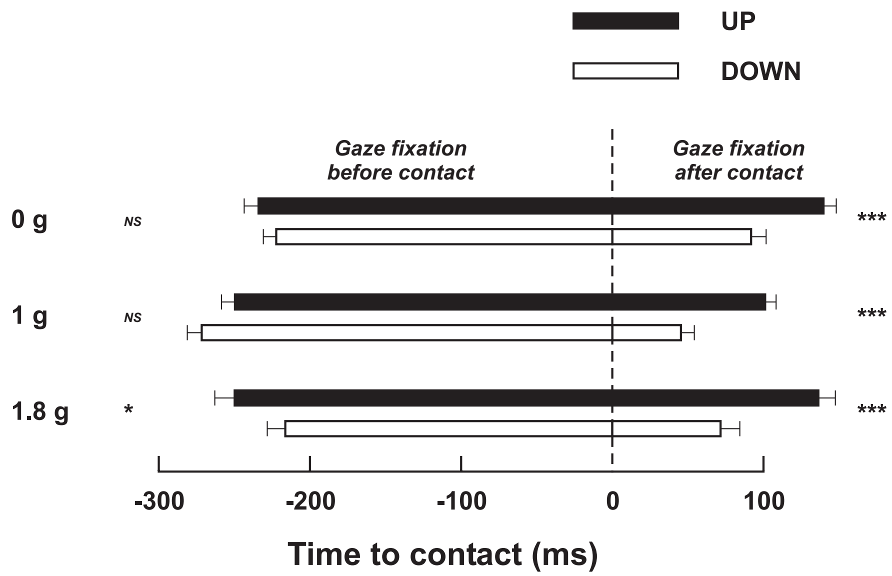

Figure 6.5: Duration of target fixations. Duration of target fixations relative to contact in upward (open rectangles) and downward (closed rectangles) movements, in 0, 1 and 1.8 g. The vertical dashed line denotes time of contact. Error bars represent 95% CI (* $= p < 0.05$, *** $= p < 0.001$).

6.5 Discussion

An increasing number of studies have employed grip force (GF), used to stabilise a hand-held object against load force (LF) tending to destabilise grip, as an index of prediction in the control of voluntary movement. Various studies have shown anticipatory adjustment of GF for different forms of LF including those dependent on position, velocity and acceleration, and with impulsive as well as smoothly varying profile (see for example Augurelle et al. (2003); Flanagan et al. (2003); Nowak and Hermsdorfer (2006); Turrell et al. (1999).

In this study, we investigated the control of GF in active collisions during parabolic flights which allowed us to examine the separate effects of inertial and gravitational components of LF. The task comprised initially a transport phase corresponding to the initial part of the movement and then a collision phase involving the period around the impact. First, the results confirmed a predictive control of GF during both the transport and the collision phases. The GF-LF coupling during the transport phase held true and improved across parabolas but we showed a strong dissociation between GF and LF at collision, with no improvement across trials. Second, microgravity allowed us to decouple the transport and the collision components from the whole GF profile. We demonstrated that the two strategies diverged some 150 ms before contact (around peak hand acceleration, PA). Third, the analysis of gaze-hand coordination revealed that the gaze generally moved ahead of the hand and that saccades were still time-locked to PA in all conditions, despite variability in the trajectories. Finally, participants adapted their oculomotor strategy to the context by increasing the duration of fixation in the most challenging conditions.

6.5.1 Microgravity highlights a switch from transport to collision modes

In the transport phase, the tight coupling between GF and LF evidences predictive control of GF as a function of LF, whatever the direction of movement and gravity level. This is in agreement with previous studies obtained in altered gravity where participants adjusted their GF according to the LF in vertical point-to-point (Nowak et al., 2001) and rhythmic movements in steady gravity phases (Augurelle et al., 2003) and even during abrupt gravity transitions (Hermsdorfer et al., 2000). However, participants programmed the collision phase differently from the transport phase as revealed by the clear dissociation between GF and LF which contrasted with their tight coupling during transport. Indeed, GF increased progressively in anticipation of the impact and reached a maximum after contact, whatever the direction of movement and the gravity environment. Further evidence for pre-programming is supported by our regression analysis which predicts GF_M on the basis of GF and GF rate before contact (Eq. 6.6).

The microgravity conditions allowed us to further investigate how the CNS programmed GF in the transport and the collision phases. On the one hand, in opposite movements performed in 0 g, participants exerted similar GF against similar LF generated by a mass being moved at equivalent magnitude of acceleration. Therefore, the GF profile contained the same transport component in up and down trials. On the other hand, the impacts were asymmetric upwards and downwards (see Fig. 6.2 C, 0 g), leading to different collision phases. Therefore, the divergence in GF profiles between the two directions some 150 ms before contact highlights the transition between the two phases. Indeed, since LF monotonically decreased between PA and TC in both directions (see LF on Fig. 6.1) the increase in GF can only be explained by a change in the strategy to anticipate the high impact loads and not by solely a transport strategy, where GF and LF should be coupled.

A striking observation in altered gravity (0 and 1.8 g) is the larger collision LF downwards. Surprisingly, our results demonstrate that participants did not adjust GF with collision LF but exerted larger GF upwards. It could be hypothesized that participants anticipated eventual symmetric impacts in both directions, and predictively adopted GF patterns as in 1 g. Although it can be argued that larger GF in upward collisions is a strategy to minimize a higher risk of dropping the object (Mrotek et al., 2004), it is however questionable as to why this GF asymmetry still persists in 0 g where potential slips are equally probable in both directions. We suggest that participants did not train enough to learn to control their actions, which is supported by conclusions reported in similar paradigms (Papaxanthis et al., 2005). Therefore, similar experiments are required in long term weightlessness environment to assess long term learning of GF-LF coupling during collisions.

6.5.2 A conceptual internal model of eye-hand coordination during a collision task

Figure 6.6 proposes a hypothetical model to describe how the CNS coordinates gaze, hand and GF motor actions during the transport of the object and at the collision.

First, given an estimate of gravity and an intended direction of movement (Target), a hand action is prepared together with a gaze saccade. It is well established that pre-programming hand actions is completed during the reaction time (Dubrowski et al., 2000). We reported that hand reaction times were influenced by direction. A similar effect has already been shown in horizontal arm movements at different eccentricities (Flanagan and Lolley, 2001) and also during collision (White et al., submitted). However, it is unlikely that this reflects a neuromuscular delay due to an increased gravitational torque upward, because it persisted in 0 g and did not increase in 1.8 g, (see Fig. 6.4 A). We therefore suggest that these longer latencies in upward movements might be a sign of preparation of a more complex motor program.

Second, participants calibrated their hand and gaze actions so as to invariably have a constant delay of about 130 ms between the peak hand acceleration and gaze saccade onset, despite important variability in their occurrences. Such a strategy allows visual feedback of the hand approaching the target in the slowing down part of the movement (Binsted et al., 2001). In addition, this constant time-locking across conditions strongly supports that arm and eye movements are closely coordinated by the CNS (Nanayakkara and Shadmehr, 2003; Saunders and Knill, 2003).

Third, provided an efference copy of the arm motor command, a forward model predicts the LF that will be generated at the fingertips as a consequence of kinematics. This forward model must also have access to an estimate of gravity. Indeed, two equivalent motor commands will induce different LF at the fingertips in, say, 1 and 1.8 g environments. A central representation of gravity in the CNS is also supported by a recent study analysing kinematic and dynamic features of arm movements (Gentili et al., 2007). The role of this forward model is to predict the required GF according to the phase of the movement, *i.e.* transport or collision. This distinction depends on current time with respect to the occurrence of PA. Therefore, if current time is before time of PA, then, a reliable linear relationship can predict the required GF from LF during transport. In contrast, after time of PA, GF could not be predicted from LF anymore near the collision. In sum, the CNS is able to predict when a switch between transport and collision strategies has to be operated, taking into account the occurrence of PA, which is embedded in the efference copy of the arm motor command.

Finally, feedbacks are necessary to control the movement and for learning, especially in new conditions. A classical view of reaching movements consists of two phases: a fast initial phase that is primarily open loop, and a slower adjustment phase under the guidance of sensory feedback (Jeannerod, 1988). Direct visual control of the hand may be of particular interest in manipulation tasks executed under vibration (Martin et al., 1991) that can be induced by collisions, for instance. Indeed, high frequencies perturb tactile and proprioceptive information (Lackner and DiZio, 1992; Roll et al., 1989). On the one hand, visual feedback can be used to update the motor program during the movement since gaze lands on the target some 250 ms before the contact occurs (Kawato, 1999; Saunders and Knill, 2003). On the other hand, longer duration of fixation after collision (especially upwards) can update the mapping between motor commands and their consequences in the collisions (Johansson et al., 2001; Sailer et al., 2005; White et al., submitted). The fact that in all conditions, the duration of fixation did not decrease with trials supports the idea that the role of visual feedback is not diminished with practice. Indeed, Starkes et al. (2002) suggested that participants learn to make better use of visual information and use online processing to optimize movements in term of physical energy and stability.

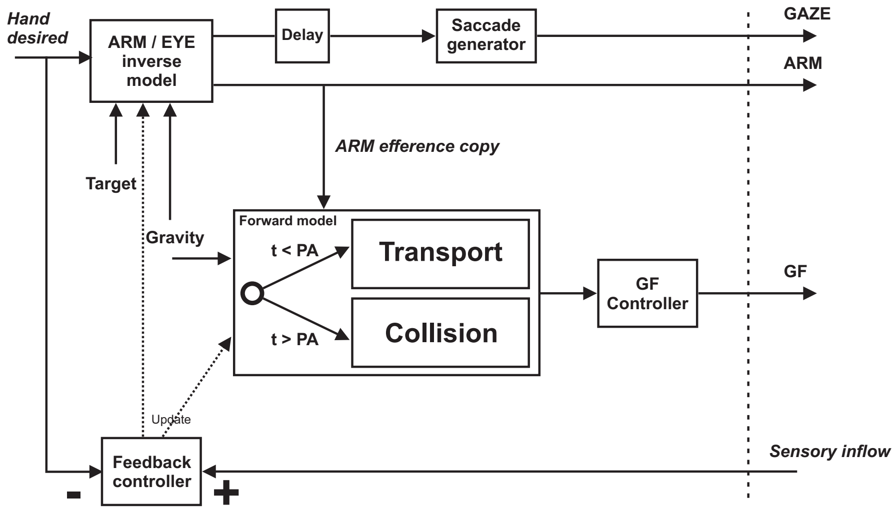

Figure 6.6: Conceptual model of eye-hand-grip coordination during a collision task. A desired hand trajectory together with an estimate of target position and ambient gravity is sent to an inverse model that issues a delayed saccade and an arm motor command. An efference copy of this arm command is sent into a forward model that computes the adequate GF, in function of the current mode. If time is before the estimated occurrence of Peak Acceleration (PA), an internal model reliably computes GF in function of LF. If time is after the estimated occurrence of PA, the GF cannot be predicted anymore with LF, in the collision mode. Sensory inflows are fed back in a controller that can correct the last part of the trajectory and updates the inverse and the forward models.

Chapter 7

Conclusions and perspectives

> There are three kinds of lies: lies, damned lies, and statistics.
>
> Mark Twain

The ability humans have to perform skilled actions is the result of adaptive changes in hands, feet, limbs and by the elaboration of the motor control system of the brain that evolved during several millions of years (Mountcastle, 2005). For instance, observing one's hands in action reveals the adroit manipulative capacity of the human, a skill of a different order from that any monkey displays. An important feature of the human hand is its muscled thumb. One of the most obvious manipulations is the opposition of thumb and fingertips - precision grip - which is regarded as an important structural adaptation in human evolutionary history (Napier, 1956). The analysis of grip force is powerful: it provides a window into the working of the human nervous system dedicated to the control of movement. Since the control of grip force is largely anticipatory, the influence of movement kinematics and dynamics on this control gives an indication of what the nervous system can and cannot anticipate.

7.1 Main findings

During their life, people learn to interact with their surrounding Newtonian environment and then calibrate their sensory motor system by experiencing causality between movements and sensory inputs. The omnipresence of gravitational attraction is deeply integrated in our everyday actions.

In this work, we had the unique opportunity to break the very strong link between weight and inertia by modifying the gravitational attraction in parabolic flights. We were able to test the robustness and versatility of internal models that control the grip force on an hand-held object when faced with new dynamic environments in a variety of dexterous manipulations. Rhythmic movements involve different neural mechanisms than discrete movements although their formal separation still remains unclear (Schaal et al., 2004). In the first three chapters we focused on GF/LF modulation in rhythmic movements as well as on more general aspects linked to efficiency of upper limb periodic motion. In the last two chapters, we turned to discrete tasks.

Before entering into more details, let us briefly summarize the main contribution of this work. In the first study (Chapters 2), we investigated a general issue related to the control of rhythmic upper limb movements in the light of mechanical properties of oscilators. In particular, altered gravity environments allowed us to draw an hypothesis to explain why movements are slowed down when gravity decreases. In the next two experiments (Chapters 3 and 4), we analysed GF/LF modulation when participants performed cyclic upper limb movements with an hand-held device. We investigated how the gravitational and inertial components of the load are treated by the internal models used to predictively control the grip force. The last two paradigms investigated how subjects controlled GF in a discrete task that involved the transport of a mass toward a target in a normal Earth environment (Chapter 5) and then in 0 and 1.8 g (Chapter 6). In this context, they had to cope with slow varying inertial forces arising from the transport of the object, and then, had to counteract the abrupt impact forces at collision. The extension to altered gravity environments allowed to shed light on the mechanisms used by the Central Nervous System to coordinate gaze, hand and grip motor actions during a task that involves transport of an object and high impact loads.

Central Pattern Generators (CPG) are known to be involved in low-level activities like walking or chewing in humans whereas rhythmic upper limb movements are much more controlled by higher brain centres than in other mammals (Marder, 2000). Like oscillators, CPG generate antiphase oscillations in the electrical activity of two groups of neurons, which alternately drive a pair of antagonist muscular groups, to induce periodic motion. A periodic system that runs at resonant frequency exchanges energy with the environment optimally. We provided evidence that CPG behave like a simple pendulum to drive efficiently the rhythmic movements, except in 0 g, where a higher level strategy takes over. Overall, we showed in Chapter 2 that changes in gravity are taken into account by the central nervous system to sustain efficient rhythmic movements. Our hypothesis reconciles contradictory findings regarding the slowing of movements in microgravity (Fisk et al., 1993; Mechtcheriakov et al., 2002).

The robust GF/LF coupling is described by a framework that contains both inverse and forward models of the arm. The inverse component predicts the required motor command to generate the intended kinematics. The forward module estimates the magnitude of the LF at the fingertips, in order to program an adequate GF (Flanagan and Wing, 1997; Kawato, 1999). Our first study gave more insights into the working of these internal models. First, we showed in Chapter 3 that hand and arm motor commands are independent, a result that has recently been confirmed (Danion, 2004; Descoins et al., 2006). Second, we provided further evidence that the forward model predicting the load can be adjusted to account for various physical contexts. This is compatible with the fact that given a context, we select the most appropriate inverse-forward module (controller-predictor) (Haruno et al., 2001) following Bayesian rules (Kording and Wolpert, 2004). Third, the controller that regulates GF is so precise that it takes into account even the subtle asymmetries in kinematics of vertical arm movements that are transmitted to LF. Finally, although shown qualitatively, the GF controller discriminates the source of the load (gravitational versus inertial) as reported by different GF exerted against similar LF but that were generated with different combinations of inertial and gravitational contributions. Our second study in Chapter 4 quantified the above results in 1 g in a simple model. Current investigations exploit data in parabolic flights to refine this model with real gravity as an input.

Whereas rhythmic movements constitute a significant proportion of our activities (*e.g.* handling a hammer, stirring into a pan, brushing our teeth), we also perform many discrete movements (*e.g.* displace an object), or a combination of the two. In addition, we interact with the close environment by inducing smooth or straight contacts, that sometimes challenge grasp stability. In Chapter 5, we designed a control experiment to characterize the task in a normal gravitational environment (1 g), to investigate the control of GF during active collisions. We identified two distinct phases in its planning. On the one hand, low forces generated during the transport phase were counteracted by the GF following similar rules as previously shown (Flanagan and Wing, 1993, 1995; Flanagan et al., 1993). However, during the collision phase that involved the period around the impact, GF was programmed to reach its maximum shortly after impact and was therefore not coupled to peak LF anymore. We suggested that the optimal adjustment of GF results from a compromise to avoid slippage and to damp the vibrations following impacts. This has been justified with a mass-damper-spring system modelling the finger/object interface. In addition, gaze behaviour was optimised to provide vision of the decelerating object in a target-centred reference frame and to allow visual feedback of the collision phase, especially in the more challenging upward trials, by increasing the fixation after contact. We concluded that participants adopted a strategy to update the correlations between motor outflows (efference copies) and their sensory consequences in order to refine their GF pattern in subsequent trials. In Chapter 6, we conducted the same experiment in parabolic flights and refined the dissociation between the transport and the collision phases in microgravity. In addition, the oculomotor strategy was strongly influenced by the direction of movement and the gravitational environment. Increased duration of gaze fixations in 0 and 1.8 g as well as longer hand reaction times in upward movements reflected the difficulty to perform upper collisions in unknown gravity environments. Finally, we showed that the timing of peak acceleration might play an important role in coordinating gaze and hand movements, and in delimiting the transition between the transport and collision modes. This strongly suggests that the eye motor system has access to an internal representation of the motor command of the arm, taking into account the action of gravity. We proposed a hypothetical model to describe how the CNS coordinates gaze, hand and GF motor actions during the transport of the object and at the collision. The obtained results clarified how the CNS coordinates arm and gaze actions to control GF in more natural dexterous manipulations.

The overall contribution of this work is to stress the importance of gravity in the neural mechanisms that guide our actions. Despite the fact gravity is usually a constant parameter throughout our lives for most of us, it is centrally represented in motor programs (Indovina et al., 2005; Papaxanthis et al., 1998). Humans learned to make the most of this force field when performing accurate skilled actions. In that sense, gravity is not a perturbation but takes an active part in the optimization process that governs our movements. Finally, it is worth mentioning that our experiments in hypergravity (1.8 g) could usually be viewed, after some adaptation, as an extrapolated version of behaviour in 1 g, by applying a gain. In contrast, microgravity (0 g) led to completely new observations. In the first case, the gravitational term is still present in the expression of the constraints. In microgravity the consequences of an acceleration induced to an object has to be learned without the action of gravity. Therefore, structurally different equations must be integrated in the nervous system. Illustrating this assertion, the Chinese Astronaut[1] reported during his recent visit to Brussels that when confronted with the problem of manipulating massive objects in a weightless environment: "*You don't move the object; it is the object that moves you*".

7.2 Future prospects

From this point, it is tempting to suggest further experiments to address open questions that are directly linked to this thesis in order to further understand the strategies implemented in the CNS to perform ubiquitous manipulation activities. Many behavioural paradigms can be imagined to address issues related to the control of movement in general.

7.2.1 Rhythmic movements

The central nervous system has the capacity to sustain very robust and competitive rhythmic movements. The pattern of GF/LF modulation is well established in cyclic upper limb movements (Blank et al., 2001; Flanagan and Wing, 1995). Therefore, this provides control conditions that can be compared to experiments in various contexts. In addition, in demanding experimental environments like parabolic flights where each second is important, rhythmic manipulations provide a larger quantity of data.

Several improvements can be envisaged in order to refine how and how fast humans integrate normal and altered gravity environments when manipulating objects. Beyond fundamental theoretical questions, it would be interesting to see how astronauts can adapt their motor strategies for such tasks to novel conditions of gravity, in the perspective of lunar missions and distant Mars exploration.

First, while it is clearly impossible to simulate altered gravity on the Earth, it is however possible to vary the contribution of gravity - which is always vertical - along the direction of movement, by tilting the whole experimental context, including the subject. In the extreme case, we can generate the interesting condition of $-1g$, by positioning the volunteer upside down, a context that should not make them sicker than during parabolic flights... This additional condition can be used to test the model presented in Chapter 3. Manipulating objects in such a posture is unusual. Therefore, we speculate that kinematic patterns would be very asymmetric. Would subjects integrate

[1] A Chinese Astronaut is a called a Taikonaut.

these asymmetries in the GF profiles, as they do in $+1g$? If it is not the case, how much time is needed to converge to a reliable control?

Second, parabolic flights induce stable gravity phases but also fast transition periods, that are predictable when the atmospheric conditions are clear. These rapid periods were successfully exploited to validate our model in the CPG study (see Chapter 4). It could be interesting to focus on these transitions to answer to specific questions regarding the duration of learning processes. To our knowledge, one study analysed how subjects controlled an object held stationary, during these rapid gravitational transitions and showed that they could anticipate the change in gravity, as measured by their GF (Hermsdorfer et al., 1999). However, in that case, (1) the inertial component remained zero because no acceleration was induced to the object and (2) they conducted the experiment with two subjects only.

Finally, one should be aware that the applied GF on a given object is idiosyncratic. Namely, subjects will adjust their grasp according to personal factors but also in function of physical properties of the fingertips and the object. Consequently, the static coefficient of friction should not be negligible in the model. It is not reasonable to assume different functions that implement internal models dedicated to the same control. Therefore, the coefficient of friction - which does not follow Amonton's law[1] - should be parameterized in the model in a more realistic manner. Indeed, fingers are made of compliant, living material. As a consequence, static friction which is at the basis of grasp stability, diverges from mechanics of rigid inert bodies (Kogut and Etsion, 2004). First, asperities, which are microscopic projections from the "average surface" play a major role in determining the coefficient of friction between materials. The pressure on an asperity may deform the contact area plastically. Therefore, frictional resistance arises from sliding objects breaking and creating bonds through asperities. Second, decreasing the temperature proportionally affects the amount of frictional force. Third, Bowden (1953) proved that Amonton's law strictly applies when there is a lower load. The reason for this independence at lower loads is that there is less pressure for the asperities in contact to deform. A PhD thesis has been started in our lab to investigate those tribological[2] aspects of prehension.

[1]The coefficient of friction is defined as the ratio between the magnitude of the frictional force and the normal force. Amonton's law states that the coefficient of friction is independent of the normal force.

[2]Tribology is the science of the mechanisms of friction, lubrication, and wear of interacting surfaces that are in relative motion.

7.2.2 Discrete movements

In our collision experiments, we did not find evidence of any scaling of GF according to expected momentum or impact forces, which was quite surprising initially. For example, Turrell et al. (1999) found a scaling between GF and the magnitude of the produced impacts. In addition, GF peaks were synchronized to the collision LF. In that context, subjects had more information only a haptic feedback of the impact: they could estimate the collision by viewing the swing of the pendulum and subsequently use this estimate to adjust their control in subsequent trials. In contrast, the targets in our experiment were stationary. Therefore, participants triggered a saccade to the target so as to be well in advance of the collision and they did not leave it until after the impact occurred.

We suggest a modified paradigm to test whether the mechanical properties of the target alter the GF strategy, for example, by replacing the foam on the target by a spring with an adjustable stiffness coefficient. In addition, we could test the subject side of the system by instructing them to apply different levels of GF, quantified as percentage of Maximum Voluntary Contraction (MVC) levels. The larger the GF, the stiffer the system. Would this maximum in GF still be delayed with respect to the impact?

Another interesting effect lay in the asymmetry in GF profiles between upward and downward collisions, even in microgravity. We hypothesized that participants would generate larger GF in upward movements to minimize the risk of dropping the object. We speculate that similar GF would be exerted when performing horizontal collisions in 1 g. This should further demonstrate that (1) gravity defines verticality and (2) that the internal model of normal gravity is robust to changes. Strikingly, larger GF in upward movements persisted in 0 g, even at the last trial. Learning movements in conflicting dynamic environments as during repeated exposures to 1, 1.8 and 0 g during parabolic flights, interferes with the consolidation of previously learned models of movements of the same type (Krakauer et al., 1999). Regarding this second point, it would be very interesting to evaluate whether the strategy applicable in short term 0 g eventually disappears in favour of a behaviour better suited to the long-term weightless environment. This experiment has been proposed as part of the "Dexterous Manipulations in Microgravity" project to fly in the International Space Station and has been selected for a definition phase.

The experiments we conducted in the present work led us to a major conclusion. All these results suggest that adaptable internal models of arm dynamics are available to a variety of motor systems, like the eye plant (Ariff et al., 2002; Nanayakkara and Shadmehr, 2003) and the grip controller. Further studies are required to reveal whether this reflects broad access to a common representation of arm dynamics or multiple, possibly redundant, representations within each motor subsystem (Davidson and Wolpert, 2005). Finally, prediction might be at the basis for the coordination of multimodal movements.

Appendix A

Experimental equipment

A.1 Objectives

In this work, we was interested in multiple aspects of human motor behaviour. First, we had to design a manipulandum capable of measuring forces and torques under each finger during a precision grip task. Second, some experiments required the measurements of eye movements. Third, we wanted to interface the whole system with a 3D position tracking system. Finally, the experimental platform had to meet design constraints since it was mostly dedicated to parabolic flight experiments.

In this section, we first cover the technical description of the equipment, from the instrumented hand-held device to the end-user software, with a special emphasis on the simplicity of usefulness. Some aeronautical details will be presented on the particular environments induced by parabolic flights manœuvres. we conclude this appendix with some suggestions for improvements of the set-up.

A.2 Mechanical design: the manipulandum

A.2.1 Abstract

Fine prehension is ubiquitous in everyday skilled hand manipulations. The anticipatory nature of the control of normal grip forces exerted against tangential loads has been extensively used to provide insights into the working of neural control of movements. We designed a new versatile device to measure the three dimensional forces and torques during a broad panel of precision grip tasks. The instrument measures constraints exerted independently on two grip surfaces by the thumb and the opposing fingers. In addition, the device can be loaded to increase the weight and/or induce torques and can be easily integrated in a variety of experimental contexts. Its compactness improves its stability during movement and allows an ergonomic manipulation for impaired persons or children.

A.2.2 Introduction

A precision grip occurs between the thumb and index finger during precise and skilled hand manipulations. In order to lift an object aloft without translational and/or rotational slips, the grip force (GF) applied normal to the grip surfaces must be large enough to counteract the destabilizing tangential forces and rotational torques acting on the fingertips (Johansson and Westling, 1984). Since the control of grip force is largely anticipatory (Flanagan and Wing, 1997), many behavioural paradigms can be imagined to address issues related to the control of movement in general.

The parallel co-ordination between grip forces (GF) and load forces (LF) applied to each contact surface of an object has been initially studied by Johansson and Westling (1984) during a motor task consisting in gripping, lifting and holding an object. Since then, the parallel change in GF and LF has been established as a general control strategy during prehension requiring grasp stability. For instance, studies reported that the GF was modulated with the fluctuations in inertial loads that arise from moving a grasped object in space as the object is accelerated and decelerated by the arm (Flanagan and Wing, 1993; Flanagan et al., 1993). Another study showed that the GF modulated approximately in phase with changes in LF induced by whole body jumping (Flanagan and Tresilian, 1994). This robust coupling between GF and LF emerges from a variety of grip configurations, like in multidigit grips (Gao et al., 2005) and for different forms of LF including those dependent on position, velocity and acceleration (Flanagan et al., 2003; Nowak and Hermsdorfer, 2004) as well as in normal or altered gravity conditions (Augurelle et al., 2003; Hermsdorfer et al., 2000).

Most studies involving precision grip (*i.e.* not involving the whole hand) were limited to tasks in which LF where unidirectional, as in horizontal or vertical movements. However, in our daily activities, objects are often grasped such that multidirectional constraints are induced between the fingers, including torques (Goodwin et al., 1998; Kinoshita et al., 1997). The objective of this study is to design a new versatile instrument capable of measuring the three dimensional forces and torques under the thumb and index finger during a variety of manipulative tasks and experimental contexts.

A.2.3 Methods

A.2.3.1 Instrumented device

The device has a cylindrical shape of 80 mm diameter and 30 mm height (Fig. A.1 A). It is equipped with two lightweight (50 g each) force-torque sensors (Mini40 F/T sensor, ATI Industrial Automation, Garner, NC) mounted back-to-back in an aluminum frame (112 g). Each sensor measures the three orthogonal force (F_x, F_y, F_z) and torque (T_x, T_y, T_z) components along the corresponding axes intersecting the center of the grasp surface. The sensing ranges for F_x, F_y and F_z are ± 40, ± 40 and ± 120 N with a 0.02, 0.02 and 0.06 N resolution, respectively. The sensing range for T_x, T_y and T_z is ± 2 Nm with a 0.001 Nm resolution. The area of each sensor is 12.5 cm^2 and distant 30 mm apart. The basis weight of the instrument is 212 g and its centre of mass is located at the middle of the line joining the centre of both grip surfaces. The device can be loaded with 6 semi-rings that are either made of tungsten carbide (84 g each) or of Ertalon (8 g each) for a loaded weight ranging from 260 g (with 6 Ertalon semi-rings) to 716 g (with 6 tungsten carbide semi-rings) (Fig. A.1 A). The semi-rings can be placed either symmetrically, so that its center of mass is at the center of the grasp surfaces or asymmetrically, so that the center of mass is off-centered from the center of the grasp surfaces. When the center of mass is off-centered, an adjustable torque can be applied by rotating the device at various angles relative to the direction of the eccentricity of the center of mass ($\pm 90^o$ no torque, 0^o maximal torque). A nylon opaque cover (22 g) gears the masses interlocking and hides the configuration so that its appearance is always visually the same.

A.2.3.2 Signal processing

The sensors are mounted back-to-back with sensor S2 rotated 22^o around its Z-axis to avoid cable congestion while minimizing distance between the two surfaces. Since the common coordinate system is centered on S1 (Figure A.1 B), the values measured by S2 are corrected according to:

$$\begin{pmatrix} \cos 22^\circ & \sin 22^\circ & 0 & 0 & 0 & 0 \\ \sin 22^\circ & -\cos 22^\circ & 0 & 0 & 0 & 0 \\ 0 & 0 & -1 & 0 & 0 & 0 \\ 0 & 0 & 0 & \cos 22^\circ & \sin 22^\circ & 0 \\ 0 & 0 & 0 & \sin 22^\circ & -\cos 22^\circ & 0 \\ 0 & 0 & 0 & 0 & 0 & -1 \end{pmatrix} \begin{pmatrix} F_x \\ F_y \\ F_z \\ T_x \\ T_y \\ T_z \end{pmatrix} \tag{A.1}$$

The total grip force (GF) was calculated as the average of the normal grip

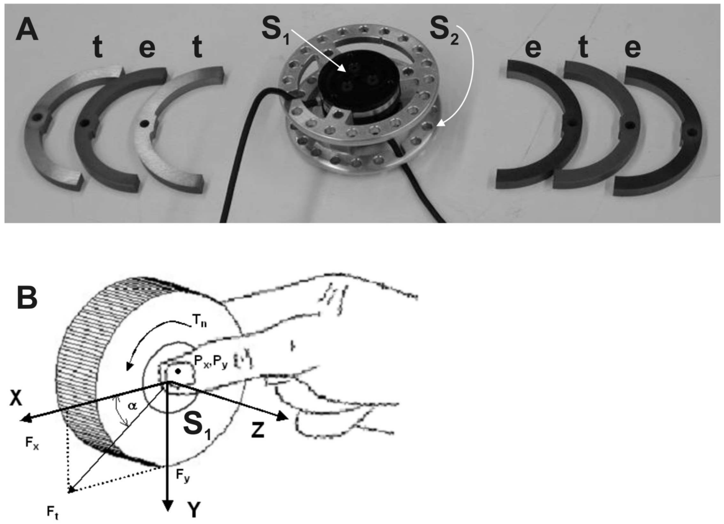

Figure A.1: The instrumented device. (A) Fragmented view with three tungsten carbide (t) and three Ertalon (e) semi-rings. (B) A precision grip task with the nylon cover. (C) The common coordinate system used to measure the load force (LF), the normal torque T_n around the Z-axis and the coordinates (P_x, P_y) of the center of pressure.

forces applied by the thumb and the fingers on each transducer. The force tangential to the grasp surface is a vector with two components:

$$\begin{pmatrix} F_{x,S} \\ F_{y,S} \end{pmatrix} \tag{A.2}$$

where S denotes the sensor (S1 or S2). The total tangential force acting on the device is calculated as follows:

$$\vec{F}_{t,S} = (\vec{F}_{x,S1} + \vec{F}_{x,S2}) + (\vec{F}_{y,S1} + \vec{F}_{y,S2}) \tag{A.3}$$

Therefore, its magnitude (in N) and direction (in deg) with respect to the reference X-axis are:

$$LF = \left\|\vec{F}_{t,S}\right\| = \sqrt{(F_{x,S1} + F_{x,S2})^2 + (F_{y,S1} + F_{y,S2})^2} \tag{A.4}$$

$$\alpha = \frac{180}{\pi} \arctan\left(\frac{F_{y,S1} + F_{y,S2}}{F_{x,S1} + F_{x,S2}}\right) \tag{A.5}$$

In addition to the forces, torques can also be measured. The normal torque that tends to rotate a sensor around its Z-axis ($T_{n,S}$) is computed as the difference between the torque measured around the Z-axis ($T_{z,S}$) and the torque due to an off-centered grip, if any:

$$T_{n,S} = T_{z,S} - (F_{y,S}P_{x,S} - F_{x,S}P_{y,S}) \tag{A.6}$$

where $(P_{x,S}, P_{y,S})^T$ are the coordinates of the center of pressure on each grasp surface, and are computed as:

$$\begin{pmatrix} P_{x,S} \\ P_{y,S} \end{pmatrix} = \begin{pmatrix} -\frac{T_{y,S}}{F_{z,S}} \\ \frac{T_{x,S}}{F_{z,S}} \end{pmatrix} \tag{A.7}$$

The total normal torque (T_n) is calculated as the average of the normal torques applied to each sensor.

A.2.3.3 Data acquisition

The signals from both sensors are synchronized and digitized in a PXI-chassis (National Instruments©, Austin, TX). The controller is an AMD 333 MHz embedded processor that samples the signals at up to 1 kHz after an analog low pass second order Bessel filter at 235 Hz. The signals are then digitally low-pass filtered using a zero-phase digital filter (autoregressive, forward and backward filter, cutoff frequency: 15 Hz).

A.2.3.4 Experimental procedure

The new device has been tested in a grip-lift task comparable to those in previous studies (see for example Johansson and Westling (1984)). An informed volunteer (male, 26 years old) was asked to grip the device, lift it 5 cm vertically off a table, hold it still in the air for 3 seconds, and then replace the object on the table. The procedure was repeated in two loading conditions: with or without generated torque. In both conditions, 3 semi-rings in tungsten carbide (heavy) and 3 in Ertalon (light) were inserted in the body, leading to an equivalent mass of 510 g. In the symmetric load condition (Torque = 0 N.mm), the heaviest rings filled the lower half-body, so that the center of mass of the object and the point of application of GF were aligned with vertical. The asymmetric condition was obtained by rotating the symmetric configuration by 90^o (Torque = 23 N.mm). The participant was asked to apply a spontaneous GF during the task.

A force is defined by its magnitude and direction but it is often useful to identify its point of application, commonly called the center of pressure, for example to investigate whether a slip occurs. Therefore in order to validate

Equation A.7, we repeated the following procedure for each sensor. We applied continuous forces with a sharp pen along four equivalently spaced diameters (45^o per section) of the circular area of the transducer, from one edge to the opposing edge. The diameters were grooved on brass surfaces covering the sensors.

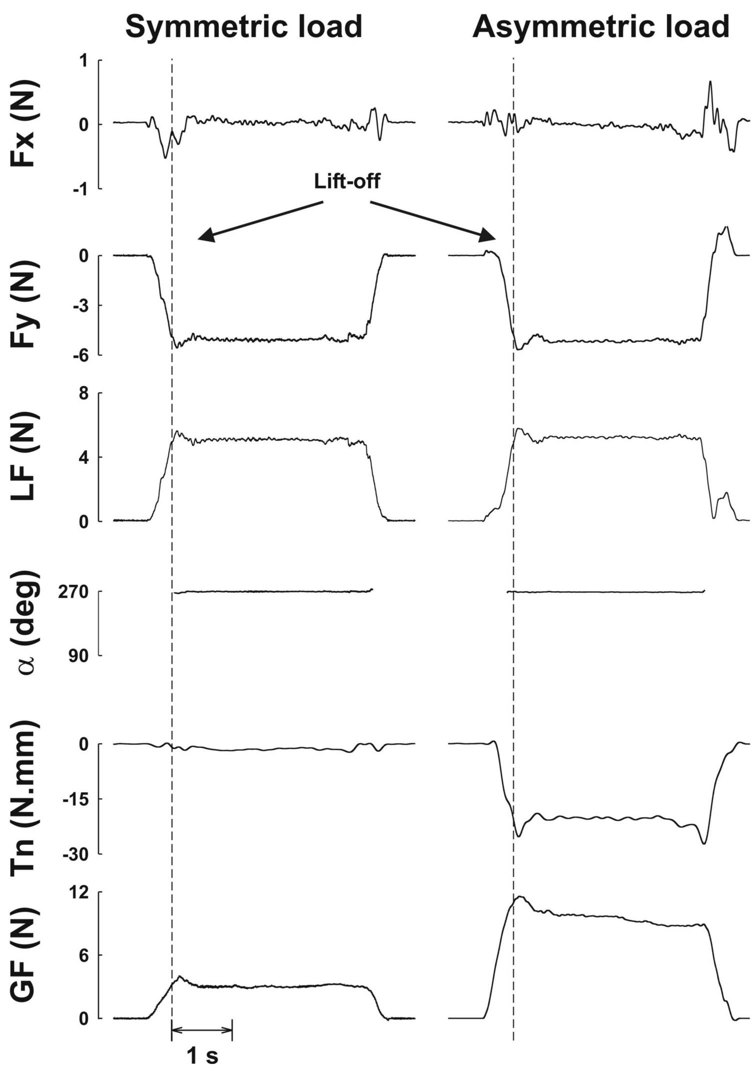

Figure A.2: Typical traces of one grip lift trial in the symmetric (left panel) and asymmetric loading conditions (right panel, $T_n = -20.7 \pm 1.11$ N.mm). Are presented as a function of time: the projection of the load force on the X-axis (A) and the Y-axis (B), the load force magnitude (C) and direction (D), the normal torque (E) and the grip force (F).

A.2.4 Results

Two typical traces of fingertip forces and torques are presented in Figure A.2, either with a symmetric load (left panel) or with an asymmetric load generating a torque of -20.7 ± 1.11 N.mm around the Z-axis (right panel). In both conditions, the mass of the device is equal to 510 g (weight of 5 N). The total tangential force (LF) is primarily due to its vertical component (F_y) because its horizontal component (F_x) was close to zero throughout the lift. Lift-off occurs when F_y reaches the device's weight (Fig. A.2, vertical dashed lines). The direction of the tangential force vector (a) is equal to 270^o after lift. While the LF are the same in both conditions, a large torque tends to rotate the object about the Z-axis in the asymmetric load condition (right panel). Consequently, the GF increases in order to prevent a rotational slip.

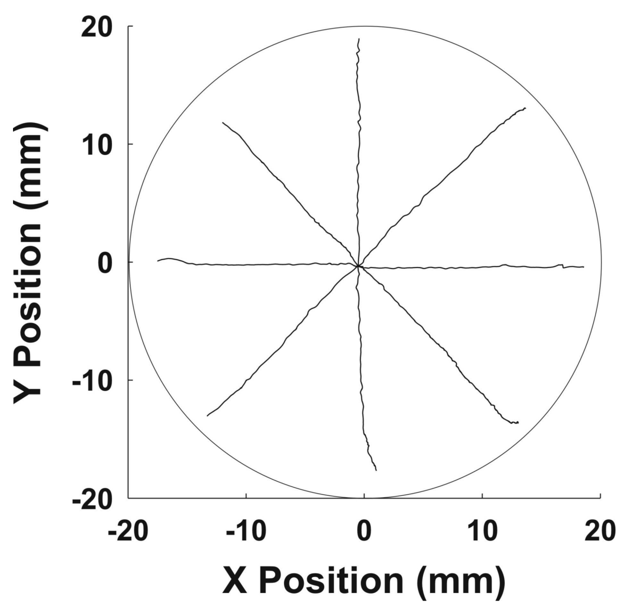

Figure A.3: Reconstructed center of pressure of a contacting force applied along four equivalently spaced diameters on the transducer's plate (circle).

Figure A.3 depicts the center of pressure in the 2D space of one sensor, calculated according to Equations A.6 and A.7. The reconstructed point of application of the force followed very closely the exact diameter ($R^2 > 0.92$, $SEM < 0.8$ mm). In addition, it is worth to note that the procedure to compute the center of pressure is insensitive to an arbitrary profile of constraint applied on the transducer.

A.2.5 Discussion and conclusion

A new device has been developed for the measurement of 3D forces and torques to study the dynamics of precision grip. It also avoids to make assumptions about the direction of the load as required when using devices measuring forces along a single axis. The holes manufactured in its circumference allow an easy integration to external equipment, like robots or motors. This versatile instrument has already provided valuable results in parabolic flights (White et al., 2005), in a TMS study (Davare et al., 2006) and in weight-dropping tasks.

A.3 Implementation

The electronic devices and the software implemented to control the acquisition process are detailed in the two following sections.

A.3.1 Hardware

In order to be as flexible as possible, we used standard products from National Instruments (Austin, TX). The acquisition system was organized on a hardware kernel (PXI-8150B) with an AMD 333 MHz embedded controller running Windows98 OS. Three additional data acquisition (DAQ) boards were plugged inside the chassis:

1. a PXI-6071E DAQ board with 64 single ended analog input channels and 2 single ended analog output channels,
2. a PXI-6533 high speed digital I/O DAQ board and
3. a PXI-8210 ethernet/SCSI adapter.

Simultaneous two dimensional (horizontal and vertical) recordings of both right and left eyes were made with the Chronos head mounted video-based eye tracker (CHRONOS VISION GmbH, Berlin, Germany). This standalone system can be triggered with a TTL low gate signal. A second video-based device (OptoTrak 3020 system, Northern Digital, Ontario, Canada) tracked in space infrared-light-emitting diodes (IREDs) that can be positioned on points of interest. This system is fed in by a clock signal to ensure synchronization. Any other custom measurements can be performed by plugging other devices on a free analog input channel on the PXI-6071E board. The two above synchronization signals (Chronos and OptoTrak) are delivered by digital outputs of the PXI-6533 DAQ. Alongside providing network access, the third one (PXI-8210) was dedicated to real-time communication with the OptoTrak system (system initialization and data download among others). Figure A.4 depicts the three main parts of the platform: the PXI controller, the Chronos and the OptoTrak systems.

A substantial development (hardware and software) was necessary to acquire data from the sensors (Mini 40 F/T transducers, ATI Industrial Automation, NC). Indeed, these were delivered with 2 standalone controllers (one per sensor), connected to a standard PC through RS-232 interface. Another alternative consisted in using ATI ISA boards plugged into (older) PC which provided signals in physical units in a proprietary software. However, on the

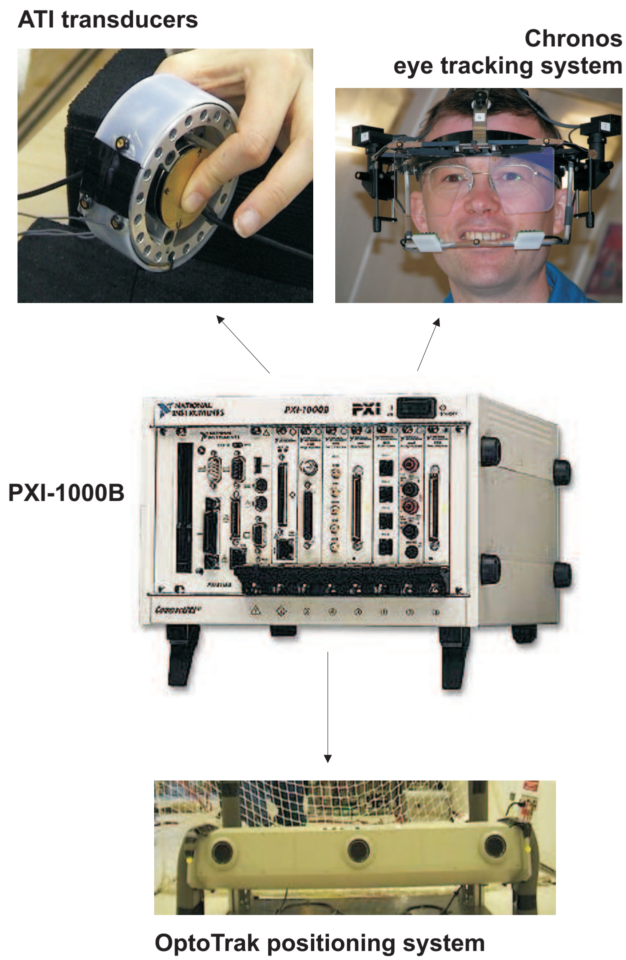

Figure A.4: The PXI-1000B chassis contains 3 DAQ boards controlling the acquisition from the force sensors, the Chronos and the OptoTrak devices.

one hand, sampling frequencies were too low to meet our needs. On the other hand, our concern was to maximize integration by piloting all the process with only one system. Therefore, we decided to program the sensors outputs with the NI materials, bypassing ATI software and a part of electronic circuitry. Figure A.5 sketches the logics to command the sensor's outputs.

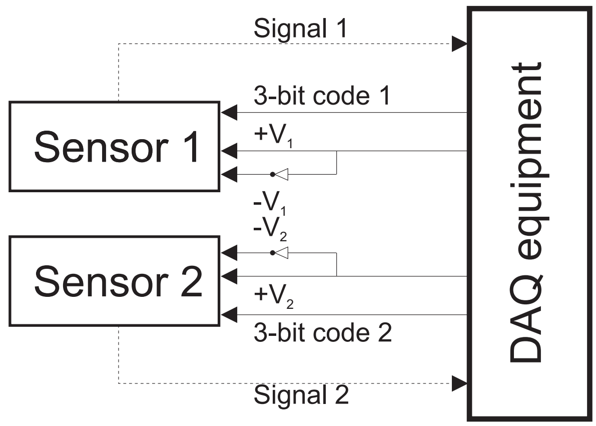

Figure A.5: Connections between the PXI and the transducers. Solid lines are control signals, dashed lines are data.

Each transducer output is plugged into a free input channel of the PXI-6071E DAQ board. Since the sensors have 6 degrees of freedom (F_x, F_y, F_z, T_x, T_y, T_z), we had to command one of the outputs by applying a 3-bit digital code to the appropriate 3 pins of a DSUB connector at the same time as a pair of bias voltages ($+V$,$-V$) in order to null offset in the circuitry. The digital code (Grey code) and output voltages were delivered by the PXI-6533 and PXI-6071E DAQ boards, respectively. I only used 7 of the 8 possibilities (2^3): 6 for F/T measurements and 1 for thermister reading to correct (by software) the offset of the strain gages due to temperature fluctuations. Following specifications, we had to loop within a time window of 1/7000 s (7 kHz) in order to output each "logical" measurement (i.e. F_x) at 1 kHz ($7000/7 = 1000$). This procedure was applied in parallel to each sensor.

A.3.2 Software

A custom software ("Microgravity") has been implemented in ANSI C language (LabWindows/CVI, National Instrument, Austin, TX) to control the hardware kernel and all the peripheral equipments. The idea was twofold. On the one hand, since we acquired data during parabolic flights, the software had to be highly reliable and user friendly. It has been tested following "white boxes" procedures and specified with flow charts. On the other hand, the software had to be used by experimenters involved in various experimental contexts. Flexibility and rapid adaptation without modifications of the code were important.

When we execute *Microgravity*, we get a splash screen offering 5 Graphic User Interfaces (GUI) modules, from the lowest level (hardware) to the highest level (logical):

1. **Configuration:** Front end panels reflecting the underlying hardware. This module allows experimenters to *configure* hardware connections (voltage range, sampling frequency, etc) on arbitrary chosen analog input channels of the boards. The configuration is done only once per experiment and can be saved in an ini file.

2. **Acquisition:** Definition of the experimental protocol and data recording. A protocol ini file contains subjects information and duration of each trial among other details. The acquisition also initializes the OptoTrak through an integrated API and DLL. Importantly, the experimenter has the possibility to monitor arbitrary signals to check the system. Each trial is triggered by a push on a START button. This event, in turn, starts *acquiring* data following the loaded configuration file, triggers other systems (Chronos and OptoTrak), displays a countdown. When the time has elapsed, all the data are transparently saved in a file indexed by the trial number. An abortion is possible at any time if something wrong happens.

3. **View:** Visualization of raw traces. This module allows a quick quality check on the data. It is possible to dispatch any signal on 1, 2 or 3 stripcharts. Working cursors and zooming tools are available. An automatic preprocessing of the data (software filtering, rotating one of the two transducers (see A.2.3.1) can optionally be launched before saving a part or the whole traces in another file for analysis or simply in ASCII file.

4. **Analysis:** A deep introspection of the traces can be achieved here. Among other possibilities, this module allows to dispatch signals in physical units on up to 6 charts on both vertical axes (see Figure A.6), change the scales, X-Y plot any signal, compute cross-correlations or FFT, etc. Obviously, it is also possible to export all or a subset of the data (possibly

downsampled) to ASCII text files for further analysis in other softwares like Matlab.

5. **Options:** Allows customization of all paths for data and ini files as well as color of traces.

Figure A.6: Analysis module of Microgravity with in a working session.

The module n (≤ 5) needs information from module(s) $< n$. Hence, as a precondition, at least one ini file created by each of the lower modules must exist in order to run the current one. A default ini file per module can be specified to be automatically loaded on start of the program. These ini files have a clear structure and can easily be edited.

As introduced in the hardware section (A.3.1), a substantial work was to control the acquisition of the two ATI transducers. Figure A.7 depicts the procedure based on a stimulus-response cycle as follows. I had to output at exactly the same time 2 bias output voltages $+V_1$ and $+V_2$ (one per sensor) and one code of 6 bits (3 bits per sensor). Then, the software had to read the response of each sensor. However, two problems arose:

1. We needed to synchronize 2 boards. The first one (PXI-6071E) performed analog output while the second one (PXI-6533) delivered the digital code with hard real time constraints.

2. The software could not read the two inputs exactly at the same moment the code and bias voltages were provided. Indeed, any electronic system needs a minimum delay to stabilize its circuitry. The reading process could only start after that transient phase.

The following solutions were implemented to solve each of these problems.

1. Synchronization of 2 boards in a PXI chassis was done by sharing a control signal on the real time backpane bus (RTSI lines) by configuring the circuitry.

2. A counter (GPCTR0) was started exactly at the time the code and the bias voltages were sent. After a programmed delay (50 ns resolution - 20 MHz onboard clock source), the counter generated a single pulse used as a read signal. By programming the delay, one can thus bypass the transitory zone, measured with an oscilloscope.

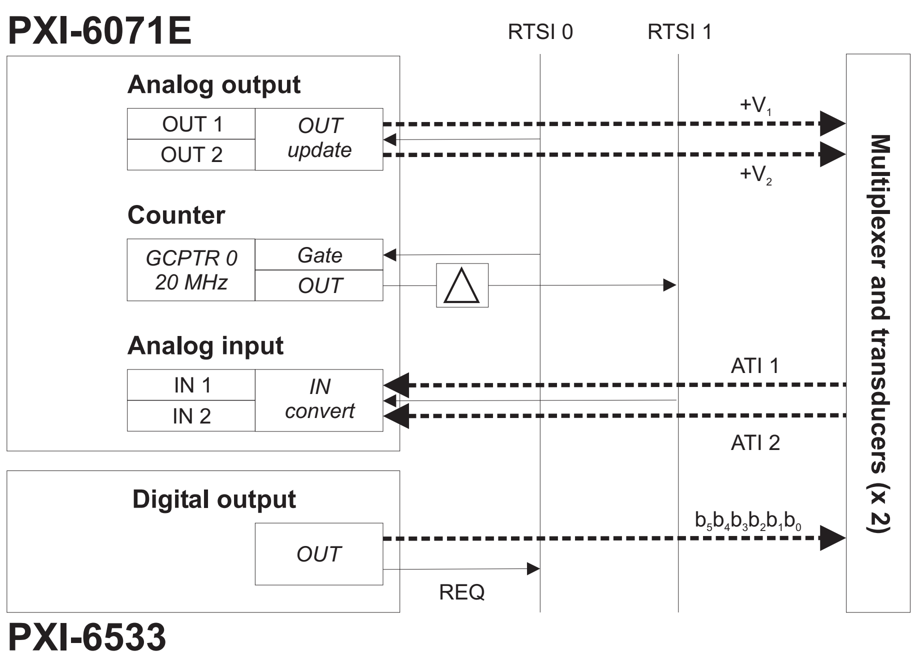

Figure A.7: Flowchart to command the transducers.

Let us detail one cycle (*e.g.* to read F_x):

1. The REQ signal is transmitted on RTSI0 at the same time a 6-bit digital code is sent (e.g. 001001).

2. This pulse is received from the RTSI0 at the gate of GPCTR0 and, simultaneously, at the "Out Update" clock.

3. The counter starts counting 1000 pulses of 50 ns each from its internal source (50 μs).

4. At the same time, 2 bias voltages are sent.

5. When the counter reaches the programmed delay, it emits a single pulse on RTSI1.

6. The "In Convert" then initiates an A/D conversion of 2 analog values.

The next cycle (to read F_y) starts with the next REQ pulse. Therefore, to acquire logical (forces and torques) signals at 1000 Hz, one physical channel is mutiplexed between 7 signals (3 forces, 3 torques and 1 measure of temperature). Consequently, real sampling frequency is seven times larger (7 kHz).

A.3.3 Parabolic flights logistics and mechanics

A.3.3.1 Campaign organization

In addition to drop towers, sounding rockets, recoverable satellites and capsules, space shuttles, and space stations, parabolic flight has become a full-fledged means of accessing microgravity. Parabolic flight was first introduced for astronaut training; but today it is mainly used for testing of space technology and for short duration scientific experiments. Moreover, it also provides hypergravity periods that can be exploited in physical and life science studies.

Such flights are conducted on the specially-configured aircraft A300 ZeroG and offer a period of up to 20 seconds of weightlessness. The aircraft is a prototype #3 of Airbus A300. Its first flight occurred in 1973 but it has few hours of mission. In fact, it is still a relatively young aircraft. It has always been used for test flights, never for transport. Structural transformations have been carried out to complain with parabolic flights: a structural follow-up of critical parts is ensured by strain gauges, hydraulic bells allows circulation of oil in 0 g phases and cabin has been accommodated for experiments.

A flight campaign originates in Bordeaux (Mérignac airport) and normally consists of three individual flights with 31 parabolas flown on each flight. On each parabola, there is a period of increased gravity (1.8 g) which lasts for 20 seconds immediately prior to and following the 20-second period of reduced gravity (see Fig. A.8).

The French company Novespace is contracted by ESA to provide the campaign logistics and supervision of the experiment technical preparation. The Centre d'Essais en Vol (CEV) provides all of the in-flight support and flight personnel. The aircraft technical support is provided by the Bordeaux-based Sogerma company.

A typical ESA campaign is normally scheduled for a period of two weeks, with the first week dedicated to experiment receipt, followed by installation, test and calibration within the aircraft. The second week is assigned to the parabolic flights themselves. At the start of the second week (on a Monday), attendance at a medical and safety briefing is mandatory by all persons planning to fly. Three flights of 31 parabolas are nominally scheduled for the Tuesday, Wednesday and Thursday mornings, with a flight duration of approximately two-and-a-half hours. In the case of inclement weather or technical problem with the aircraft, a flight is delayed to the afternoon of the same day or morning of the next day. The Friday of the second week is reserved as a back-up flight day.

A.3.3.2 Parabolic flight manœvre

From a steady horizontal flight, the aircraft gradually pulls up its nose and starts climbing at an angle of approximately 45 degrees (Fig. A.8). This "injection" phase lasts for about 20 seconds, during which the aircraft experiences an acceleration of around 1.8 times the gravity level at the surface of the Earth. The engine thrust is then reduced to the minimum required to compensate for air-drag, and the aircraft then follows a free-fall ballistic trajectory (a parabola) lasting approximately 20 seconds, during which weightlessness is achieved. At the end of this period, the aircraft must pull out of the parabolic arc, a manœuvre which gives rise to another (noisier) 20-second period of 1.8 g on the aircraft, after which it returns to normal level flight attitude.

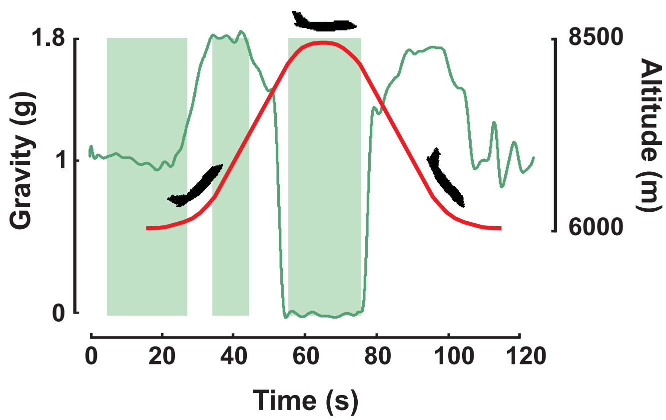

Figure A.8: A single parabolic flight profile in function of time. Gravity is on the left axis and altitude is on the right axis.

According to the free-fall state definition (see 1.5), various flight parameters must be controlled by two flight engineers in order to have only the weight as resultant force. During the microgravity period, 4 forces are continuously monitored. On the one hand, the weight (W) and the thrust (T, produced by the engine) depend on the aircraft:

$$W = mg \tag{A.8}$$

$$T = ma \tag{A.9}$$

On the other hand, the drag (D, resistant force parallel to the relative wind) and the lift (L, perpendicular to the relative wind) are 2 aerodynamical forces:

$$D = \rho\frac{v^2}{2}AC_D(\alpha) \tag{A.10}$$

$$L = \rho\frac{v^2}{2}AC_L(\alpha) \tag{A.11}$$

where ρ is the air density, v is the true airspeed, A is the relevant area (typically taken to be the wing area) and C_D and C_L are the lift and drag coefficients, respectively. These two parameters are mainly function of α, the angle of attack of the wing, and are remarkably insensitive to physical parameters like temperature. Figure A.9 contrasts a horizontal 1 g-flight with a 0 g-portion of flight.

In 1 g, since the velocity of the plane is considered constant, we have:

$$\vec{W} + \vec{T} + \vec{L} + \vec{D} = \vec{0} \tag{A.12}$$

In a 0 g-flight, the aircraft is controlled so that the resulting force is equal to the weight:

$$\vec{T} + \vec{L} + \vec{D} = \vec{0} \tag{A.13}$$

These profiles are flown repeatedly, with a period of 3 minutes between the start of two consecutive parabolas (a 1-minute parabolic phase resulting from 20 seconds at 1.8 g + 20 seconds of weightlessness + 20 seconds at 1.8 g), followed by a 2-minute "rest" period in 1 g. Throughout the flight, all personnel are kept continuously informed of the campaign status (countdown to the next parabola, number of minutes of rest period, etc.).

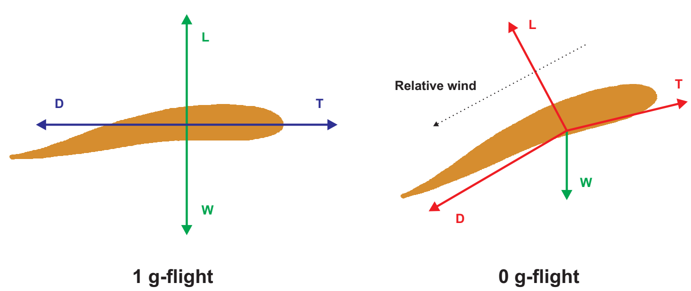

Figure A.9: Force balance on the wings in 0 and 1 g.

A.4 Future improvements

Since the beginning of its service in 2000, our experimental setup flew 8 parabolic flight campaigns which represents around 750 parabolas or 4 hours 30 minutes of microgravity and was transported on 16000 km. Our setup had a hard life these last five years. Electronic systems and particularly embedded systems technologies evolve rapidly. Therefore, it is often a better strategy to create a new device, taking into account past experience rather than updating the current one.

Several improvements can be made on the current system. First, the manipulandum should be further miniaturized in order to ease manipulation by children and especially children who have motor deficits. Second, closed-loop protocols should be envisaged. More and more interesting paradigms address the study of human behaviour but adapting the task in function of an online event. A real-time operating system (QNX or real time Linux kernel (Lillicrap and Katerine, 2004)) could be more reliable than a general purpose one. The availability of the DAQ drivers reduce the choice of OS.

As we mentioned in the conclusion of this work, some of these improvements are currently implemented in a new prototype that already flown in a recent parabolic flight campaign to qualify for flight in the International Space Station (ISS).

Appendix B

A model of the upper limb

In this appendix, we show that more complex versions of periodic systems, namely double compound pendulums and spherical pendulums, present the same variations in function of gravity as the model presented in Chapter 3. First we create a model of the upper arm and forearm with a double compound pendulum. Then, the assumption to confine motion in a plane will be raised by approaching the trajectory performed by our subjects with a mono-segmental spherical pendulum. The system of differential equations will be derived and resolved in both cases. The normal mode of the system will be calculated as a function of gravity. We expect that the principal frequency increases with gravity, as is reflected in our data, in both models.

B.1 Problem statement

The following figure describes how the upper limb is modeled. Two rods assumed cylindrical (upper arm with mass m_u and length L_u ; lower arm with mass m_l and length L_l) are free to move in the X, Y plane around two joints (shoulder and elbow). The centers of mass of each rod are positioned at r_u and r_l from the nearest joint and are not centred in the limb. The two unknows are the angular displacements $q_u(t)$ and $q_l(t)$.

B.2 Resolution with Lagrange's equations

The problem will be resolved in the framework of Lagrangian dynamics. This formalism reduces to Newton's law and treats problems from rather general viewpoints. The Lagrangian is given by:

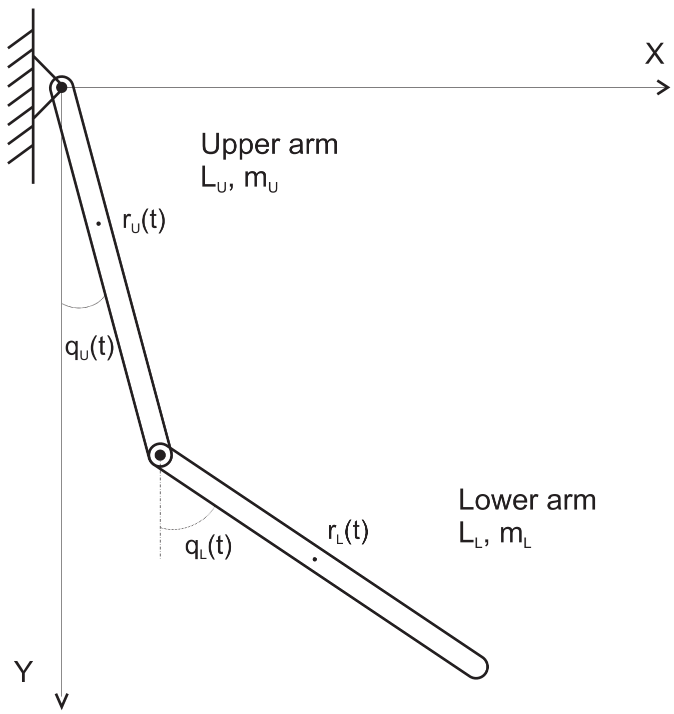

Figure B.1: A double compound pendulum model of the upper limb. Lengths, masses and positions of the center of mass of the segments are denoted by L_i,M_i and r_i and angular displacements with respect to Y are given by $q_U(t)$. The index i denotes the upper (U) or lower (L) segment.

$$\frac{d}{dt}\left(\frac{\partial T}{\partial \dot{\mathbf{q}}}\right) - \frac{\partial T}{\partial \mathbf{q}} = \mathbf{Q}_f \tag{B.1}$$

where $\mathbf{q}$ is a generalized coordinate, $\mathbf{Q}$ is the generalized force, and T is the kinetic energy. Bold values denote vectors. In the following developments, the indices u and l refer to the upper and lower limbs respectively.

B.2.1 Kinematics

The position vector of the center of the mass of the upper and lower limbs are:

$$\mathbf{r}_u = x_u\ \hat{\mathbf{x}} + y_u\ \hat{\mathbf{y}} \tag{B.2}$$

$$\mathbf{r}_u = r_u \sin q_u\ \hat{\mathbf{x}} + r_u \cos q_u\ \hat{\mathbf{y}} \tag{B.3}$$

where x_u, u_u are the coordinates of the upper center of mass. Similarly for the lower link, we have:

$$\mathbf{r}_l = x_l\ \hat{\mathbf{x}} + y_l\ \hat{\mathbf{y}} \tag{B.4}$$

$$\mathbf{r}_l = \mathbf{L}_u + r_l \sin q_l\ \hat{\mathbf{x}} + r_l \cos q_l\ \hat{\mathbf{y}} \tag{B.5}$$

$$\mathbf{r}_l = (L_u \sin q_u + r_l \sin q_l)\ \hat{\mathbf{x}} + (L_u \cos q_u + r_l \cos q_l)\ \hat{\mathbf{y}} \tag{B.6}$$

By simple derivation with respect to time, we get the velocities:

$$\mathbf{v}_u = r_u \dot{q}_u \cos q_u\ \hat{\mathbf{x}} - r_u \dot{q}_u \sin q_u\ \hat{\mathbf{y}} \tag{B.7}$$

$$\mathbf{v}_l = (L_u \dot{q}_u \cos q_u + r_l \dot{q}_l \cos q_l)\ \hat{\mathbf{x}} - (L_u \dot{q}_u \sin q_u + r_l \dot{q}_l \sin q_l)\ \hat{\mathbf{y}} \tag{B.8}$$

These velocities will be used to compute the kinetic energies in the Lagrangian.

B.2.2 Dynamics

In this section, we mainly focus on the procedure to follow in order to get the moments of inertia of the system which is a necessary step to compute the kinetic energy involved in the Lagrangian. The forces due to gravity are also described.

B.2.2.1 Forces due to gravity

In this system, only the gravitational force is constraining the movement. It is acting on both links following:

$$\mathbf{G}_u = m_u \sigma g \; \hat{\mathbf{y}} \tag{B.9}$$
$$\mathbf{G}_l = m_l \sigma g \; \hat{\mathbf{y}} \tag{B.10}$$

The parameter σ will be used to vary the gravity arbitrarily in order to test the model and to confront its prediction with our read data.

B.2.2.2 Moments of inertia

We consider the two links as cylinders with known dimensions (radius R, length L and mass m) and position of centers of mass (r). However, the inertial behaviour of the links are quite different since the lower arm is assumed to rotate about the shoulder (at the extremity of the cylinder) while the upper limb is allowed to rotate about its centre of mass.

By definition, the inertia of a body with density ρ and total mass M is:

$$I = \int_0^M r^2 dm \tag{B.11}$$

Since $M = \rho dV$,

$$I = \rho \int_x \int_y \int_z r^2 dV \tag{B.12}$$

Let us consider first the lower link which rotates about an axis parallel to the z-axis (see Fig. B.1) passing through its center of mass CM). By symmetry, the integration of the whole cylinder is eight times the inertia of the volume shown on the Figure B.2:

The bounds of the above integrals (Eq. B.12) are explained in the following expression:

$$I = 8\rho \int_{x=0}^{\frac{L}{2}} \int_{y=0}^{R} \int_{z=0}^{\sqrt{R^2-y^2}} (x^2 + y^2) \; dx \; dy \; dz \tag{B.13}$$

After some manipulations, we get the inertia of the lower limb around the z-axis:

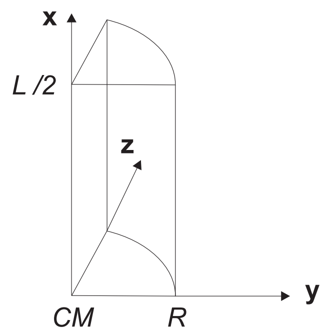

Figure B.2: Domain of integration to get the inertia of a cylinder

$$I_l = \frac{m_l L_l^2}{12} + \frac{m_l R_l^2}{4} \tag{B.14}$$

However, for the upper limb, we assumed that it turns about the shoulder joint. The parallel axis theorem states the following property. Let I be the moment of inertia about axis AB and I_c be the moment of inertia about an axis parallel to AB and passing through the center of mass. Then, if r_u is the distance between the center of mass and AB, we have $I = I_c + Mr_u^2$. From the application of this theorem, it follows:

$$I_u = I_{u,C_u} + I_{u,A} \tag{B.15}$$

$$I_u = \frac{m_u L_u^2}{12} + \frac{m_u R_u^2}{4} + I_{u,A} \tag{B.16}$$

Since $I_{u,A} = m_u r_u^2$:

$$I_u = \frac{m_u L_u^2}{12} + \frac{m_u R_u^2}{4} + m_u r_u^2 \tag{B.17}$$

The term dependent on the radius R of the cylinder in (B.16) and (B.17) is very small compared to the others.

B.2.3 Kinetic energy

To evaluate the Lagrange's equations, the kinetic energy for both links has to be calculated. The upper link is only in rotational motion. Hence:

$$T_u = \frac{I_u \dot{q}_u^2}{2} \tag{B.18}$$

The kinetic energy of the lower link is due to the translation and rotation and can be expressed as:

$$T_l = \frac{I_l\dot{q}_l^2}{2} + \frac{m_l\vec{v}_l^2}{2} \tag{B.19}$$
$$T_l = \frac{I_l\dot{q}_l^2}{2} + \frac{m_l}{2}\left(Lu^2\dot{q}_u^2 + r_l^2\dot{q}_l^2 + 2L_u r_l\dot{q}_u\dot{q}_l^2\cos(q_l - q_u)\right) \tag{B.20}$$

The total kinetic energy of the system writes:

$$T = T_u + T_l \tag{B.21}$$

B.2.4 Lagrangian formulation

In this section, we combine all the above developments to formulate the two Lagrange's equations that lead to the equations of motion.

B.2.4.1 Left hand side: kinetic energy

The left hand sides of Lagrange's equations for the upper limb are:

$$\begin{aligned}\frac{\partial T}{\partial \dot{q}_u} &= I_u\dot{q}_u + m_l L_u^2\dot{q}_u + m_l L_u r_l\dot{q}_l\cos(q_l - q_u)\\ \frac{d}{dt}\left(\frac{\partial T}{\partial \dot{q}_u}\right) &= I_u\ddot{q}_u + m_l L_u^2\ddot{q}_u + m_l L_u r_l\ddot{q}_l\cos(q_l - q_u) -\\ &\quad m_l L_u r_l\dot{q}_l(\dot{q}_l - \dot{q}_u)\sin(q_l - q_u)\end{aligned} \tag{B.22}$$

Similarly, for the angular displacement of the lower link:

$$\begin{aligned}\frac{\partial T}{\partial \dot{q}_l} &= I_l\dot{q}_l + m_l r_l^2\dot{q}_l + m_l L_u r_l\dot{q}_u\cos(q_l - q_u)\\ \frac{d}{dt}\left(\frac{\partial T}{\partial \dot{q}_l}\right) &= I_l\ddot{q}_l + m_l r_l^2\ddot{q}_l + m_l L_u r_l\ddot{q}_u\cos(q_l - q_u) -\\ &\quad m_l L_u r_l\dot{q}_u(\dot{q}_l - \dot{q}_u)\sin(q_l - q_u)\end{aligned} \tag{B.23}$$

The partial derivatives with respect to angular displacements are easily computed from above:

$$\frac{\partial T}{\partial q_u} = m_l L_u r_l\dot{q}_l\dot{q}_u\sin(q_l - q_u) \tag{B.24}$$
$$\frac{\partial T}{\partial q_l} = -m_l L_u r_l\dot{q}_l\dot{q}_u\sin(q_l - q_u) \tag{B.25}$$

B.2.4.2 Right hand side: generalized forces

Up to now, we only took into account the gravitational forces. Their expressions were given in Section B.2.2.1. The generalized forces associated to q are:

$$\mathbf{Q} = \vec{\mathbf{F}}_{c_u} \frac{\partial \vec{\mathbf{r}}_{c_u}}{\partial \mathbf{q}} + \vec{\mathbf{F}}_{c_l} \frac{\partial \vec{\mathbf{r}}_{c_l}}{\partial \mathbf{q}} \tag{B.26}$$

The evaluation of (B.26) both for q_u and q_l yields the two generalized forces Q_u and Q_l:

$$Q_u = \sigma g (m_u r_u - m_l L_u) \sin q_u \tag{B.27}$$

$$Q_l = -\sigma g m_l r_l \sin q_l \tag{B.28}$$

In the two above expressions, $g = 9.81 \text{ ms}^{-2}$ and $\sigma \in [0;2]$ is a parameter used to vary gravity.

B.3 The equations of motion

If we integrate all the previous steps, the Lagrange's equations lead directly to the equations of motion:

$$\begin{aligned} &\left(I_u + m_l L_u^2\right) \ddot{q}_u + m_l L_u r_l \ddot{q}_l \cos(q_l - q_u) - \\ &m_l L_u r_l \dot{q}_l^2 \sin(q_l - q_u) + \sigma g \sin q_u \left(m_l L_u - m_u r_u\right) = 0 \end{aligned} \tag{B.29}$$

$$\begin{aligned} &\left(I_l + m_l r_l^2\right) \ddot{q}_l + m_l L_u r_l \ddot{q}_u \cos(q_l - q_u) + \\ &m_l L_u r_l \dot{q}_u^2 \sin(q_l - q_u) + \sigma g m_l r_l \sin q_l = 0 \end{aligned} \tag{B.30}$$

It is worth to note that if we simplify the model assumptions by considering two identical links, well established equations in the simplified case are found.

B.4 Finding the normal modes

B.4.1 Assumption of small oscillations

In the following, we find the normal modes under assumptions of small oscillations. More precisely, $\sin\theta \approx \theta$, $\cos\theta \approx 1$. Moreover, the second order terms are neglected $\dot{\theta}^2\theta \approx 0$. Applying these simplifications, (B.29) and (B.30) reduce to:

$$\left(I_u + m_l L_u^2\right)\ddot{q}_u + m_l L_u r_l \ddot{q}_l \quad + \sigma g \left(m_l L_u - m_u r_u\right) q_u \quad = 0 \tag{B.31}$$

$$\left(I_l + m_l r_l^2\right)\ddot{q}_l + m_l L_u r_l \ddot{q}_u \quad + \sigma g m_l r_l q_l \quad = 0 \tag{B.32}$$

Let $q_u(t) = A_u \cos\omega t$ and $q_l(t) = A_l \cos\omega t$. Since the angular variables appear in the above equations only on even order of derivation, the time dependence can be canceled. Hence, it follows a system of two equations where the amplitudes A_u and A_l are the unknown, for a fixed ω:

$$\begin{array}{rrl} \left[\left(I_u + m_l L_u^2\right) + \sigma g \left(m_u r_u - m_l L_u\right)\right]\ A_u + & \omega^2 m_l L_u r_l\ A_l & = 0 \\ \omega^2 m_l L_u r_l\ A_u + & \left[\left(I_l + m_l r_l^2\right)\omega^2 - \sigma g m_l r_l\right]\ A_l & = 0 \end{array}$$

In order to avoid the trivial solution $A_u = A_l = 0$, we must ensure that the determinant of the following (symmetric) matrix be equal to 0:

$$\det \begin{vmatrix} I_u\omega^2 + m_l L_u^2 \omega^2 + \sigma g \left(m_u r_u - m_l L_u\right) & \omega^2 m_l L_u r_l \\ \omega^2 m_l L_u r_l & I_l \omega^2 + m_l r_l^2 \omega^2 + -\sigma g m_l r_l \end{vmatrix} = 0$$

This leads to a bisquarred equation in ω:

$$\begin{array}{rr} \left[\left(I_u + m_l L_u^2\right)\left(I_l + m_l r_l^2\right) - m_l^2 L_u^2 r_l^2\right]\omega^4 & + \\ \left[\sigma g \left(m_u r_u - m_l L_u\right)\left(I_l + m_l r_l^2\right) - \sigma g m_l r_l \left(I_u + m_l L_u^2\right)\right]\omega^2 & - \\ \sigma^2 g^2 m_l r_l \left(m_u r_u - m_l L_u\right) & = 0 \end{array}$$

If we denote the coefficients by a, b and c, we get:

$$a\omega^4 + b\omega^2 + c = 0 \tag{B.33}$$

Since $\omega = \frac{2\pi}{T}$, the normal modes follow directly:

$$T = 2\pi\sqrt{\frac{2a}{-b \pm \sqrt{b^2 - 4ac}}} \tag{B.34}$$

The evolution of the principal mode in function of gravity is shown on Figure B.3. Note that values of the period rise toward infinity when g decreases to 0ms^{-2}.

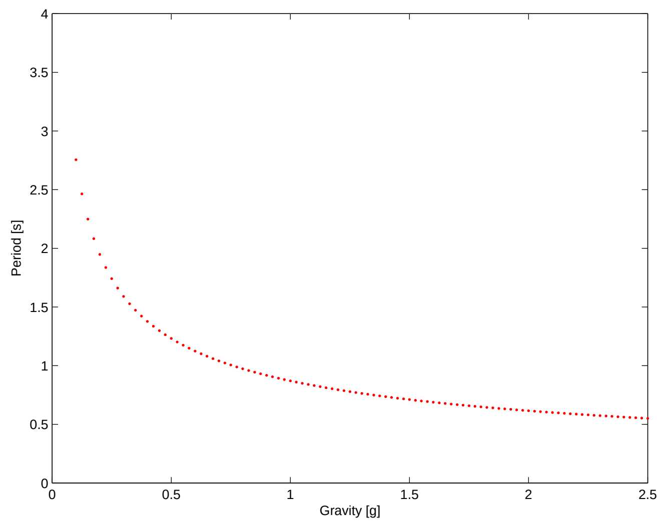

Figure B.3: Natural frequency of the upper limb in function of gravity under assumption of small oscillations

B.5 Resolution of the equations

In order to solve the equations of motion (B.29 and B.30), we have to reduce the system to a first-order set of equations, following the form:

$$\dot{x} = f(x,t) \tag{B.35}$$

B.5.1 Reduction of the system

Let define the following auxiliary variables:

$$\begin{array}{ll} x_1 = q_u & y_l = q_l \\ x_2 = \dot{q}_u & y_2 = \dot{q}_l \end{array}$$

By plugging the above definitions in the equations of motion, we can isolate first-derivative in the left-hand side:

$$\left\{ \begin{array}{lcl} \left(I_u + m_l L_u^2\right) \dot{x}_2 + m_l L_u r_l \dot{y}_2 \cos(y_1 - x_1) & = & m_l L_u r_l y_2^2 \sin(y_1 - x_1) - \\ & & \sigma g \left(m_l L_u - m_u r_u\right) \sin x_1 \\ \left(I_l + m_l r_l^2\right) \dot{y}_2 + m_l L_u r_l \dot{x}_2 \cos(y_1 - x_1) & = & -m_l L_u r_l x_2^2 \sin(y_1 - x_1) \\ & & -\sigma g m_l r_l \sin y_1 \end{array} \right.$$

Defining the right-hand side of the above expression by $f(x_1, y_1, x_2, y_2)$, and adapting matrix formalism, we can write:

$$\begin{pmatrix} (I_u + m_l L_u^2) & m_l L_u r_l \cos(y_1 - x_1) \\ m_l L_u r_l \cos(y_1 - x_1) & (I_l + m_l r_l^2) \end{pmatrix} \begin{pmatrix} \dot{x}_2 \\ \dot{y}_2 \end{pmatrix} = f(x_1, y_1, x_2, y_2)$$

Therefore, we meet the requirements for the equation of motion to be solved in Matlab (ode45 function, since the problem is non stiff):

$$\begin{pmatrix} \dot{x}_2 \\ \dot{y}_2 \end{pmatrix} = \begin{pmatrix} (I_u + m_l L_u^2) & m_l L_u r_l \cos(y_1 - x_1) \\ m_l L_u r_l \cos(y_1 - x_1) & (I_l + m_l r_l^2) \end{pmatrix}^{-1} f(x_1, y_1, x_2, y_2)$$

The two other variables follow from definition:

$$\begin{pmatrix} \dot{x}_1 \\ \dot{y}_1 \end{pmatrix} = \begin{pmatrix} x_2 \\ y_2 \end{pmatrix}$$

B.5.2 Simulations

In this section, we present some numerical simulations of our double compound pendulum model. On the figure below, we depict the evolution of q_u and q_l over time for the following initial conditions:

$$\begin{pmatrix} q_u \\ q_l \\ \dot{q}_u \\ \dot{q}_l \end{pmatrix} = \begin{pmatrix} \pi/8 \\ \pi/5 \\ 0 \\ 0 \end{pmatrix}$$

The two links are initially displaced to the right at different swing angles. Then the system is let free to oscillate. Since there is no damping, the amplitudes of oscillations remain constant over time. Note that although the behaviours of both links are periodic, the lower one adopts a more complicated pattern. We were interested to see how gravity influences the natural frequency of the system for a given initial condition. Therefore, we resolved the equations of motion for a range of gravity parameterized by σ. The range covered 0.1 g to 3 g. The period reaches infinity in microgravity. In order to calculate the period, we applied a FFT over the upper link signal. At this point, we see that the assumptions of small oscillations (red trace) is a good approximation of the real system (blue dots) and that this model reproduces the trend we observed in our data.

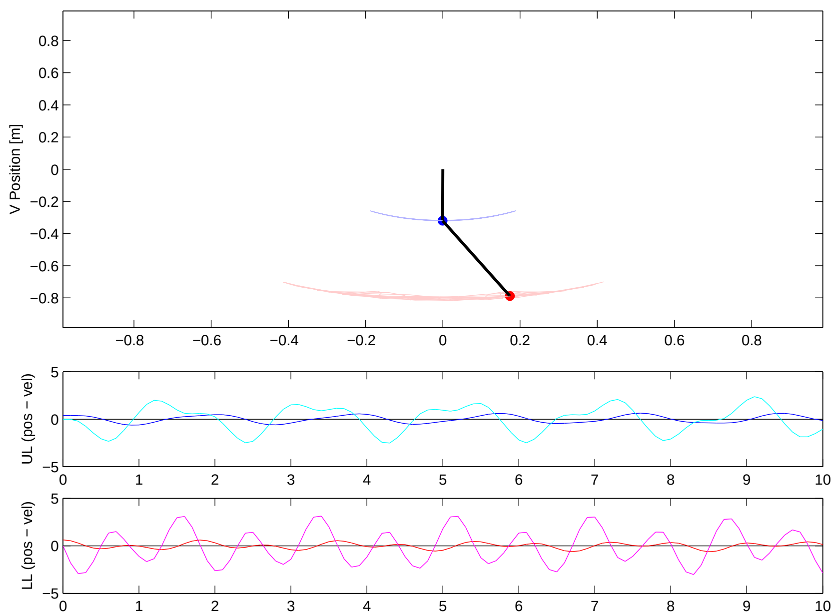

Figure B.4: Simulation of the double compound pendulum during 10 seconds. The upper panel presents a 2D diagram of the system. The two panels below show the positions and velocities for the upper (UL) and lower (LL) links, respectively. Positions are depicted in dark blue and red. Velocities are plotted in light blue and magenta.

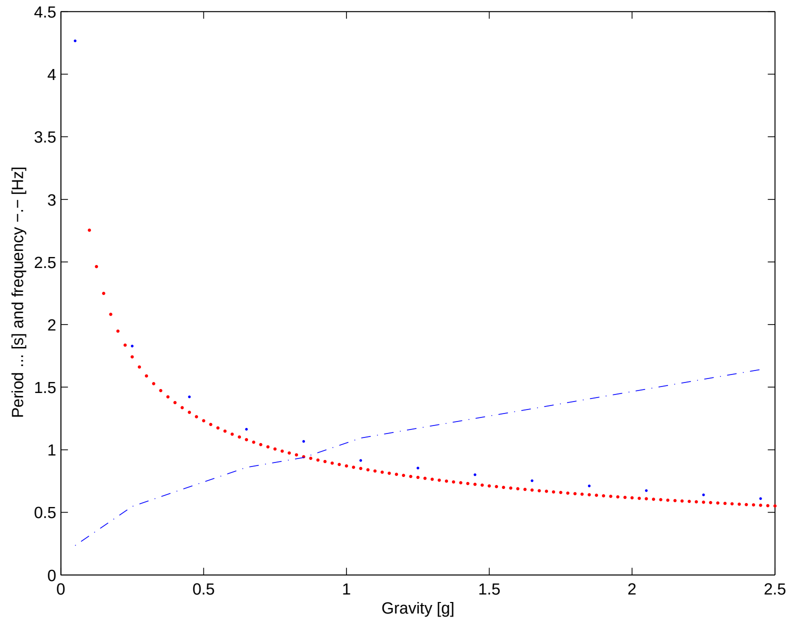

Figure B.5: Period and natural frequency in function of gravity. Assumption of small oscillations in red. Unsimplified system with blue dots. The dash-dotted curve shows the frequency.

B.6 The spherical pendulum

In this section, we modeled the upper limb with a spherical pendulum under the action of gravity (g) in order to approach the real system more closely. Because its motion takes place on a sphere, we used spherical coordinates to derive the equations of motion (Fig. B.6). The dynamics of motion can be described by the Lagrangian $L = T - V$ where T and V represent the kinetic and potential energies respectively. Kinetic energy is always given by:

$$T = \frac{1}{2}mv^2 \tag{B.36}$$

with $v = \dot{x} + \dot{y} + \dot{z}$. Assuming the system reaches a maximum potential energy when $\theta = 0$ and a minimum potential energy when $\theta = \pi$, then:

$$V = mgz = mgl\cos\theta \tag{B.37}$$

The Lagrangian is then given by:

$$L = \frac{1}{2}\left[(l\dot{\theta})^2 + (l\dot{\phi}\sin\theta)^2\right] - mgl\cos\theta \tag{B.38}$$

The angular momentum p_θ and p_ϕ of the pendulum with respect to θ and ϕ are introduced using the Lagrangian:

$$\begin{aligned} p_\theta = \frac{\partial L}{\partial \dot{\theta}} &= ml^2\dot{\theta} \\ p_\phi = \frac{\partial L}{\partial \dot{\phi}} &= ml^2\dot{\phi}\sin^2\theta \end{aligned}$$

Conservative systems can be modeled using Hamilton's equations: $-\frac{\partial p_i}{\partial t} = \frac{\partial H}{\partial q_i}$ and $\frac{\partial q_i}{\partial t} = \frac{\partial H}{\partial p_i}$, where p_i and q_i are the canonical conjugates state variables, and the Hamiltonian $H = T+V = const$. After substitution of the momentums into the Lagrangian, we obtain the Hamiltonian:

$$H = \frac{1}{2m}\left[\frac{p_\theta^2}{l^2} + \frac{p_\phi^2}{l^2\sin^2\theta}\right] \tag{B.39}$$

In our problem, we have $q_1 = \theta$, $q_2 = \phi$, $p_1 = p_\theta$ and $p_2 = p_\phi$. Applying these conditions, we derive the equations of motion of an undamped free spherical pendulum:

$$\begin{aligned} \dot{\theta} &= \frac{p_\theta}{ml^2} \\ \dot{p_\theta} &= \frac{\cos\theta p_\phi^2}{ml^2\sin^3\theta} + mgl\sin\theta \\ \dot{\phi} &= \frac{p_\theta}{ml^2\sin^2\theta} \\ \dot{p_\phi} &= 0 \end{aligned}$$

In practice, the pendulum is recalled to its rest position (collinear with the Y-axis) by either passive (muscular stiffness) or active (muscular force) mechanisms. Therefore, we implemented restoring torques around the X-axis (θ) and Z-axis (ϕ) proportional to angular displacements. We solved the system numerically using a Predictor-Corrector method with Runge-Kutta of order four as the predictor (MATLAB, Mathworks Inc.).

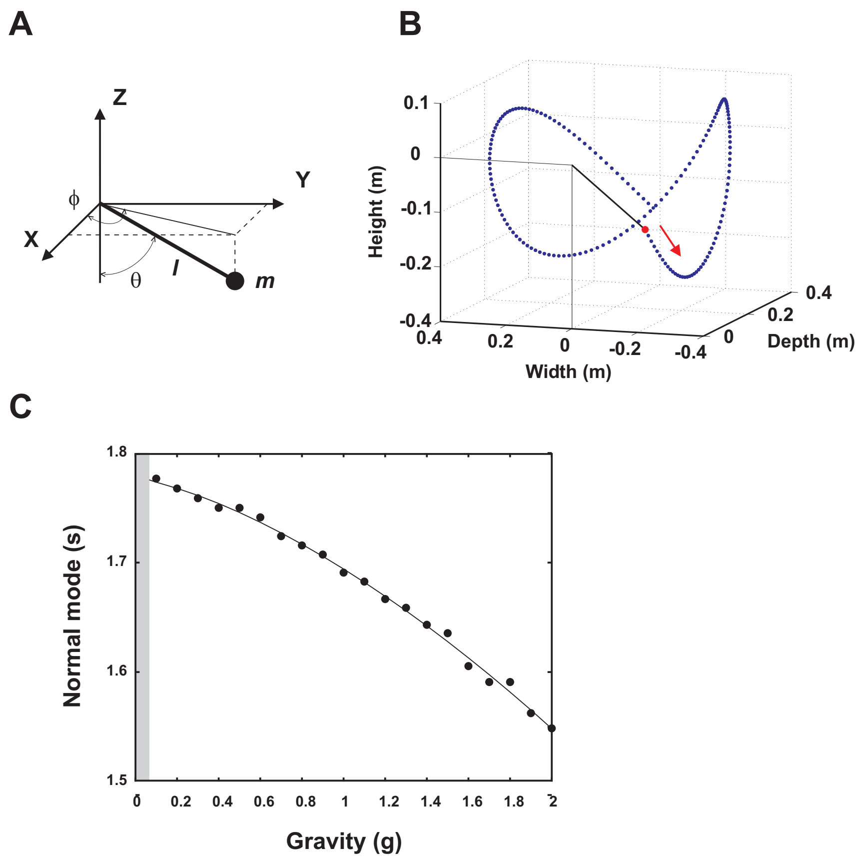

Figure B.6: The two-degrees of freedom spherical pendulum model. (A) Pendulum of mass m and rigid chord of length l attached to the origin. The position of m is specified by the spherical transformations: $x = l \sin\theta \cos\phi$, $y = l \sin\theta \sin\phi$ and $z = l \cos\phi$. (B) Simulation of one cycle ($T = 1.73$ s) after integration of the equations of motions for the following parameters: $g = 9.81$ ms^{-2}, $m = 0.8$ kg, $l = 0.8$ m, damping coefficients $= 0.2$ s^{-1}. Initial conditions: $\theta(0) = \frac{3\pi}{8}$, $\phi(0) = 0$, $p_\theta(0) = 5$ Nms and $p_\phi(0) = 10$ Nms. Blue dots are spaced by 200 ms. (C) Natural frequency as a function of gravity computed by DFT over 100 seconds for the actuated (green) or unactuated (red) pendulum model. Thin black line are a polynomial fit of degree 4.

References

K. Abahnini and L. Proteau. The role of peripheral and central visual information for the directional control of manual aiming movements. *Can J Exp Psychol*, 53(2):160–75, 1999. 1196-1961 (Print) Journal Article Research Support, Non-U.S. Gov't. 15

M. O. Abe and N. Yamada. Modulation of elbow joint stiffness in a vertical plane during cyclic movement at lower or higher frequencies than natural frequency. *Exp Brain Res*, 153(3):394–9, 2003. 0014-4819 (Print) Journal Article. 41

R. A. Andersen, L. H. Snyder, A. P. Batista, C. A. Buneo, and Y. E. Cohen. Posterior parietal areas specialized for eye movements (lip) and reach (prr) using a common coordinate frame. *Novartis Found Symp*, 218:109–22; discussion 122–8, 171–5, 1998. 96

R. W. Angel, W. Alston, and H. Garland. Functional relations between the manual and oculomotor control systems. *Exp Neurol*, 27(2):248–57, 1970. 95

D. E. Angelaki and J. D. Dickman. Spatiotemporal processing of linear acceleration: primary afferent and central vestibular neuron responses. *J Neurophysiol*, 84(4):2113–32, 2000. 0022-3077 (Print) Journal Article Research Support, U.S. Gov't, Non-P.H.S. Research Support, U.S. Gov't, P.H.S. 77

D. E. Angelaki, A. G. Shaikh, A. M. Green, and J. D. Dickman. Neurons compute internal models of the physical laws of motion. *Nature*, 430(6999): 560–4, 2004. 1476-4687 (Electronic) Journal Article Research Support, U.S. Gov't, Non-P.H.S. Research Support, U.S. Gov't, P.H.S. 77

G. Ariff, O. Donchin, T. Nanayakkara, and R. Shadmehr. A real-time state predictor in motor control: study of saccadic eye movements during unseen reaching movements. *J Neurosci*, 22(17):7721–9, 2002. 18, 124

C. G. Atkeson. Learning arm kinematics and dynamics. *Annu Rev Neurosci*, 12:157–83, 1989. 18

C. G. Atkeson and J. M. Hollerbach. Kinematic features of unrestrained vertical arm movements. *J Neurosci*, 5(9):2318–30, 1985. 23

A. S. Augurelle, M. Penta, O. White, and J. L. Thonnard. The effects of a change in gravity on the dynamics of prehension. *Exp Brain Res*, 148(4): 533–40, 2003. 23, 24, 28, 45, 46, 47, 59, 60, 62, 93, 101, 107, 112, 113, 126

P. Bedard and L. Proteau. On the role of static and dynamic visual afferent information in goal-directed aiming movements. *Exp Brain Res*, 138(4):419–31, 2001. 96

M. Berger, S. Mescheriakov, E. Molokanova, S. Lechner-Steinleitner, N. Seguer, and I. Kozlovskaya. Pointing arm movements in short- and long-term space-flights. *Aviat Space Environ Med*, 68(9):781–7, 1997. 41

N Bernstein. *The Co-ordination and Regulation of Movement*. A.M. Wing, P. Haggard, J.R. Flanagan (Eds) Hand and Brain, 1967. 6, 10, 41

S. M. Beurze, S. Van Pelt, and W. P. Medendorp. Behavioral reference frames for planning human reaching movements. *J Neurophysiol*, 96(1):352–62, 2006. 0022-3077 (Print) Journal Article Research Support, Non-U.S. Gov't. 96

B. Biguer, M. Jeannerod, and C. Prablanc. The coordination of eye, head, and arm movements during reaching at a single visual target. *Exp Brain Res*, 46(2):301–4, 1982. 0014-4819 (Print) Journal Article Research Support, Non-U.S. Gov't. 11

G. Binsted, R. Chua, W. Helsen, and D. Elliott. Eye-hand coordination in goal-directed aiming. *Hum Mov Sci*, 20(4-5):563–85, 2001. 114

S. J. Blakemore, S. J. Goodbody, and D. M. Wolpert. Predicting the consequences of our own actions: the role of sensorimotor context estimation. *J Neurosci*, 18(18):7511–8, 1998. 60, 67

R. Blank, A. Breitenbach, M. Nitschke, W. Heizer, S. Letzgus, and J. Hermsdorfer. Human development of grip force modulation relating to cyclic movement-induced inertial loads. *Exp Brain Res*, 138(2):193–9, 2001. 121

J. Blouin, N. Teasdale, C. Bard, and M. Fleury. Directional control of rapid arm movements: the role of the kinetic visual feedback system. *Can J Exp*

Psychol, 47(4):678–96, 1993. 1196-1961 (Print) Journal Article Research Support, Non-U.S. Gov't. 15

J. Blouin, G. M. Gauthier, and J. L. Vercher. Internal representation of gaze direction with and without retinal inputs in man. *Neurosci Lett*, 183(3):187–9, 1995. 0304-3940 (Print) Clinical Trial Journal Article Research Support, Non-U.S. Gov't. 11

O. Bock. Problems of sensorimotor coordination in weightlessness. *Brain Res Brain Res Rev*, 28(1-2):155–60, 1998. 35, 63

F. P. Bowden. Friction on snow and ice. *Proceedings of the Royal Society of London. Series A, Mathematical and Physical Sciences*, 217(1131):462–478, 1953. 122

T. Brown. The intrinsic factors in the act of progression in the mammal. *Proc Roy Soc Lond B Biol Sci*, 84:308–319, 1911. Journal article. 14, 34

C. A. Buneo, M. R. Jarvis, A. P. Batista, and R. A. Andersen. Direct visuomotor transformations for reaching. *Nature*, 416(6881):632–6, 2002. 0028-0836 (Print) Journal Article. 96

E. Burdet, R. Osu, D. W. Franklin, T. E. Milner, and M. Kawato. The central nervous system stabilizes unstable dynamics by learning optimal impedance. *Nature*, 414(6862):446–9, 2001. 95

R. E. Burke. The central pattern generator for locomotion in mammals. *Adv Neurol*, 87:11–24, 2001. 0091-3952 (Print) Journal Article Review. 34

D. P. Carey. Eye-hand coordination: eye to hand or hand to eye? *Curr Biol*, 10(11):R416–9, 2000. 96

A. H. Clarke, J. Ditterich, K. Druen, U. Schonfeld, and C. Steineke. Using high frame rate cmos sensors for three-dimensional eye tracking. *Behav Res Methods Instrum Comput*, 34(4):549–60, 2002. 81, 102

L. A. Cohen. Role of eye and neck proprioceptive mechanisms in body orientation and motor coordination. *J Neurophysiol*, 24:1–11, 1961. 0022-3077 (Print) Journal Article. 12

M. A. Conditt, F. Gandolfo, and F. A. Mussa-Ivaldi. The motor system does not learn the dynamics of the arm by rote memorization of past experience. *J Neurophysiol*, 78(1):554–60, 1997. 22

J. D. Crawford, W. P. Medendorp, and J. J. Marotta. Spatial transformations for eye-hand coordination. *J Neurophysiol*, 92(1):10–9, 2004. 96

F. Danion. How dependent are grip force and arm actions during holding an object? *Exp Brain Res*, 158(1):109–19, 2004. 119

M. Davare, M. Andres, G. Cosnard, J. L. Thonnard, and E. Olivier. Dissociating the role of ventral and dorsal premotor cortex in precision grasping. *J Neurosci*, 26(8):2260–8, 2006. 132

P. R. Davidson and D. M. Wolpert. Widespread access to predictive models in the motor system: a short review. *J Neural Eng*, 2(3):S313–9, 2005. 1741-2560 (Print) Journal Article Review. 124

P. R. Davidson and D. M. Wolpert. Internal models underlying grasp can be additively combined. *Exp Brain Res*, 155(3):334–40, 2004. 17, 19, 22, 77

P. R. Davidson, D. M. Wolpert, S. H. Scott, and J. R. Flanagan. Common encoding of novel dynamic loads applied to the hand and arm. *J Neurosci*, 25(22):5425–9, 2005. 19

P. T. de Jong, J. M. de Jong, B. Cohen, and L. B. Jongkees. Ataxia and nystagmus induced by injection of local anesthetics in the neck. *Ann Neurol*, 1(3):240–6, 1977. 0364-5134 (Print) Journal Article Research Support, U.S. Gov't, P.H.S. 12

F. Delcomyn. Neural basis of rhythmic behavior in animals. *Science*, 210 (4469):492–8, 1980. 0036-8075 (Print) Journal Article Research Support, U.S. Gov't, P.H.S. 14

Y. N. Delevoye-Turrell, F. X. Li, and A. M. Wing. Efficiency of grip force adjustments for impulsive loading during imposed and actively produced collisions. *Q J Exp Psychol A*, 56(7):1113–28, 2003. 80

M. Demont. Tuned oscillations in the swimming scallop pectenmaximus. *Can J Zool*, 68(4):786–791, 1990. 41

M. Descoins, F. Danion, and R. J. Bootsma. Predictive control of grip force when moving object with an elastic load applied on the arm. *Exp Brain Res*, 172(3):331–42, 2006. 20, 119

M. Desmurget, D. Pelisson, Y. Rossetti, and C. Prablanc. From eye to hand: planning goal-directed movements. *Neurosci Biobehav Rev*, 22(6):761–88, 1998. 11, 80, 96

V. Dietz. Do human bipeds use quadrupedal coordination? *Trends Neurosci*, 25(9):462, 2002. 34

J. B. Dingwell, C. D. Mah, and F. A. Mussa-Ivaldi. Experimentally confirmed mathematical model for human control of a non-rigid object. *J Neurophysiol*, 91(3):1158–70, 2004. 20

P. Dizio and J. R. Lackner. Motor adaptation to coriolis force perturbations of reaching movements: endpoint but not trajectory adaptation transfers to the nonexposed arm. *J Neurophysiol*, 74(4):1787–92, 1995. 20

A. Dubrowski, J. Lam, and H. Carnahan. Target velocity effects on manual interception kinematics. *Acta Psychol (Amst)*, 104(1):103–18, 2000. 10, 114

C. Dugas and A. M. Smith. Responses of cerebellar purkinje cells to slip of a hand-held object. *J Neurophysiol*, 67(3):483–95, 1992. 0022-3077 (Print) Journal Article Research Support, Non-U.S. Gov't. 18

B. B. Edin. Quantitative analyses of dynamic strain sensitivity in human skin mechanoreceptors. *J Neurophysiol*, 92(6):3233–43, 2004. 0022-3077 (Print) Journal Article Research Support, Non-U.S. Gov't. 77

A. Einstein. On the relativity principle and the conclusions drawn from it. *Jahrbuch der Radioaktivitaet und Elektronik*, 4, 1907. 67

J. Epelboim, R. M. Steinman, E. Kowler, Z. Pizlo, C. J. Erkelens, and H. Collewijn. Gaze-shift dynamics in two kinds of sequential looking tasks. *Vision Res*, 37(18):2597–607, 1997. 95

E. Espinoza and A. M. Smith. Purkinje cell simple spike activity during grasping and lifting objects of different textures and weights. *J Neurophysiol*, 64(3):698–714, 1990. 0022-3077 (Print) Journal Article Research Support, Non-U.S. Gov't. 18

C. Fernandez and J. M. Goldberg. Physiology of peripheral neurons innervating otolith organs of the squirrel monkey. i. response to static tilts and to long-duration centrifugal force. *J Neurophysiol*, 39(5):970–84, 1976. 0022-3077 (Print) Journal Article Research Support, U.S. Gov't, Non-P.H.S. Research Support, U.S. Gov't, P.H.S. 77

J. Fisk, J. R. Lackner, and P. DiZio. Gravitoinertial force level influences arm movement control. *J Neurophysiol*, 69(2):504–11, 1993. 63, 119

Flanagan and Johansson. *Hand movements. In: Ramashandran VS (ed) Encyclopedia of the human brain.* Academic Press, San Diego, 2002. 44

J. R. Flanagan and S. Lolley. The inertial anisotropy of the arm is accurately predicted during movement planning. *J Neurosci*, 21(4):1361–9, 2001. 18, 114

J. R. Flanagan and J. R. Tresilian. Grip-load force coupling: a general control strategy for transporting objects. *J Exp Psychol Hum Percept Perform*, 20 (5):944–57, 1994. 44, 60, 66, 126

J. R. Flanagan and A. M. Wing. Modulation of grip force with load force during point-to-point arm movements. *Exp Brain Res*, 95(1):131–43, 1993. 10, 44, 59, 66, 76, 80, 94, 100, 119, 126

J. R. Flanagan and A. M. Wing. The stability of precision grip forces during cyclic arm movements with a hand-held load. *Exp Brain Res*, 105(3):455–64, 1995. 10, 17, 44, 61, 66, 67, 76, 80, 94, 100, 119, 121

J. R. Flanagan and A. M. Wing. The role of internal models in motion planning and control: evidence from grip force adjustments during movements of hand-held loads. *J Neurosci*, 17(4):1519–28, 1997. 17, 44, 59, 66, 67, 80, 119, 126

J. R. Flanagan, J. Tresilian, and A. M. Wing. Coupling of grip force and load force during arm movements with grasped objects. *Neurosci Lett*, 152(1-2): 53–6, 1993. 80, 100, 119, 126

J. R. Flanagan, M. K. Burstedt, and R. S. Johansson. Control of fingertip forces in multidigit manipulation. *J Neurophysiol*, 81(4):1706–17, 1999a. 44, 59

J. R. Flanagan, E. Nakano, H. Imamizu, R. Osu, T. Yoshioka, and M. Kawato. Composition and decomposition of internal models in motor learning under altered kinematic and dynamic environments. *J Neurosci*, 19(20):RC34, 1999b. 44, 59, 61

J. R. Flanagan, P. Vetter, R. S. Johansson, and D. M. Wolpert. Prediction precedes control in motor learning. *Curr Biol*, 13(2):146–50, 2003. 20, 80, 93, 112, 126

T. Flash and N. Hogan. The coordination of arm movements: an experimentally confirmed mathematical model. *J Neurosci*, 5(7):1688–703, 1985. 12, 20

H. Forssberg, A. C. Eliasson, H. Kinoshita, R. S. Johansson, and G. Westling. Development of human precision grip. i: Basic coordination of force. *Exp Brain Res*, 85(2):451–7, 1991. 19

D. W. Franklin, E. Burdet, R. Osu, M. Kawato, and T. E. Milner. Functional significance of stiffness in adaptation of multijoint arm movements to stable and unstable dynamics. *Exp Brain Res*, 151(2):145–57, 2003. 95

F. Gao, M. L. Latash, and V. M. Zatsiorsky. Internal forces during object manipulation. *Exp Brain Res*, 165(1):69–83, 2005. 126

R. Gentili, V. Cahouet, and C. Papaxanthis. Motor planning of arm movements is direction-dependent in the gravity field. *Neuroscience*, 145(1):20–32, 2007. 0306-4522 (Print) Journal Article. 115

Z. Ghahramani, D. M. Wolpert, and M. I. Jordan. Generalization to local remappings of the visuomotor coordinate transformation. *J Neurosci*, 16 (21):7085–96, 1996. 22

C. Ghez, J. Gordon, and M. F. Ghilardi. Impairments of reaching movements in patients without proprioception. ii. effects of visual information on accuracy. *J Neurophysiol*, 73(1):361–72, 1995. 0022-3077 (Print) Journal Article Research Support, Non-U.S. Gov't Research Support, U.S. Gov't, P.H.S. 12

S. J. Goodbody and D. M. Wolpert. Temporal and amplitude generalization in motor learning. *J Neurophysiol*, 79(4):1825–38, 1998. 22

S. J. Goodbody and D. M. Wolpert. The effect of visuomotor displacements on arm movement paths. *Exp Brain Res*, 127(2):213–23, 1999. 13

L. Goodman, M. A. Riley, S. Mitra, and M. T. Turvey. Advantages of rhythmic movements at resonance: minimal active degrees of freedom, minimal noise, and maximal predictability. *J Mot Behav*, 32(1):3–8, 2000. 0022-2895 (Print) Journal Article. 41

A. W. Goodwin, P. Jenmalm, and R. S. Johansson. Control of grip force when tilting objects: effect of curvature of grasped surfaces and applied tangential torque. *J Neurosci*, 18(24):10724–34, 1998. 126

A. M. Gordon, H. Forssberg, R. S. Johansson, and G. Westling. The integration of haptically acquired size information in the programming of precision grip. *Exp Brain Res*, 83(3):483–8, 1991. 19

A. M. Gordon, H. Forssberg, R. S. Johansson, A. C. Eliasson, and G. Westling. Development of human precision grip. iii. integration of visual size cues during the programming of isometric forces. *Exp Brain Res*, 90(2):399–403, 1992. 19

A. M. Gordon, G. Westling, K. J. Cole, and R. S. Johansson. Memory representations underlying motor commands used during manipulation of common and novel objects. *J Neurophysiol*, 69(6):1789–96, 1993. 10, 19

A. M. Gordon, H. Forssberg, and N. Iwasaki. Formation and lateralization of internal representations underlying motor commands during precision grip. *Neuropsychologia*, 32(5):555–68, 1994. 19

P. L. Gribble, S. Everling, K. Ford, and A. Mattar. Hand-eye coordination for rapid pointing movements. arm movement direction and distance are specified prior to saccade onset. *Exp Brain Res*, 145(3):372–82, 2002. 18

FS Grodins. *Control theory and biological systems.* Columbia Univ Pr, 1963. 3

P. Gysin, T. R. Kaminski, and A. M. Gordon. Coordination of fingertip forces in object transport during locomotion. *Exp Brain Res*, 149(3):371–9, 2003. 44, 60, 66

C. M. Harris and D. M. Wolpert. Signal-dependent noise determines motor planning. *Nature*, 394(6695):780–4, 1998. 13

M. Haruno, D. M. Wolpert, and M. Kawato. Mosaic model for sensorimotor learning and control. *Neural Comput*, 13(10):2201–20, 2001. 19, 119

N. G. Hatsopoulos. Coupling the neural and physical dynamics in rhythmic movements. *Neural Comput*, 8(3):567–81, 1996. 34, 35

N. G. Hatsopoulos and W. H. Warren Jr. Resonance tuning in rhythmic arm movements. *J Mot Behav*, 28(1):3–14, 1996. 14, 35

J. Hermsdorfer, C. Marquardt, J. Philipp, A. Zierdt, D. Nowak, S. Glasauer, and N. Mai. Grip forces exerted against stationary held objects during gravity changes. *Exp Brain Res*, 126(2):205–14, 1999. 45, 78, 122

J. Hermsdorfer, C. Marquardt, J. Philipp, A. Zierdt, D. Nowak, S. Glasauer, and N. Mai. Moving weightless objects. grip force control during microgravity. *Exp Brain Res*, 132(1):52–64, 2000. 45, 59, 62, 63, 78, 107, 113, 126

N. Hogan. An organizing principle for a class of voluntary movements. *J Neurosci*, 4(11):2745–54, 1984. 12

Holt. The force-driven harmonic oscillator as a model for human locomotion. *Hum Mov Sci*, 1990. 14, 41

K. J. Holt, S. F. Jeng, R. R. Rr, and J. Hamill. Energetic cost and stability during human walking at the preferred stride velocity. *J Mot Behav*, 27(2): 164–178, 1995. 0022-2895 (Print) Journal article. 41

H. Imamizu, Y. Uno, and M. Kawato. Internal representations of the motor apparatus: implications from generalization in visuomotor learning. *J Exp Psychol Hum Percept Perform*, 21(5):1174–98, 1995. 22

I. Indovina, V. Maffei, G. Bosco, M. Zago, E. Macaluso, and F. Lacquaniti. Representation of visual gravitational motion in the human vestibular cortex. *Science*, 308(5720):416–9, 2005. 24, 120

T. Iwasaki and M. Zheng. Sensory feedback mechanism underlying entrainment of central pattern generator to mechanical resonance. *Biol Cybern*, 94(4): 245–61, 2006. 0340-1200 (Print) Journal Article. 34, 35

M. Jeannerod. *The neural and behavioural organization of goal directed movements*. Oxford, clarendon press edition, 1988. 15, 115

P. Jenmalm and R. S. Johansson. Visual and somatosensory information about object shape control manipulative fingertip forces. *J Neurosci*, 17(11):4486–99, 1997. 21, 44

R. S. Johansson and K. J. Cole. Grasp stability during manipulative actions. *Can J Physiol Pharmacol*, 72(5):511–24, 1994. 17

R. S. Johansson and G. Westling. Roles of glabrous skin receptors and sensorimotor memory in automatic control of precision grip when lifting rougher or more slippery objects. *Exp Brain Res*, 56(3):550–64, 1984. 10, 11, 44, 77, 126, 129

R. S. Johansson and G. Westling. Signals in tactile afferents from the fingers eliciting adaptive motor responses during precision grip. *Exp Brain Res*, 66 (1):141–54, 1987. 11, 14, 77

R. S. Johansson and G. Westling. Programmed and triggered actions to rapid load changes during precision grip. *Exp Brain Res*, 71(1):72–86, 1988. 11, 19, 80, 94, 100

R. S. Johansson, C. Hager, and R. Riso. Somatosensory control of precision grip during unpredictable pulling loads. ii. changes in load force rate. *Exp Brain Res*, 89(1):192–203, 1992a. 11, 94, 100

R. S. Johansson, R. Riso, C. Hager, and L. Backstrom. Somatosensory control of precision grip during unpredictable pulling loads. i. changes in load force amplitude. *Exp Brain Res*, 89(1):181–91, 1992b. 11

R. S. Johansson, G. Westling, A. Backstrom, and J. R. Flanagan. Eye-hand coordination in object manipulation. *J Neurosci*, 21(17):6917–32, 2001. 80, 93, 96, 100, 115

Jordan and Wolpert. *Computational motor control. The Cognitive Neurosciences (601-620).* Gazzaniga, (Ed.). Cambridge, MIT Press, 1999. 10, 12

P. S. Katz. Intrinsic and extrinsic neuromodulation of motor circuits. *Curr Opin Neurobiol*, 5(6):799–808, 1995. 0959-4388 (Print) Journal Article Review. 42

M. Kawato. Internal models for motor control and trajectory planning. *Curr Opin Neurobiol*, 9(6):718–27, 1999. 17, 44, 60, 67, 77, 115, 119

M. Kawato, T. Kuroda, H. Imamizu, E. Nakano, S. Miyauchi, and T. Yoshioka. Internal forward models in the cerebellum: fmri study on grip force and load force coupling. *Prog Brain Res*, 142:171–88, 2003. 18

H. Kinoshita, L. Backstrom, J. R. Flanagan, and R. S. Johansson. Tangential torque effects on the control of grip forces when holding objects with a precision grip. *J Neurophysiol*, 78(3):1619–30, 1997. 126

L. Kogut and I. Etsion. A static friction model for elastic-plastic contacting rough surfaces. *Transactions of the ASME*, 126:34–40, 2004. 122

K. P. Kording and D. M. Wolpert. Bayesian integration in sensorimotor learning. *Nature*, 427(6971):244–7, 2004. 22, 119

J. W. Krakauer, M. F. Ghilardi, and C. Ghez. Independent learning of internal models for kinematic and dynamic control of reaching. *Nat Neurosci*, 2(11): 1026–31, 1999. 123

P.N. Kugler and M.T. Turvey. *Information, natural law, and the self-assembly of rhythmic movement.* Hillsdale, NJ, lawrence erlbaum edition, 1987. 14, 34

J. R. Lackner and P. DiZio. Gravitoinertial force level affects the appreciation of limb position during muscle vibration. *Brain Res*, 592(1-2):175–80, 1992. 115

J. R. Lackner and P. Dizio. Rapid adaptation to coriolis force perturbations of arm trajectory. *J Neurophysiol*, 72(1):299–313, 1994. 21

J. R. Lackner and P. DiZio. Motor function in microgravity: movement in weightlessness. *Curr Opin Neurobiol*, 6(6):744–50, 1996. 35

J. R. Lackner and P. Dizio. Gravitoinertial force background level affects adaptation to coriolis force perturbations of reaching movements. *J Neurophysiol*, 80(2):546–53, 1998. 13

F. Lacquaniti, C. Terzuolo, and P. Viviani. The law relating the kinematic and figural aspects of drawing movements. *Acta Psychol (Amst)*, 54(1-3):115–30, 1983. 12

K.S. Lashley. Basic neural mechanisms in behavior. *Psychological Review*, 37: 1–24, 1930. 6

S. Lazzari, J. L. Vercher, and A. Buizza. Manuo-ocular coordination in target tracking. i. a model simulating human performance. *Biol Cybern*, 77(4): 257–66, 1997. 18

T. L. Lillicrap and P. Katerine. Learning dancing with neurons. *Nat Louxor Bar*, 27(2):248–57, 2004. 143

D. C. Lin and W. Z. Rymer. Damping in reflexively active and areflexive lengthening muscle evaluated with inertial loads. *J Neurophysiol*, 80(6):3369–72, 1998. 0022-3077 (Print) Journal Article Research Support, U.S. Gov't, P.H.S. 95

E. Marder. Motor pattern generation. *Curr Opin Neurobiol*, 10(6):691–8, 2000. 0959-4388 (Print) Journal Article Research Support, Non-U.S. Gov't Research Support, U.S. Gov't, P.H.S. Review. 34, 118

E. Marder and R. L. Calabrese. Principles of rhythmic motor pattern generation. *Physiol Rev*, 76(3):687–717, 1996. 0031-9333 (Print) Journal Article Research Support, Non-U.S. Gov't Research Support, U.S. Gov't, P.H.S. Review. 14

E. Marder and J. M. Goaillard. Variability, compensation and homeostasis in neuron and network function. *Nat Rev Neurosci*, 7(7):563–74, 2006. 1471-003X (Print) Journal Article Research Support, N.I.H., Extramural Research Support, Non-U.S. Gov't Review. 42

B. J. Martin, J. P. Roll, and N. Di Renzo. The interaction of hand vibration with oculomanual coordination in pursuit tracking. *Aviat Space Environ Med*, 62(2):145–52, 1991. 0095-6562 (Print) Journal Article Research Support, Non-U.S. Gov't. 115

J. McIntyre, M. Lipshits, M. Zaoui, A. Berthoz, and V. Gurfinkel. Internal reference frames for representation and storage of visual information: the role of gravity. *Acta Astronaut*, 49(3-10):111–21, 2001a. 18, 44

J. McIntyre, M. Zago, A. Berthoz, and F. Lacquaniti. Does the brain model newton's laws? *Nat Neurosci*, 4(7):693–4, 2001b. 23, 41

S. Mechtcheriakov, M. Berger, E. Molokanova, G. Holzmueller, W. Wirtenberger, S. Lechner-Steinleitner, C. De Col, I. Kozlovskaya, and F. Gerstenbrand. Slowing of human arm movements during weightlessness: the role of vision. *Eur J Appl Physiol*, 87(6):576–83, 2002. 41, 119

B. Mehta and S. Schaal. Forward models in visuomotor control. *J Neurophysiol*, 88(2):942–53, 2002. 20

D. M. Merfeld, L. Zupan, and R. J. Peterka. Humans use internal models to estimate gravity and linear acceleration. *Nature*, 398(6728):615–8, 1999. 25

R. C. Miall and R. Ivry. Moving to a different beat. *Nat Neurosci*, 7(10): 1025–6, 2004. 1097-6256 (Print) Comment News. 41

P. Morasso. Spatial control of arm movements. *Exp Brain Res*, 42(2):223–7, 1981. 12

B Mountcastle. *The Sensory Hand. Neural mechanisms of somatic sensations.* Harvard University Press, 2005. 117

L. A. Mrotek, B. A. Hart, P. K. Schot, and L. Fennigkoh. Grip responses to object load perturbations are stimulus and phase sensitive. *Exp Brain Res*, 155(4):413–20, 2004. 96, 114

E. Nakano, H. Imamizu, R. Osu, Y. Uno, H. Gomi, T. Yoshioka, and M. Kawato. Quantitative examinations of internal representations for arm trajectory planning: minimum commanded torque change model. *J Neurophysiol*, 81(5):2140–55, 1999. 13

T. Nanayakkara and R. Shadmehr. Saccade adaptation in response to altered arm dynamics. *J Neurophysiol*, 90(6):4016–21, 2003. 19, 114, 124

J. R. Napier. The prehensile movements of the human hand. *J Bone Joint Surg Br*, 38-B(4):902–13, 1956. 0301-620X (Print) Journal Article. 117

S. Neggers and H. Bekkering. Coordinated control of eye and hand movements in dynamic reaching. *Hum Mov Sci*, 21(3):37, 2002. 96

W. L. Nelson. Physical principles for economies of skilled movements. *Biol Cybern*, 46(2):135–47, 1983. 12, 41

D. A. Nowak and J. Hermsdorfer. Predictive and reactive control of grasping forces: on the role of the basal ganglia and sensory feedback. *Exp Brain Res*, 173(4):650–60, 2006. 94, 112

D. A. Nowak and J. Hermsdorfer. Sensorimotor memory and grip force control: does grip force anticipate a self-produced weight change when drinking with a straw from a cup? *Eur J Neurosci*, 18(10):2883–92, 2003. 19

D. A. Nowak and J. Hermsdorfer. Predictability influences finger force control when catching a free-falling object. *Exp Brain Res*, 154(4):411–6, 2004. 126

D. A. Nowak, J. Hermsdorfer, J. Philipp, C. Marquardt, S. Glasauer, and N. Mai. Effects of changing gravity on anticipatory grip force control during point-to-point movements of a hand-held object. *Motor Control*, 5(3):231–53, 2001. 66, 100, 113

D. A. Nowak, S. Glasauer, and J. Hermsdorfer. How predictive is grip force control in the complete absence of somatosensory feedback? *Brain*, 127(Pt 1):182–92, 2004a. 17

D. A. Nowak, J. Hermsdorfer, E. Schneider, and S. Glasauer. Moving objects in a rotating environment: rapid prediction of coriolis and centrifugal force perturbations. *Exp Brain Res*, 157(2):241–54, 2004b. 80, 93

D. A. Nowak, K. Rosenkranz, J. Hermsdorfer, and J. Rothwell. Memory for fingertip forces: passive hand muscle vibration interferes with predictive grip force scaling. *Exp Brain Res*, 156(4):444–50, 2004c. 21

C. Papaxanthis, T. Pozzo, K. E. Popov, and J. McIntyre. Hand trajectories of vertical arm movements in one-g and zero-g environments. evidence for a central representation of gravitational force. *Exp Brain Res*, 120(4):496–502, 1998. 23, 35, 62, 78, 120

C. Papaxanthis, T. Pozzo, and J. McIntyre. Kinematic and dynamic processes for the control of pointing movements in humans revealed by short-term exposure to microgravity. *Neuroscience*, 135(2):371–83, 2005. 114

J. Pelz, M. Hayhoe, and R. Loeber. The coordination of eye, head, and hand movements in a natural task. *Exp Brain Res*, 139(3):266–77, 2001. 96, 100

C. Prablanc, J. F. Echallier, E. Komilis, and M. Jeannerod. Optimal response of eye and hand motor systems in pointing at a visual target. i. spatio-temporal characteristics of eye and hand movements and their relationships when varying the amount of visual information. *Biol Cybern*, 35(2):113–24, 1979. 95, 96

C. Prablanc, D. Pelisson, and M. A. Goodale. Visual control of reaching movements without vision of the limb. i. role of retinal feedback of target position in guiding the hand. *Exp Brain Res*, 62(2):293–302, 1986. 0014-4819 (Print) Journal Article. 11

B. M. Quaney, D. L. Rotella, C. Peterson, and K. J. Cole. Sensorimotor memory for fingertip forces: evidence for a task-independent motor memory. *J Neurosci*, 23(5):1981–6, 2003. 21

M. H. Raibert. A model for sensorimotor control and learning. *Biol Cybern*, 29 (1):29–36, 1978. 0340-1200 (Print) Journal Article Research Support, U.S. Gov't, P.H.S. 21

J. P. Roll, J. P. Vedel, and E. Ribot. Alteration of proprioceptive messages induced by tendon vibration in man: a microneurographic study. *Exp Brain Res*, 76(1):213–22, 1989. 115

R. Ronsse, O. White, and P. Lefevre. Computation of gaze orientation under unrestrained head movements. *J Neurosci Methods*, 159(1):158–69, 2007. 82, 84, 102, 103

H. Ross, E. Brodie, and A. Benson. Mass discrimination during prolonged weightlessness. *Science*, 225(4658):219–21, 1984. 23

H. E. Ross and M. F. Reschke. Mass estimation and discrimination during brief periods of zero gravity. *Percept Psychophys*, 31(5):429–36, 1982. 23

H. E. Ross, E. E. Brodie, and A. J. Benson. Mass-discrimination in weightlessness and readaptation to earth's gravity. *Exp Brain Res*, 64(2):358–66, 1986. 23

Y. Rossetti, M. Desmurget, and C. Prablanc. Vectorial coding of movement: vision, proprioception, or both? *J Neurophysiol*, 74(1):457–63, 1995. 0022-3077 (Print) Clinical Trial Journal Article Research Support, Non-U.S. Gov't. 12

P. Saels, J. L. Thonnard, C. Detrembleur, and A. M. Smith. Impact of the surface slipperiness of grasped objects on their subsequent acceleration. *Neuropsychologia*, 37(6):751–6, 1999. 19

U. Sailer, J. R. Flanagan, and R. S. Johansson. Eye-hand coordination during learning of a novel visuomotor task. *J Neurosci*, 25(39):8833–42, 2005. 115

R. L. Sainburg, M. F. Ghilardi, H. Poizner, and C. Ghez. Control of limb dynamics in normal subjects and patients without proprioception. *J Neurophysiol*, 73(2):820–35, 1995. 13, 22

J. A. Saunders and D. C. Knill. Humans use continuous visual feedback from the hand to control fast reaching movements. *Exp Brain Res*, 152(3):341–52, 2003. 15, 115

S. Schaal and D. Sternad. Origins and violations of the 2/3 power law in rhythmic three-dimensional arm movements. *Exp Brain Res*, 136(1):60–72, 2001. 13

S. Schaal, D. Sternad, R. Osu, and M. Kawato. Rhythmic arm movement is not discrete. *Nat Neurosci*, 7(10):1136–43, 2004. 118

R. A. Scheidt, J. B. Dingwell, and F. A. Mussa-Ivaldi. Learning to move amid uncertainty. *J Neurophysiol*, 86(2):971–85, 2001. 21

P. Senot, M. Zago, F. Lacquaniti, and J. McIntyre. Anticipating the effects of gravity when intercepting moving objects: differentiating up and down based on nonvisual cues. *J Neurophysiol*, 94(6):4471–80, 2005. 25

D. J. Serrien, P. Kaluzny, U. Wicki, and M. Wiesendanger. Grip force adjustments induced by predictable load perturbations during a manipulative task. *Exp Brain Res*, 124(1):100–6, 1999. 94, 100

R. Shadmehr and T. Brashers-Krug. Functional stages in the formation of human long-term motor memory. *J Neurosci*, 17(1):409–19, 1997. 22

R. Shadmehr and H. H. Holcomb. Inhibitory control of competing motor memories. *Exp Brain Res*, 126(2):235–51, 1999. 22

R. Shadmehr and F. A. Mussa-Ivaldi. Adaptive representation of dynamics during learning of a motor task. *J Neurosci*, 14(5 Pt 2):3208–24, 1994. 13, 18, 20, 21

A. M. Smith. Does the cerebellum learn strategies for the optimal time-varying control of joint stiffness? *Behavioral Brain Sciences*, 19:399–410, 1996. 18

A.M. Smith. *Some cerebellar and cortical contributions to reaching and grasping. Vision and action: The control of grasping*. Ablex Publishing Corporation, Norwood, NJ, 1990. 18

B. C. Smits-Engelsman, S. P. Swinnen, and J. Duysens. The advantage of cyclic over discrete movements remains evident following changes in load and amplitude. *Neurosci Lett*, 396(1):28–32, 2006. 0304-3940 (Print) Journal Article. 41

J. F. Soechting and M. Flanders. Moving in three-dimensional space: frames of reference, vectors, and coordinate systems. *Annu Rev Neurosci*, 15:167–91, 1992. 0147-006X (Print) Journal Article Research Support, U.S. Gov't, P.H.S. Review. 11

J. Starkes, W. Helsen, and D. Elliott. A menage a trois: the eye, the hand and on-line processing. *J Sports Sci*, 20(3):217–24, 2002. 15, 115

V.A. Stelmach, G.E.; Diggles. Control theories in motor behavior. *Acta Psychologica*, 50(1):83–105, 1982. 2

Y. N. Turrell, F. X. Li, and A. M. Wing. Grip force dynamics in the approach to a collision. *Exp Brain Res*, 128(1-2):86–91, 1999. 80, 93, 94, 95, 100, 112, 123

Y. Uno, M. Kawato, and R. Suzuki. Formation and control of optimal trajectory in human multijoint arm movement. minimum torque-change model. *Biol Cybern*, 61(2):89–101, 1989. 13

R. J. van Beers, D. M. Wolpert, and P. Haggard. When feeling is more important than seeing in sensorimotor adaptation. *Curr Biol*, 12(10):834–7, 2002. 16

J. L. Vercher, S. Lazzari, and G. Gauthier. Manuo-ocular coordination in target tracking. ii. comparing the model with human behavior. *Biol Cybern*, 77(4): 267–75, 1997. 18

P. Viviani and T. Flash. Minimum-jerk, two-thirds power law, and isochrony: converging approaches to movement planning. *J Exp Psychol Hum Percept Perform*, 21(1):32–53, 1995. 12

P. Viviani and R. Schneider. A developmental study of the relationship between geometry and kinematics in drawing movements. *J Exp Psychol Hum Percept Perform*, 17(1):198–218, 1991. 12

R. C. Wagenaar and R. E. van Emmerik. Resonant frequencies of arms and legs identify different walking patterns. *J Biomech*, 33(7):853–61, 2000. 0021-9290 (Print) Journal Article. 14

G. Westheimer. Spatial vision. *Annu Rev Psychol*, 35:201–26, 1984. 0066-4308 (Print) Journal Article Review. 11

O. White, J. McIntyre, A. S. Augurelle, and J. L. Thonnard. Do novel gravitational environments alter the grip-force/load-force coupling at the fingertips? *Exp Brain Res*, 163(3):324–34, 2005. 68, 78, 132

O. White, J. L. Thonnard, A. M. Wing, R. M. Bracewell, and P. Lefevre. Eye-hand coordination in high impact loads. submitted. 100, 102, 114, 115

C. A. Williams and S. P. Deweerth. A comparison of resonance tuning with positive versus negative sensory feedback. *Biol Cybern*, 2007. 0340-1200 (Print) Journal article. 35

AM Wing. *Hand and Brain. The neurophysiology and psychology of hand movements.* Pergamon Press, Oxford, 1996. 80, 100

A. G. Witney, P. Vetter, and D. M. Wolpert. The influence of previous experience on predictive motor control. *Neuroreport*, 12(4):649–53, 2001. 21

A. G. Witney, A. Wing, J. L. Thonnard, and A. M. Smith. The cutaneous contribution to adaptive precision grip. *Trends Neurosci*, 27(10):637–43, 2004. 17

D. M. Wolpert and Z. Ghahramani. Computational principles of movement neuroscience. *Nat Neurosci*, 3 Suppl:1212–7, 2000. 21, 22

D. M. Wolpert and M. Kawato. Multiple paired forward and inverse models for motor control. *Neural Netw*, 11(7-8):1317–1329, 1998. 22, 60, 61, 67

D. M. Wolpert, Z. Ghahramani, and M. I. Jordan. An internal model for sensorimotor integration. *Science*, 269(5232):1880–2, 1995. 44, 67, 80

R.S. Woodworth. *The accuracy of voluntary movement*, volume 3. 1899. 15

M. Zago and F. Lacquaniti. Visual perception and interception of falling objects: a review of evidence for an internal model of gravity. *J Neural Eng*, 2 (3):S198–208, 2005. 18

M. Zago, G. Bosco, V. Maffei, M. Iosa, Y. P. Ivanenko, and F. Lacquaniti. Internal models of target motion: expected dynamics overrides measured kinematics in timing manual interceptions. *J Neurophysiol*, 91(4):1620–34, 2004. 25

V. M. Zatsiorsky, F. Gao, and M. L. Latash. Motor control goes beyond physics: differential effects of gravity and inertia on finger forces during manipulation of hand-held objects. *Exp Brain Res*, 2004. 67, 76, 77

E. P. Zehr, T. J. Carroll, R. Chua, D. F. Collins, A. Frigon, C. Haridas, S. R. Hundza, and A. K. Thompson. Possible contributions of cpg activity to the control of rhythmic human arm movement. *Can J Physiol Pharmacol*, 82 (8-9):556–68, 2004. 0008-4212 (Print) Journal Article Review. 14, 34

D. Zhu, S. T. Moore, and T. Raphan. Robust pupil center detection using a curvature algorithm. *Comput Methods Programs Biomed*, 59(3):145–57, 1999. 82

List of Figures

1.1 Basic concepts of system control theory 4
1.2 Feedback control system 5
1.3 Feedforward control system 5
1.4 Combination of feedback and feedforward approaches 7
1.5 Illustration of feedback and feedforward approaches 7
1.6 Planning module upstream of hybrid feedback/feedforward architecture 9
1.7 Direction-dependent precision of visual and proprioceptive localization 16
1.8 Grip force-load force coupling 17
1.9 Explicit knowledge of object properties is not sufficient to adjust prediction of GF 20
1.10 Adaptation of GF to LF across parabolas for a non-experienced subject 24
1.11 Anticipatory EMG in a ball catching task in 1 and 0 g 24

2.1 Parabolic flight manœuvre and typical trajectory performed by the participants 38
2.2 Period as a function of gravity 40

3.1 Experimental set-up with the hand-held device 47
3.2 Seven typical cycles of movement in the stable 0, 1 and 1.8 g . 52
3.3 Mean load force, grip force and their ratio across levels of load 55
3.4 Gravitational and inertial gains of as a function of load 57
3.5 Asymmetry index across trials 58

4.1 The manipulandum with half rings and the set-up 69
4.2 GF-LF relationship across different masses 72
4.3 Influence of mass and frequency on the GF-LF linear regression 73

4.4 GF regulation for a given LF 74
4.5 Model confronted to real data 76

5.1 Equipment and participant posture 83
5.2 Typical collisions upwards and downwards 87
5.3 Grip force-Load force coupling during transport and collision phases 88
5.4 Pre-programming of grip force maximum 90
5.5 Gaze and hand coupling in the transport phase 91
5.6 Gaze and hand coupling in the collision phase 93
5.7 Mass-damper-spring model 98

6.1 Typical collisions in microgravity 106
6.2 GF-LF coupling in transport and collision phases 107
6.3 Evolution of grip force over time 108
6.4 Eye-hand coordination 110
6.5 Duration of target fixations 112
6.6 Conceptual model of eye-hand-grip coordination during a collision task 116

A.1 The manipulandum and its reference frame 128
A.2 Typical lift trials with symmetric and asymmetric loadings . . 130
A.3 Reconstructed center of pressure of a contacting force 131
A.4 Main components of the set-up 134
A.5 Connections sketch between the PXI and the transducers . . . 135
A.6 Analysis module of Microgravity 137
A.7 Flowchart to command the transducers 138
A.8 A single parabolic flight profile 141
A.9 Force balance on the wings in 0 and 1 g 142

B.1 The double compound pendulum model 146
B.2 Domain of integration to get the inertia of a cylinder 149
B.3 Natural frequency of upper limb in function of gravity 153
B.4 Simulation of the double compound pendulum during 10 seconds 155
B.5 Period and natural frequency in function of gravity 156
B.6 Spherical pendulum model 158

List of Tables

1.1 Comparison between microgravity platforms 27

3.1 Mean accelerations along the three axes and in the three gravity phases 46
3.2 The four levels of equivalent tangential load forces 49

4.1 Mass combinations in the manipulandum 68

Index

A300 ZeroG, 140
acceleration profile, 41
acquisition, 136
action, 3
actuators, 1
adaptation, 60
Amonton's law, 122
analysis, 137
angle of attack, 142
angular momentum, 157
anisotropy, 18
asymmetry, 56, 62, 123
ATI, 127

ballistic trajectory, 141
Bayesian, 22
behaviour, 1
bell-shaped, 12, 85
Bordeaux, 140

C language, 135
calibrate, 117
campaign, 140
center of pressure, 129
central pattern generators, 14, 34
Centre d'Essais en Vol, 140
centrifugal, 25
cerebellum, 17, 18
Chronos, 81, 133
closed-loop, 96
coefficient of friction, 122
coefficient of restitution, 97
collision phase, 94, 105
collisions, 80, 100
compliant, 122
compression, 85
compromise, 97
configuration, 136
conflicting, 123
consolidation, 123
contacts, 119
controller, 60
coriolis effects, 25
correlation, 107
cost function, 8, 12
counter, 138
cross-correlation, 53
customization, 137

damping, 95, 97
deafferented, 17
decouple, 112
degrees of freedom, 6
delays, 6
digital code, 135
dissociation, 109, 113
divergence, 109
Divide and Conquer, 2
double compound pendulums, 145
drag, 141
drop tower, 26
dropping, 77

efference copy, 6, 66, 115

EMG, 18, 94
energy cost, 41
Equivalence Principle, 67
Ertalon, 127
ESA, 140
explicit knowledge, 19
extraretinal signals, 11
eye-centred, 96

feedback, 2, 4, 14, 115
feedforward, 4, 60, 95
FFT, 154
fixation, 92, 96, 111, 115
force field, 21
forces, 126
forward model, 17, 60, 115
Foton, 26
free-fall, 26
frequency, 67
friction, 10

gain, 67, 76, 120
gaze, 81
gaze-hand coordination, 81
generalization, 22
goals, 2
Graphic User Interfaces, 136
gravitational, 50
gravitational gain, 61
gravitoinertial, 60
gravity, 23, 120
grip force, 10, 17, 44, 117
grip force rate, 19

Hamiltonian, 157
haptic, 44, 123
high-level control, 62
hypergravity, 120, 140

idiosyncratic, 122
impact forces, 89
implicit knowledge, 19
inertial, 18, 50
inertial forces, 86
inertial gain, 61
injection, 141
instabilities, 96
internal models, 10, 67, 123
International Space Station, 27, 123
inverse system model, 3

kinetic energy, 95, 149

LabWindows/CVI, 135
Lagrangian dynamics, 145
learning, 19
lift, 141
likelihood, 22
linear relationship, 67
load force, 10, 17, 44
locomotion, 34, 66
long-term weightless, 123
look-up, 21
lunar missions, 121

manipulandum, 125
mapping, 80, 115
Mars exploration, 121
mass discrimination, 23
mass-damper-spring, 97
maximum, 113
Maximum Voluntary Contraction, 123
microgravity, 112, 113, 120
Mini40, 127
minimum jerk, 12
minimum variance, 13
mistakes, 2
model, 114
modulation, 76

module, 60
moment of inertia, 149
momentum, 123
monitoring, 136
motion-sensitive, 77
multidirectional, 126
multimodal, 124
multiple regression, 89
mutiplexed, 139

neurons, 77
noise, 3, 13
normal modes, 151
Novespace, 140

offset, 67, 76, 135
open-loop, 96
options, 137
OptoTrak, 133
oscillators, 14, 118
otoliths, 25, 77

parabola, 141
parabolic flight, 25, 27, 140
parallel axis theorem, 149
Parietal Reach Area, 96
peak acceleration, 96
pendulum, 37
perturbation, 120
planning, 8
potential energy, 156
pre-programmed, 89
precision grip, 117, 126
prediction, 124
prior, 22
proprioception, 16
pull-out, 141
pull-up, 141
Purkinje, 18
PXI controller, 133
PXI-6071E, 133, 137
PXI-6533, 133, 137
PXI-8210, 133

reaction times, 90, 110, 114
reference frame, 11
reference trajectory, 3
reflex, 80, 94, 100
replanning, 8
resonance tuning, 39
resonant frequency, 14, 34, 118
retinal coordinates, 96
rhythmic, 13
risk, 114
RTSI lines, 138

saccade, 84
semi-circular canals, 25
semi-rings, 127
sensorimotor memory, 21, 97
sensory processing, 2
single-cell, 18
slippage, 95
smooth pursuit, 90
Sogerma, 140
sounding rockets, 26
spherical pendulum, 156
stability, 97
state, 3
stereotyped, 12
stiffness, 95, 97
stimulus-response cycle, 137
strain gages, 135
structural perturbations, 20
sub-goals, 2
supra-spinal, 42
surface texture, 67
swing, 94, 123

switch, 115
symmetric, 109
synchronize, 137
system model, 3

temperature, 122, 135
temporal coupling, 60
thermister, 135
thrust, 141
time-locking, 92, 96, 111, 114
time-to-contact, 24
torque change, 13
torques, 126
transducer, 135
transition, 113, 122
transport phase, 94, 105
tribology, 122
TTL, 133
tungsten carbide, 127
two-thirds power law, 12

underwater, 25
upside down, 121

vestibular cortex, 24
vibration, 115
virtual reality, 25
visual acuity, 11
visual cues, 19
visual feedback, 114
visualization, 136
visuo-manual, 97
voluntary GF, 67

weight, 141
workspace memory, 22